EFFECTS OF SHEAR REINFORCEMENT ON THE IMPACT BEHAVIOR OF REINFORCED CONCRETE SLABS

A Thesis Submitted to the
the Graduate School of Engineering and Sciences of
İzmir Institute of Technology
in Partial Fulfillment of the Requirements for the Degree of

MASTER OF SCIENCE

in Civil Engineering

by
Yonca ARSAN

July 2014
İZMİR

We approve the thesis of **Yonca ARSAN**

Examining Committee Members:

Assist. Prof.Dr. Selçuk SAATCI
Department of Civil Engineering, İzmir Institute of Technology

Assoc. Prof. Dr. Cemalettin DÖNMEZ
Department of Civil Engineering, İzmir Institute of Technology

Assist. Prof. Dr. Mert Yücel YARDIMCI
Department of Civil Engineering, Gediz University

10 July 2014

Assist. Prof.Dr. Selçuk SAATCI
Supervisor, Department of Civil Engineering
İzmir Institute of Technology

Prof.Dr. Gökmen TAYFUR
Head of the Department of
Civil Engineering

Prof.Dr. R.Tuğrul SENGER
Dean of the Graduate School of
Engineering and Sciences

ACKNOWLEDGMENTS

First of all, I would like to express my gratitude for my supervisor Assist. Prof. Dr. Selçuk SAATCI for his endless support, guidance and patience over the course of this thesis and the laboratory work required.

I would like to thank our laboratory technician Cemal Kılıç, CE Research Assistant Hasan Yavuz Ersöz and my beloved colleague Süleyman Yaşayanlar for their help in and out of the laboratory. Without them, this study would be very laborious and dull. Also, I would like to thank the research assistants of civil engineering for their help during the course of tough work.

My special thanks to the technicians of our neighbor laboratory, Laboratory of Mechanics, for sharing their experience, guidance and assistance.

Finally, I would like to thank my parents for their amazing, everlasting support and patience. This thesis is dedicated to them.

ABSTRACT

EFFECTS OF SHEAR REINFORCEMENT ON THE IMPACT BEHAVIOR OF REINFORCED CONCRETE SLABS

Design of reinforced concrete (RC) members against impact loads is required for many structures such as industrial facilities, military protective structures, and infrastructures. This study presents experimental investigation for strengthening RC slabs under impact loads using shear reinforcement. Slabs were strengthened against punching shear with two methods: using shear studs as shear reinforcement and using steel fiber reinforced concrete (SFRC) instead of plain concrete.

Eight RC slabs with dimensions of 2150x2150x150 mm were tested. Four of the specimens, two identical pairs, were cast with shear studs around the point of impact. Remaining four specimens, again two identical pairs, were cast with 1% steel fibers. Pairs in each group contained two different levels of longitudinal reinforcement. For each pair, one specimen was tested under static loading, whereas its identical twin was tested under impact loads.

Specimens were tested with a test setup that provides simply supported conditions. Support loads, displacements, accelerations, and strains on bars were measured during the tests.

The study revealed that using shear studs and SFRC prevents brittle punching shear failure for both static and impact loading. Specimens with steel fibers reached the highest load carrying capacity for static test while specimens with shear reinforcement carried a smaller load for large deformations. Specimens with SFRC displayed a close to static behavior under impact loading, influenced only slightly by inertial forces due to impact. Specimens with shear studs were largely influenced by inertial forces and scabbing occurred at some areas. Specimens with steel fibers endured more impacts compared to control specimens and specimens with shear studs due to their higher energy dissipating capabilities.

ÖZET

BETONARME DÖŞEMELERDE KAYMA DONATISININ DARBE DAVRANIŞI ÜZERİNE ETKİLERİ

Düşük hızlı darbeye maruz kalan betonarme elemanların güçlendirilmesi, stratejik önemi olan altyapı tesislerinde, askeri, endüstriyel ve benzeri yapılarda önem taşımaktadır. Bu çalışmada, kayma donatısı ile güçlendirilmiş betonarme döşemelerin, darbe yükü altındaki deneysel araştırma sonuçları sunulmaktadır. Kayma donatısı olarak ya kesme donatısı ya da normal beton yerine kancalı uçlu çelik fiber katılmış beton kullanılmıştır.

Testlerde, 2150x2150x150 mm boyutlarındaki 8 adet betonarme döşeme kullanılmıştır. Örneklerden 4 tanesi (birbirlerinin aynısı olarak imal edilen çiftlerden iki tanesi) darbe noktasının etrafında kesme donatısı ile güçlendirilmiştir. Diğer 4 örnekte ise (birbirinin aynı olarak imal edilen diğer iki çift) hacim olarak % 1'lik kancalı uçlu çelik fiber katılmış beton kullanılmıştır. Her gruptaki çiftlerin boyuna donatı aralığı olarak 150 mm ve 200 mm olarak seçilmiştir. Her çift döşemeden biri statik yük altında diğer eşi ise darbe yükü altında test edilmiştir.

Deney düzeneği, döşemelere basit mesnet koşulları sağlamaktadır. Deney sırasında yük, deplasman, ivme ve donatılarda birim uzama ölçülmüştür.

Bu çalışma, çelik fiber ve kesme donatısı kullanımı ile, gerek statik gerekse darbe yükü altında gevrek kırılmanın önüne geçildiği görülmüştür. Statik yük altında en yüksek deformasyona kesme donatılı döşemeler ulaşmış ve en yüksek yük taşıma kapasitesi çelik fiberli döşemelerde görülmüştür. Çelik fiberli döşemeler, darbe anındaki atalet kuvvetlerinden çok az etkilenmiş ve rijit bir davranış sergilemişlerdir. Kesme donatısı olan döşemeler ise, atalet kuvvetlerinden daha fazla etkilenmiş ve döşemelerin alt yüzünde dökülmeler olmuştur. Çelik fiberli döşemeler, kesme donatılı döşemelere göre daha fazla sayıda darbeye dayanmışlardır.

TABLE OF CONTENTS

LIST OF FIGURES

Figure **Page**

LIST OF TABLES

Table **Page**

CHAPTER 1

INTRODUCTION

Impact loads on reinforced concrete structures can be generated from a number of different events including aircraft or ground vehicle crashes, gas tank explosions, industrial accidents, tornado generated missiles, rocks falling on concrete shelters, ship collisions to bridge piers, terrorist bombings, and artilleries. During the impact, the target has to absorb a large amount of energy in a very short duration. Depending on the energy absorption and dissipation capacity of the structure affected by the impact, the missile could penetrate the target or could cause scabbing of material at the impact location or spalling at the rear face. The system could also respond globally by flexural failure. Depending on the damage state of the target and the missile, impact on structures can be categorized in two: a soft impact, when the missile is deformed more than the target, and a hard impact when the target suffers the real damage compared to the missile. The state of the damage on the structure is the main interest in most studies, which could be local damage or global response or both. The damage could be considered under seven cases: Penetration, cone cracking and plugging, spalling, radial cracking, scabbing, perforation and overall structural responses are the possible failure types (Figure 1.1.). Penetration, cone cracking, spalling and scabbing are accepted as the local impact effects.

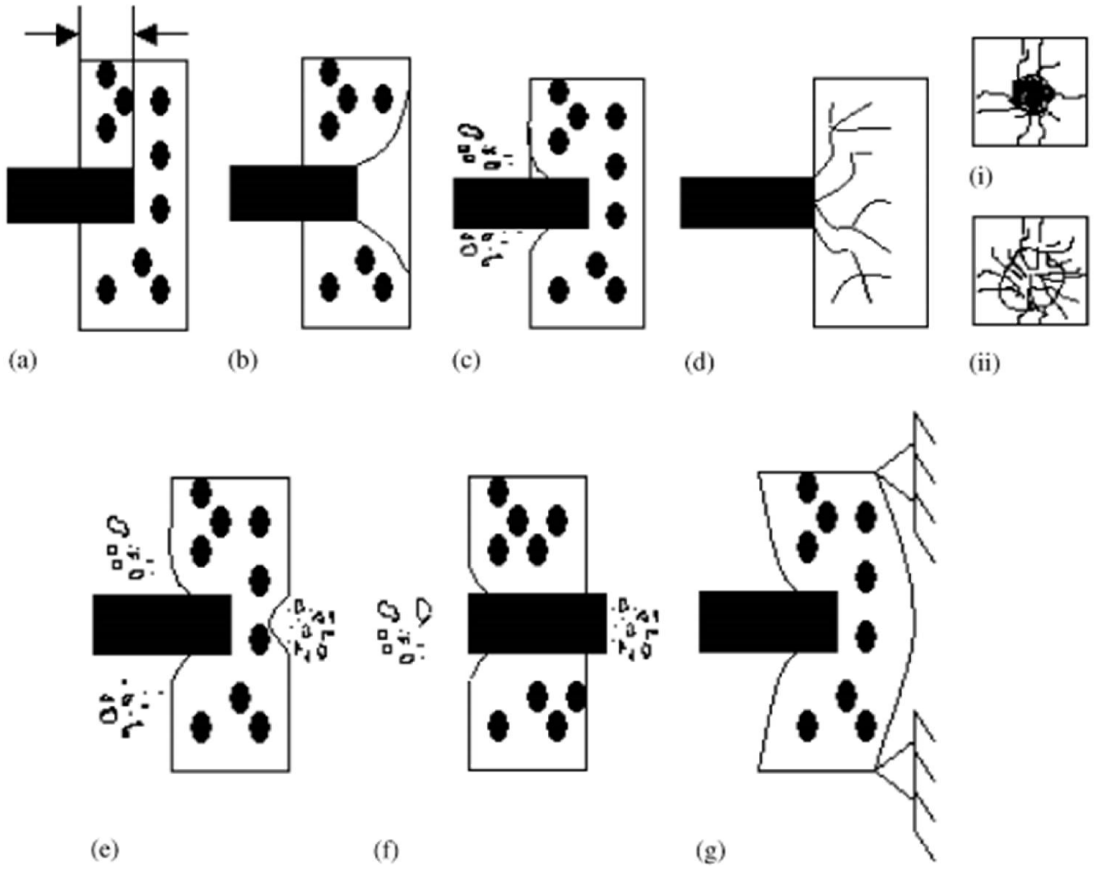

Figure 1.1. a) Penetration, b) Cone cracking, c) Spalling, d) Cracks on i) proximal face and ii) distal face, e) Scabbing, f) Perforation and g) Overall target response (Source: Li et al, 2005)

Reinforced concrete (RC) slabs support gravity loads and live loads in structures. During impact, RC slabs can be exposed to extreme dynamic loads. These unexpected loads influence slab's ability to transfer the force to other structural elements such as beams and columns. As a result of impact, RC slab could locally fail or as an extreme situation, the whole structure could collapse.

In literature, there exist numerous studies regarding impact on reinforced concrete slabs. However, great majority of these studies are towards the investigation of local damage due to the demand from the military and nuclear energy industry, which are mostly concerned from high velocity missiles. On the other hand, global failure is the main concern for the impacts on civil structures, and the studies in this area are quite limited.

The study presented here is a work that proceed the work by Batarlar (2013), aimed towards understanding the global behavior of RC slabs under impact loading. In

Batarlar's study, the brittle punching mechanism was found to be the main failure mechanism for the slabs subjected to impact loads. In this study, slab specimens, identical in dimension and reinforcement to the ones tested by Batarlar, were designed to have increased punching resistance and tested under impact loading. In order to increase the punching capacity of the slabs, two approaches were followed: increasing the tension capacity of concrete by adding steel fibers into the concrete mix, and using shear studs around the impact area that would act as stirrups and thus increase the shear capacity. Both these methods were found effective against punching failure in static conditions, but their effectiveness under impact conditions were not fully investigated.

In the following chapter, a brief review of the literature on the subject is provided. Chapter 3 presents the details of the experimental program. Discussions on the obtained results are presented in Chapter 4, which is followed by the concluding chapter.

CHAPTER 2

LITERATURE REVIEW

2.1. Introduction

The subject of impact loading is being investigated by a number of researchers for the past few decades. This chapter provides short summaries of important studies regarding the behavior of slabs under impact loading. Following section describes a few studies on the impact behavior of slabs. Study of Batarlar (2013), which precedes the current study, is summarized in more detail in this section. Current study aims to investigate the effects of shear reinforcement, in terms of shear studs and steel fibers, on the impact behavior of slabs. Therefore, Sections 2.3 and 2.4 briefly describes a few studies on the effects of steel fiber reinforcement and shear studs on the behavior of reinforced concrete slabs, respectively.

2.2. Impact Loading on RC Slabs

In a study carried out by Zinnedin and Krauthammer (2007), nine slabs with dimensions of 90x1524x3353 mm were tested under impact loading (Figure 2.1). Effects of locations of welded steel wires, the section area of these steel bars and the impact drop height on the impact behavior were investigated in this study. It was found that at lower drops, the failure mode of the specimen was flexural and at higher drops, it was punching shear failure.

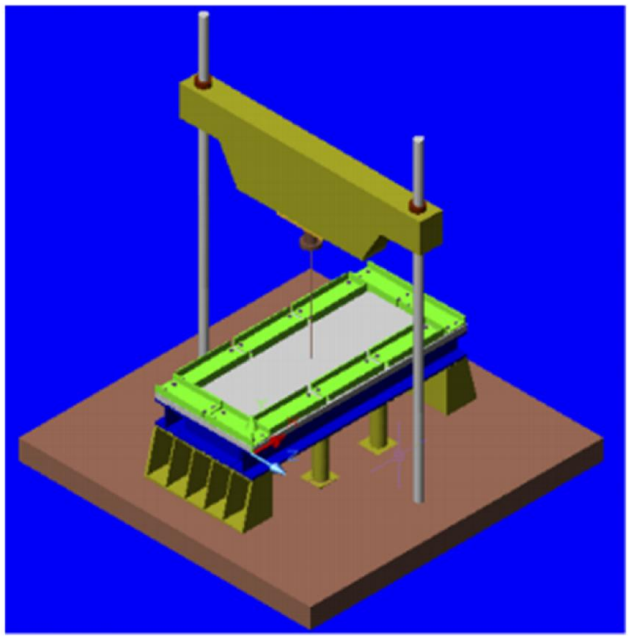

Figure 2.1. Precision impact testing system
(Source: Zinnedin and Krauthammer, 2007)

Another study was made by Kishi et al. (2011). Slabs with three kinds of support conditions were tested under impact and the results were compared to numerical analysis (Figure 2.2). It was found that maximum impact forces did not vary with support conditions as well as maximum deflections. Impact forces obtained from numerical analysis was relatively smaller compared to experimental results.

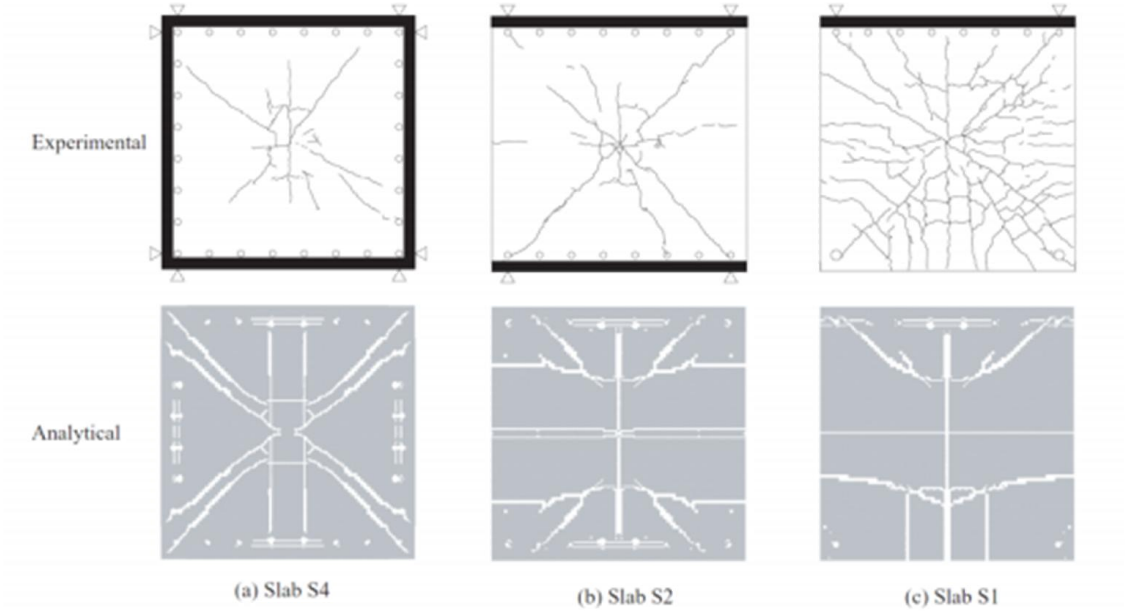

Figure 2.2. Crack patterns
(Source: Kishi et al., 2011)

The study of Batarlar (2013) precedes the current study and it served as the basis for the current experimental program. Both studies used the same test setup in Izmir Institute of Technology Structural Laboratory (Figure 2.4). Support conditions, dimensions of the specimens and longitudinal reinforcements of the specimens are also same. Considering the new parameters used on this study, Batarlar specimens will be regarded as control specimens.

Batarlar cast three identical pairs of reinforced concrete (RC) slabs where each pair had different reinforcement ratio. One specimen from each pair was tested under a slow (static) loading rate while the other was tested under a rapid (impact) loading rate. The spacing of the reinforcement bars was taken as 100, 150 and 200 mm respectively for each pair, using ϕ 8 mm reinforcing bars (Figure 2.3). Specimens had reinforcement on both top and bottom of the slab, in both principle directions.

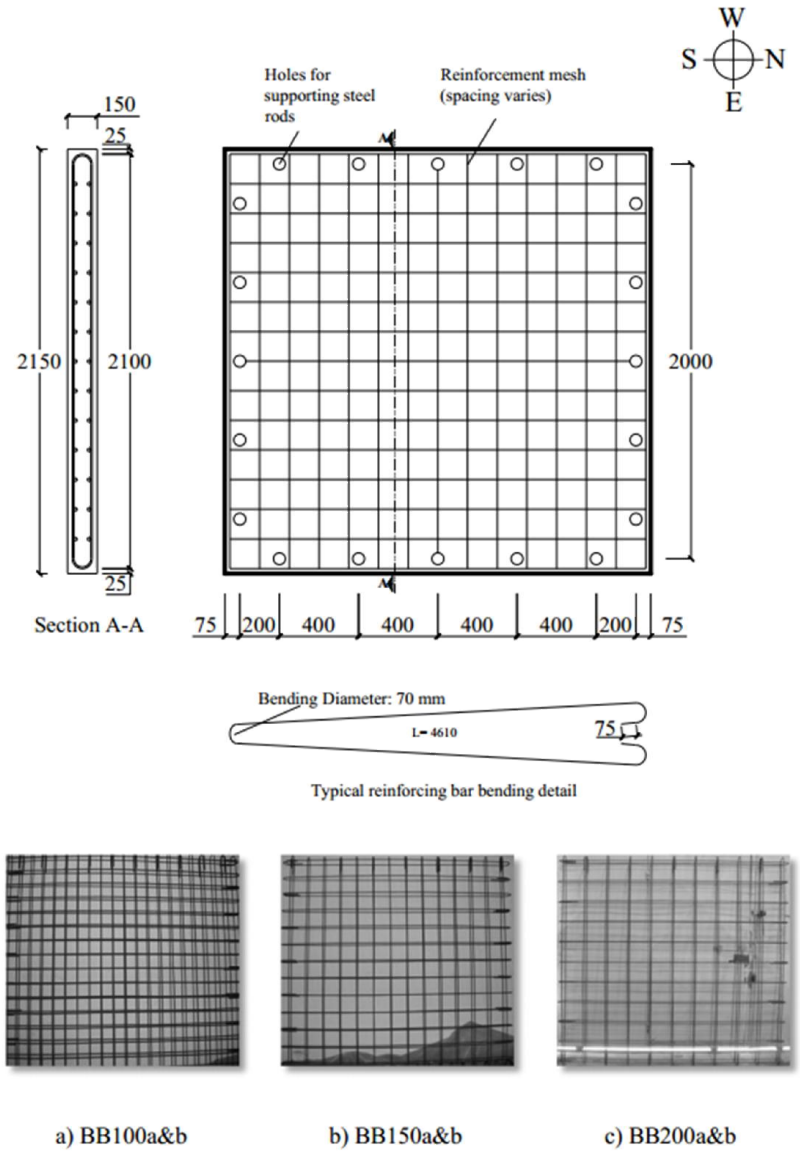

Figure 2.3. Reinforcement layout of Batarlar (2013)

All slabs had dimensions of 2150x2150x150 mm. Simply supported boundary conditions were provided by twenty hinges along the perimeter of the specimen. Hinges and load cells were connected to a circular shaft which enables free rotation but disables lifting of edges.

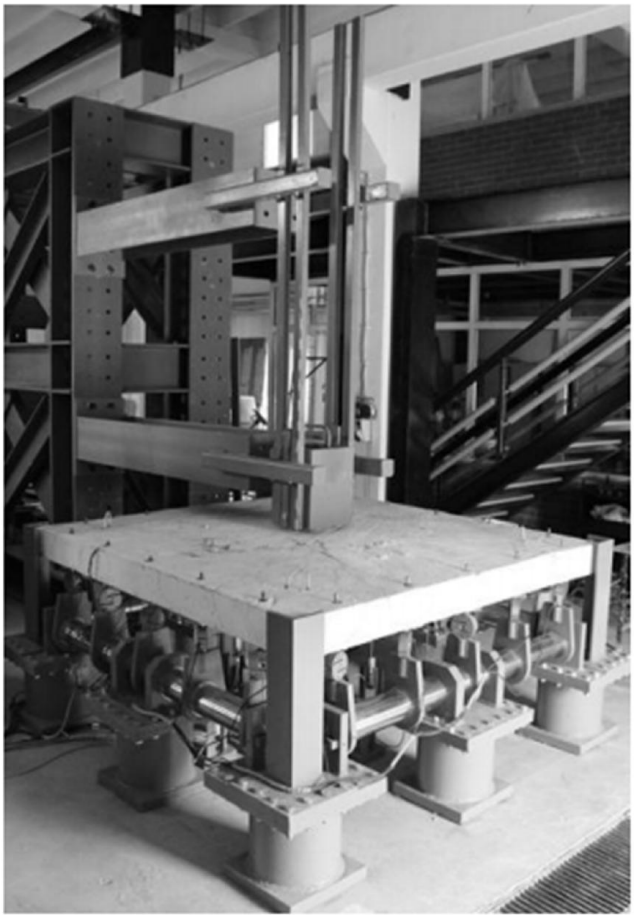

Figure 2.4. Impact testing setup
(Source: Batarlar, 2013)

Under the specimen, resistive linear positioning transducers (RLPT) have been placed. These RLPTs have been elongated with extension rods and attached to the bottom of the slab with fixing plugs inside drilled holes. For the static tests, an RLPT was placed at the top center of the slab to record the deflection.

To measure the strains of the reinforcing bars, 12 strain gauges (SG) were used for each specimen. Data from all load cells, RLPTs and accelerometers (used in impact testing) have been recorded with a data acquisition system.

During the static tests, the load was applied by a hydraulic jack at the bottom center of the slab. The hydraulic jack was actuated manually and was paused amid tests in order to document the newly formed cracks and the widened old cracks. To monitor the load during testing, a load cell was placed between the hydraulic jack and the specimen.

All static tests ended with sudden cracking sound and punching failure. Going through the data, it was seen that as the spacing between the bars increased, the load bearing capacity has decreased, while the ductility has increased leading to higher midpoint displacements. On all the static tested slabs, punching shear cones formed and these formations can be seen from the cracks on the tension side of the specimen (Figure 2.5, Figure 2.6 and Figure 2.7). Also, slabs with lesser reinforcement ratios, had less but wider cracks compared with slabs with higher reinforcement ratios where cracks were more in number but narrower.

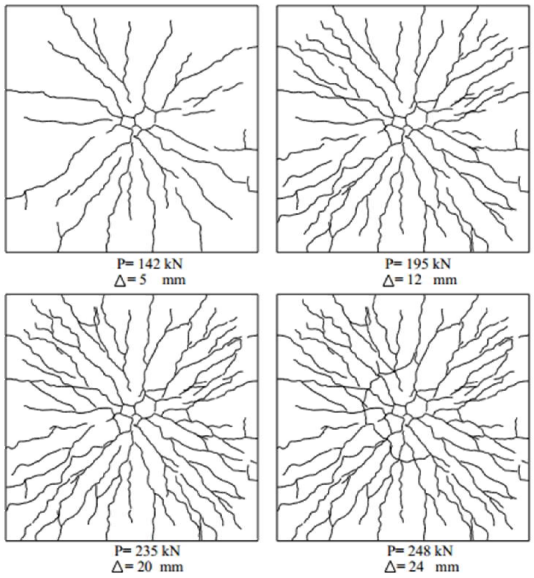

Figure 2.5. Crack distribution of specimen BB100a
(Source: Batarlar, 2013)

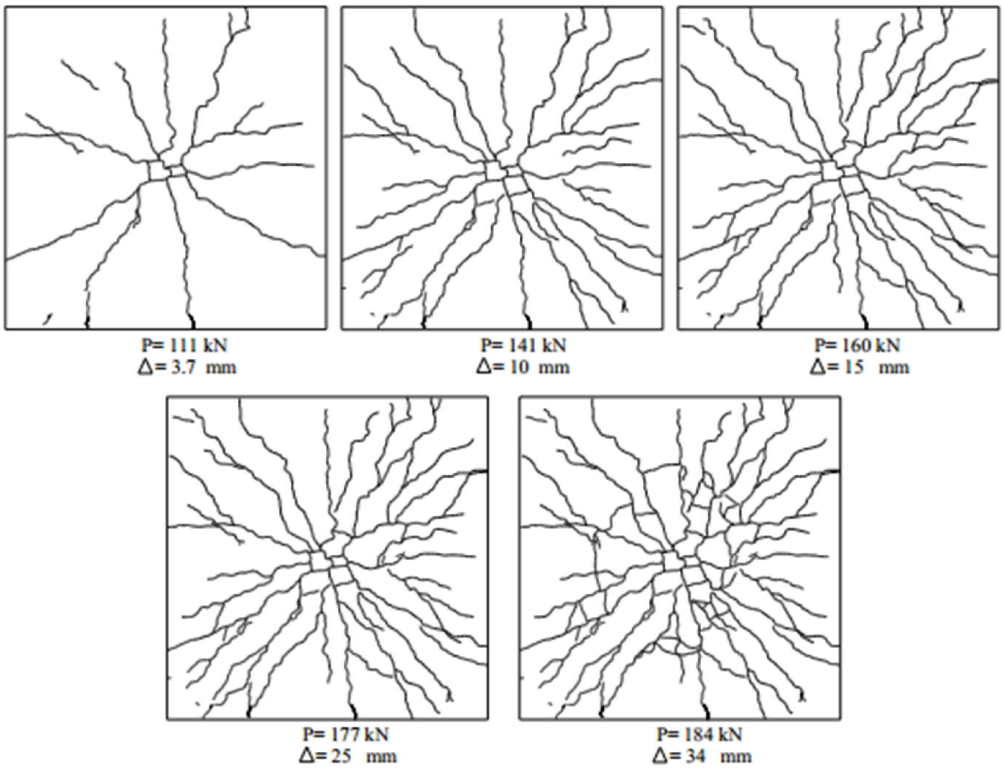

Figure 2.6. Crack distribution of specimen BB150a
(Source: Batarlar, 2013)

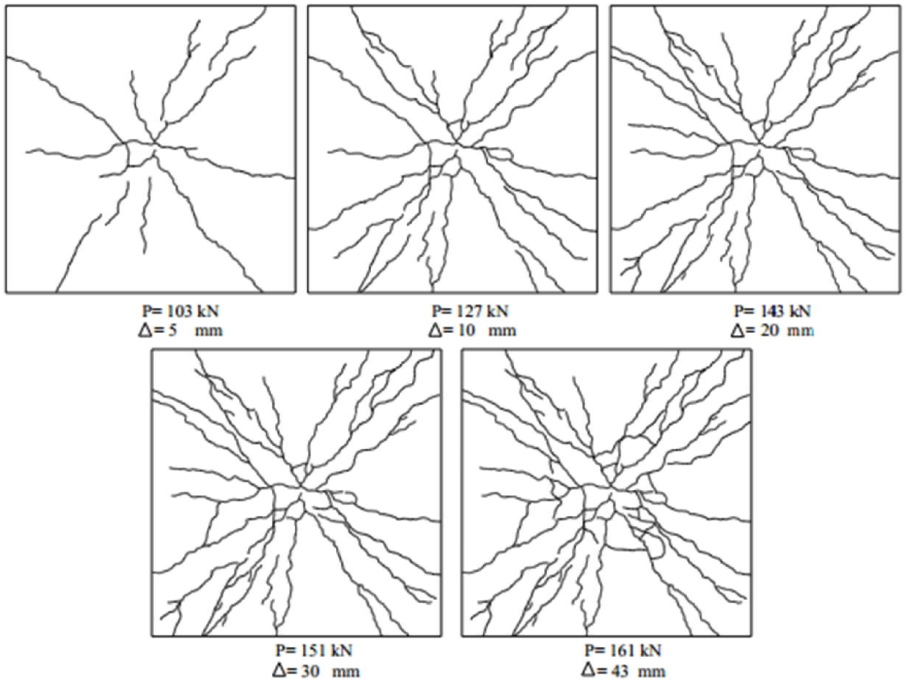

Figure 2.7. Crack distribution of specimen BB200a
(Source: Batarlar, 2013)

For impact tests, the test setup has been altered. A drop tower, with a drop height of 2.5 m, was installed. To prevent any damage to the hydraulic jack during the course of impact, the piston has been removed from underneath the specimen, also making more room for RLPTs. To obtain acceleration data, a total of seven accelerometers have been placed, two on the drop weight and five on the slab.

For all impact specimens, tests were carried out until punching failure was seen. Failure was due to the circular cracks forming a punching cone and widened diagonal cracks. Local penetration due to impact was also seen on the top surface of the slabs at the impact point.

The same test setup was also used for the current study. Test specimen dimensions and longitudinal reinforcement ratios were identical. This study further investigated the effects of the application of shear studs as shear reinforcement and steel fiber reinforced concrete (SFRC) instead of plain RC. Following sections briefly describe a few significant studies in the literature about the effects of shear studs and steel fiber reinforced concrete.

2.3. Steel Fibers

Randomly distributed steel fibers in the concrete mixture enhance the shear resistance of the member. Fibers transfer tensile stresses across diagonal cracks and increase aggregate interlock by reducing crack width. Using steel FRC is an effective way to increase the toughness and the impact resistance of the material. Although it is more prone to corrosion unlike its alternatives like Polyolefin and polyvinyl alcohol, randomly distributed steel fibers perform better.

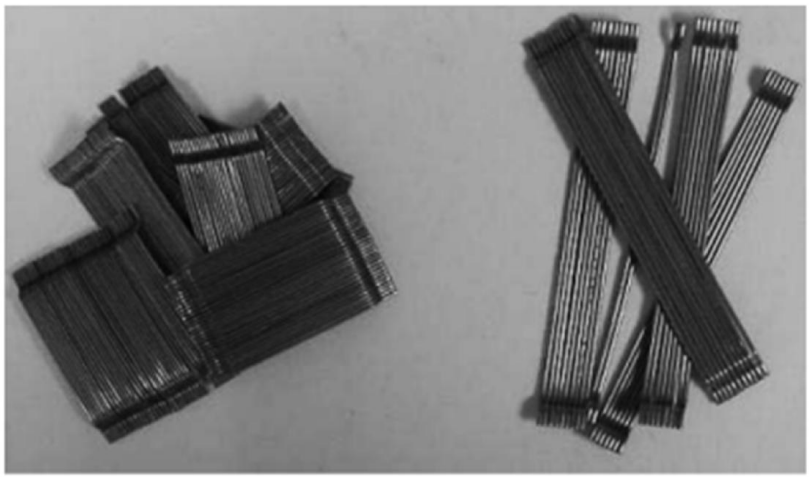

Figure 2.8. Hooked end steel fibers with different lengths; a) 30 mm, b) 60mm (Source: Dinh et al., 2010)

In a study of Xu and Mindess (2006), round concrete panels with steel and synthetic fibers were tested at the University of British Columbia under static and impact loading. Round panels, with a diameter of 635 mm and a thickness of 58 mm, were prepared with various combinations of welded wire meshes (WWM) and fibers, with two concrete strength levels. Transducers, accelerometers and a load cell were used as instrumentation. This way, the load at the moment of first crack, overall load - deflection curve and the energy consumed was recorded. A drop weight test setup was used for impact loading (Figure 2.9). Both static and impact loading was applied at the center. According to the static test results, panels with steel fibers showed increased strength and toughness compared to synthetic fibers for normal concrete strength. As for the impact tests, drop height ranged between 50 and 500 mm. Peak load increased with increased drop height. For impact tests, contribution of steel fibers, compared to synthetic fibers, were not as effective as static test. Overall, it was clear that specimens with steel fiber were less strain rate sensitive compared to specimens that were without.

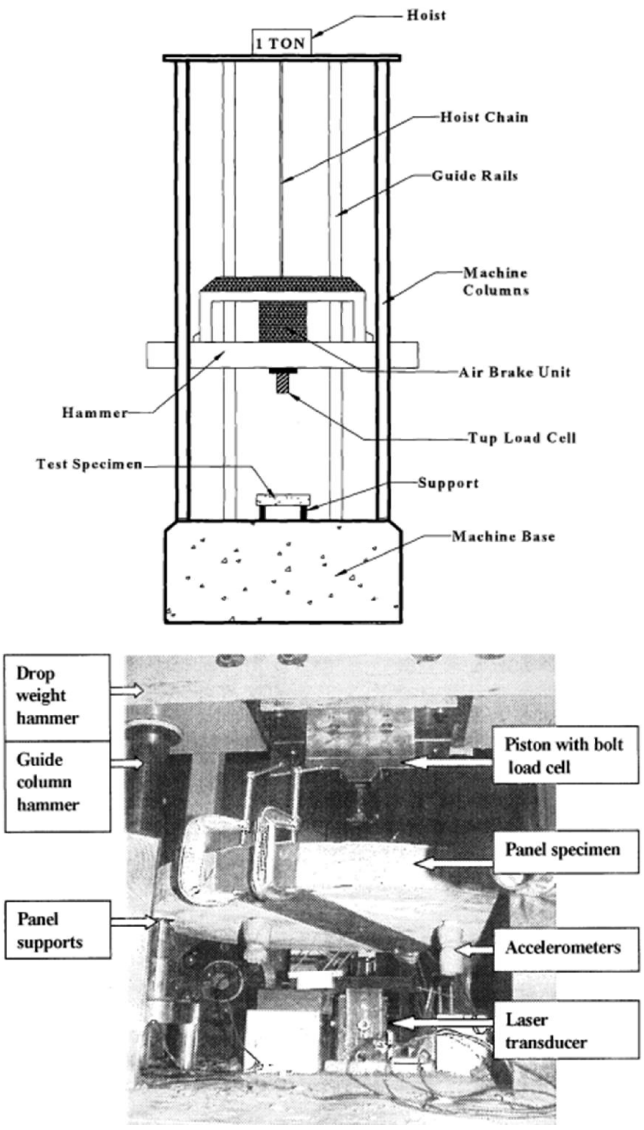

Figure 2.9. Test setup of Xu and Mindess (2006)

For its ability to increase punching strength compared to regular RC, SFRC also can be used on beams, slabs on grade and slab-column connections other than just slabs. In a study of Cheng and Parra-Montesinos (2010), FRC slab-column connections were tested under monotonically increased concentrated load. Slabs had dimensions of 1520x1520x152 mm. There were four parameters: steel fiber geometry, fiber strength, fiber content and flexural reinforcement ratio. Inside the slabs, only flexural reinforcement was provided, in both principle directions. Properties of specimen can be seen in Table 2.1. The column stub in the middle of the slab is where the load was

applied. To provide the simply supported boundary conditions, the perimeter of the slab had been supported with a steel tube topped with a rubber band, but the edges were not restrained from vertical movement. Effective depth “d” was taken as 127 mm for all ten specimens. (Figure 2.10)

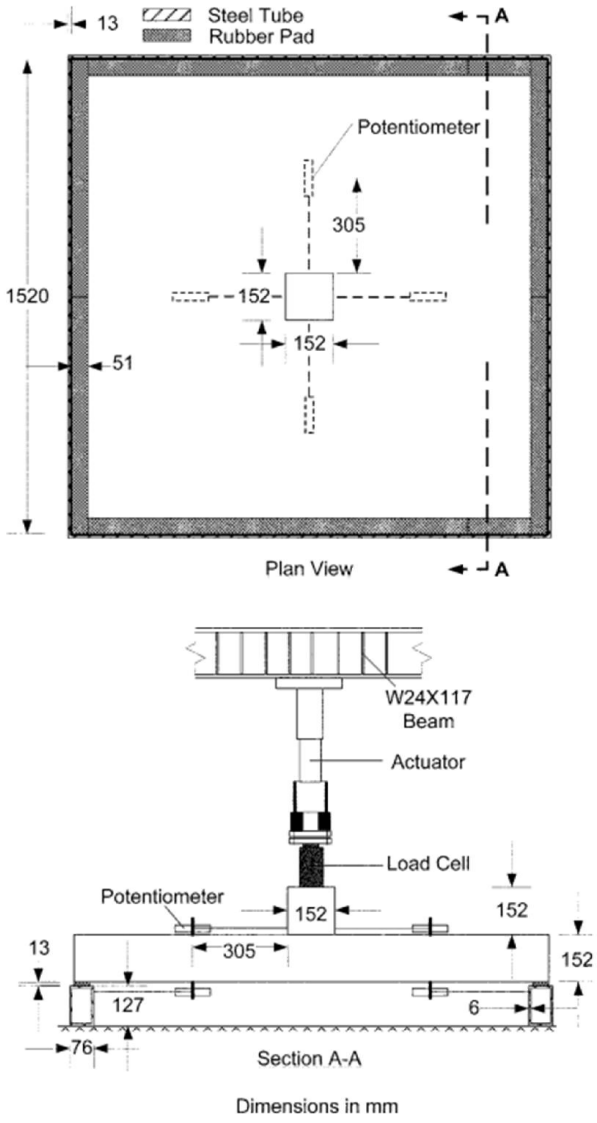

Figure 2.10. Test configurations of Cheng and Parra-Montesinos (2010)

A total of ten specimens including two plain RC, four FRC and four FRC/plain concrete specimens were tested. The last four casted with steel fibers only in a 762 mm square region in the middle of the slab (two slab thicknesses away from column stub)

and the rest was casted with regular concrete. Specimens were equipped with strain gauges and potentiometers to measure the strain and rotation.

Table 2.1. Material and fiber properties of Cheng and Parra-Montesinos (2010)

Specimen	Concrete		Steel fibers			Steel bars		
	Material	Strength, MPa	Fiber type (V_f)	L_f (d_f), mm	f_u, MPa	ρ, %	f_y, MPa	f_u, MPa
S1	Plain	47.7	—	—	—	0.83	471	697
S2						0.56		
S3	FRC	25.4	Hooked (1%)	30 (0.55)	1100	0.83	455	670
S4						0.56		
S5	FRM*	59.3	Twisted (1.5%)	35 (0.5)†	1800	0.83	471	689
	Plain	45.7	—	—	—			
S6	FRM*	57.9	Twisted (1.5%)	35 (0.5)†	1800	0.56		
	Plain	35.0	—	—	—			
S7	FRC	31.0	Hooked (1.5%)	30 (0.55)	1100	0.83	449	681
S8						0.56		
S9	FRC*	46.1	Hooked (1.5%)	30 (0.38)	2300	0.83		
	Plain	40.7	—	—	—			
S10	FRC*	59.1	Hooked (1.5%)	30 (0.38)	2300	0.56		
	Plain	50.6	—	—	—			

*Only in central 76 x 76 cm (30 x 30 in.) region of slab.
†Equivalent diameter.
Notes: FRC is fiber-reinforced concrete; FRM is fiber-reinforced mortar; V_f is fiber volume fraction; L_f is fiber length; d_f is fiber diameter; ρ is reinforcement ratio in each direction (0.83%: No. 13M at 10 cm [4 in.]; 0.56%: No. 13M at 15 cm [6 in.]); f_y is yield strength; and f_u is ultimate strength.
1 cm = 0.394 in.; 1 cm = 10 mm; 1 MPa = 0.145 ksi.

Monotonically increased load, with a rate of 3.8 mm/min, had been applied through vertically oriented hydraulic actuator and a steel reaction frame, which was connected to the actuator. Tests were stopped when significant loss of load carrying capacity was observed. At the end of each test, the cracks on the bottom of the slab were marked. Although it was visible from the cracks that column stub punched through the slab, it was not evident that each test specimen failed by punching shear failure. Specimens with 10 cm reinforcement bar spacing reached higher peak loads compared to specimens with 15 cm reinforcement bar spacing. However little or no ductility was observed for specimens with higher reinforcement ratios.

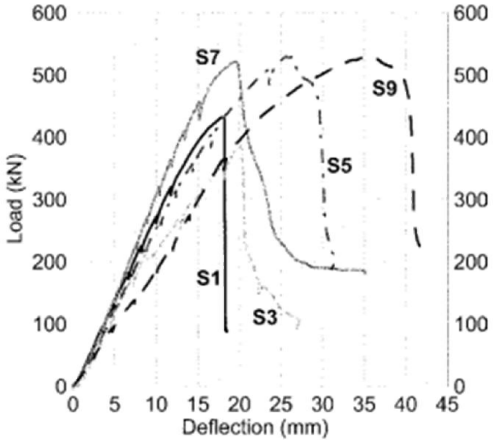

(a) Specimens with ρ = 0.83%

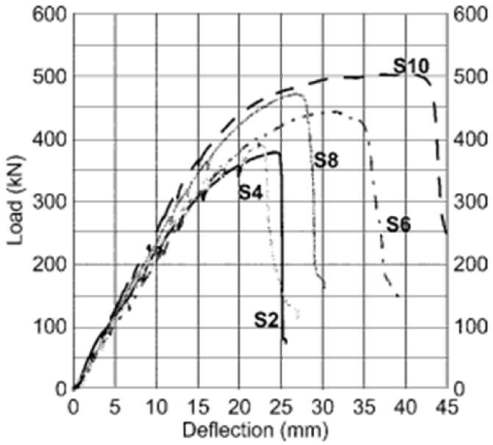

(b) Specimens with ρ = 0.56%

Figure 2.11. Load- deflection response of specimens with 0.83 % reinforcement ratio and 0.56 % reinforcement ratio (Source: Cheng and Parra-Montesinos, 2010)

From the specimens with 10 cm bar spacing; it was observed that additional steel fibers have led to an increase in ductility and normalized shear strength. Also according to the results, peak normalized strength values were greater than ACI Code regulations regarding strength factor applicable to the test results. In terms of initial stiffness, no improvement was monitored.

From outcome of test results, it is visible that the presence of fibers led to an increase in punching shear strength and changed the failure mode from brittle to ductile. Specimens with hooked steel fibers showed higher normalized punching shear strength compared to specimens with twisted steel fibers. This comparison was made between specimens with same fiber volume ratio. For the specimens made from FRC and plain

concrete, no distress at the interface was present. This means that steel FRC can be used on specific areas of the structure along with regular concrete.

Steel fibers can also be used in RC beams. According to the research of Dinh et al. (2010), using steel fibers 0.75% or higher in volume fraction meets the need of minimum stirrup reinforcement required by ACI Committee 318. 28 SFRC and RC beams were tested under monotonically increased concentrated load as a part of this research. Beams had 2 different kinds of depths, 455 and 685 mm. Other parameters include fiber volume fraction, fiber aspect ratio, fiber length, fiber strength and longitudinal reinforcement ratio. Two fiber samples are in Figure 2.8. Strains and deflections were measured by strain gauges on longitudinal reinforcement and linear potentiometers. Crack distribution was recorded after failure. For RC beams without stirrup reinforcement, a single inclined crack was observed. Multiple diagonal cracks were observed for all SFRC beams with at least two main inclined cracks (Figure 2.12). RC beams with minimum amount of stirrup reinforcement showed little improvement compared to SFRC beams. Also, average shear stress versus displacement responses indicated that longitudinal reinforcement changes the occurrence of shear failure before or after flexural yielding. For beams with longitudinal reinforcement ratio of 2%, flexural yielding occurred. However for a ratio of 2.7%, no yielding occurred.

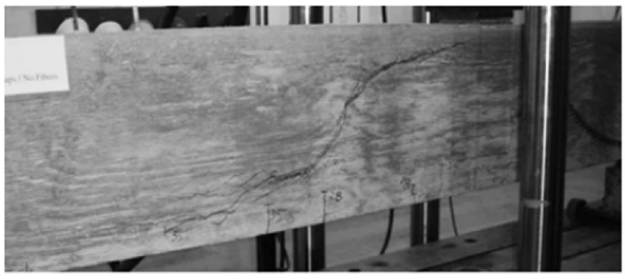

(a) Beam B18-0a (regular concrete and no stirrups)

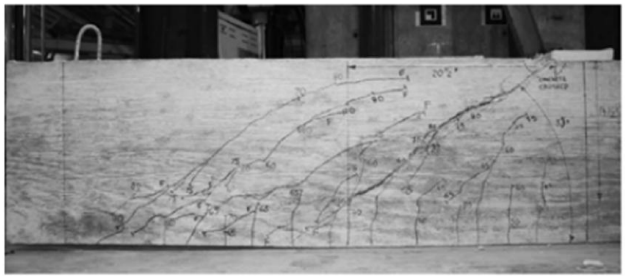

(b) Beam B18-1a (SFRC with 0.75% volume fraction of Type 1 fibers)

Figure 2.12. Cracking patterns for regular RC and SFRC
(Source: Dinh et al., 2010)

2.4. Shear Studs

Whether installed on existing slab-column connections as retrofit or applied internally as shear reinforcement, shear studs increase the punching shear capacity of reinforced concrete slabs. Shear studs, headed studs or headed bars are usually manufactured with smooth or deformed bars with forged or welded heads at both ends. Shear studs, placed perpendicular to the slab axis, can be used instead of conventional stirrup reinforcement. Shear studs are often preferred to conventional reinforcement since they are easy to install and their anchorage is better compared to conventional single legged stirrup. (Figure 2.13)

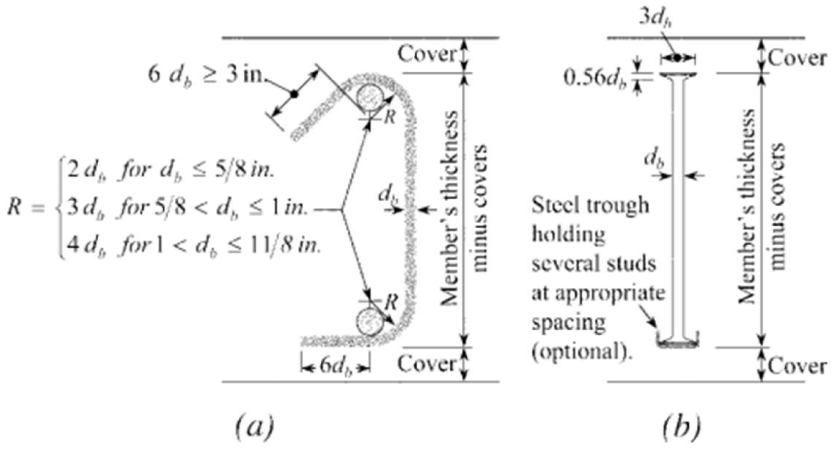

Figure 2.13. a) Conventional single-leg stirrup with hooks satisfying minimum requirements of ACI 318-05 and b) Stud with forged heads (Source: Ghali and Youkim, 2005)

In a study of El-Salakawy et al. (2002), four full scale slab-column connections were tested to failure with applied concentrated load and moment combinations. Each specimen was manufactured as a unique piece. One of the specimens had an opening in front of the column and shear reinforcement in addition to the longitudinal reinforcement. One specimen had an opening but no shear reinforcement. One specimen had neither an opening nor any shear reinforcement. Remaining specimen had shear reinforcement but no opening. As shear reinforcement, shear bolts were used.

Figure 2.14. Removing the damaged concrete
(Source: El-Salakawy et al., 2002)

As a result of loading, specimens with no shear reinforcement failed by punching whereas the others failed by flexure. As second phase of the program, all specimens were strengthened, except the one with shear reinforcement and no opening, and tested to failure again. Strengthening was done by replacing the damaged concrete with a new patch, three effective slab depths deep and installing shear bolts in the replaced zone (Figure 2.14). As a result of strengthening, specimens that failed by punching during the first phase, failed by flexure. Load capacities of these specimens were increased by 26 and 41 %.

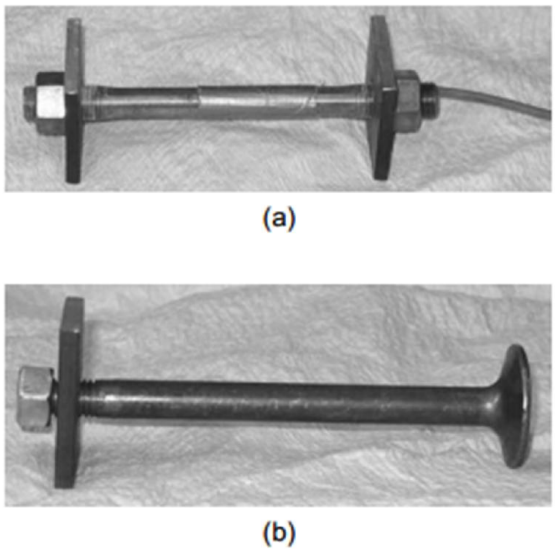

Figure 2.15. a) Steel rod and b) Shear bolt
(Source: El-Salakawy et al., 2002)

According to several studies (El-Salakawy et al., 2003; Adetifa and Polak, 2005; Bu and Polak, 2009), retrofitting using shear studs (shear bolts or shear rods, Figure 2.15) on existing slab – column connections, strengthens the connection and changes its failure mode from brittle to ductile. Shear studs can be inserted to drilled holes perpendicular to the surface of the slab all the way through slabs depth (Figure 2.16).

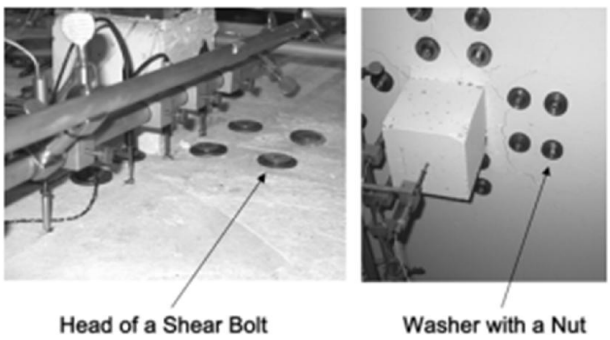

Figure 2.16. Shear bolt applied to a slab-column connection
(Source: Adetifa and Polak, 2005)

In studies involving shear studs, a number of different distributions of shear studs around the column were employed. Alongside that, control specimens and specimens with openings in front of the column were also tested to compare the results. Researchers have applied various loads and/or moments on the specimens in experiments. As for the results independent from the loading type, it was seen that applying shear studs increased the ductility of the connection. This change was proportional to rows of shear bolts used around the column. Also formation of shear cracks was prevented compared to control specimens.

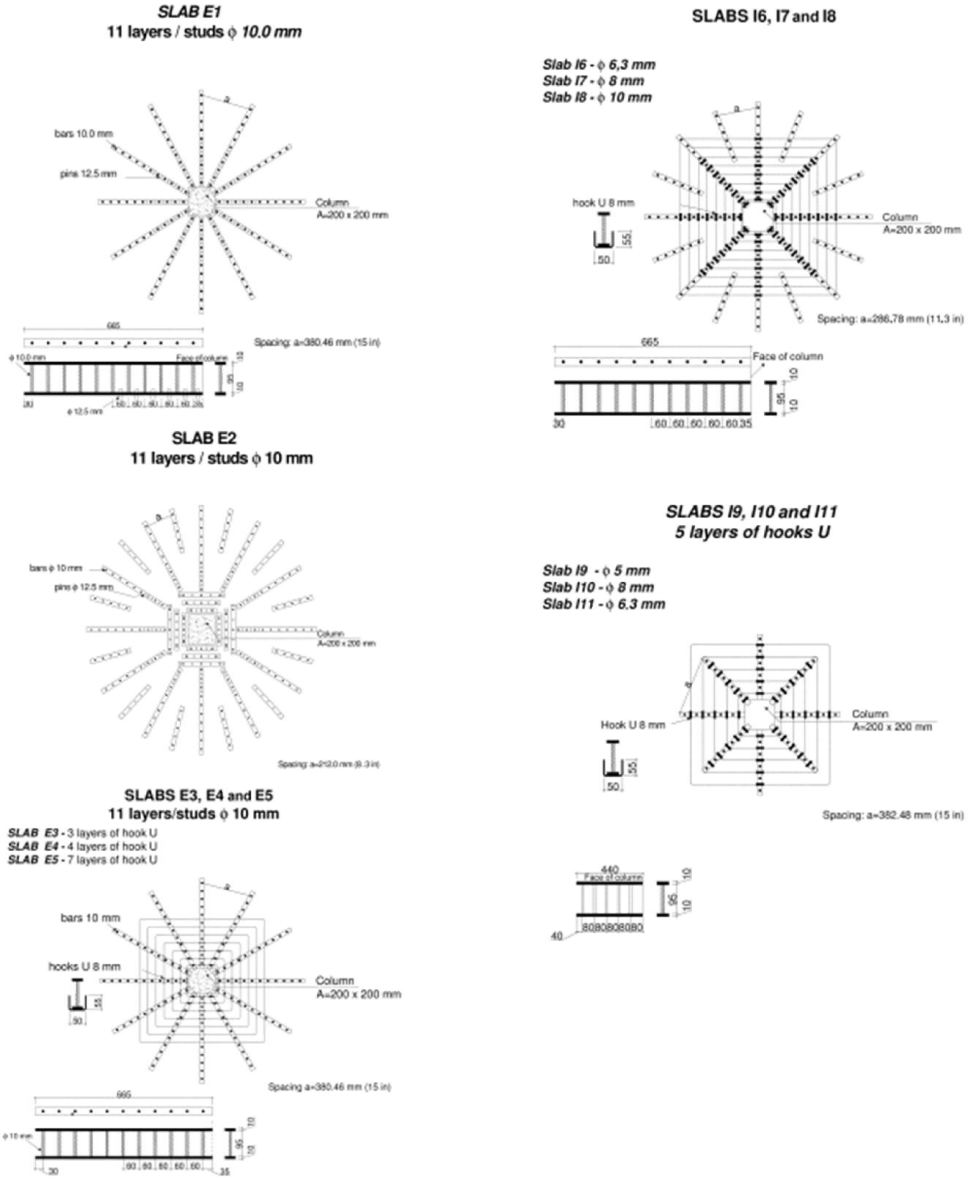

Figure 2.17. Shear reinforcement details for specimens of Trautwein et al (2011)

In a study of Trautwein et al. (2011), in order to find the punching strength of RC slabs with shear reinforcement that does not embrace flexural reinforcement, 11 slabs were tested under concentric load (Figure 2.17). Selected parameters were shear reinforcement type and distribution. Shear reinforcement in question forms from shear studs and studs with U hooks. These reinforcements were placed between the flexural reinforcement radially in various layers. Results of the study were comparable with similar studies that had embracing shear reinforcement. Punching strength of RC slabs with unbraced shear reinforcement was much higher than RC slabs without shear reinforcement.

CHAPTER 3

EXPERIMENTAL PROGRAM

In this study, four RC slabs strengthened with shear studs and four manufactured with steel fiber reinforced concrete (SFRC) were tested under static and impact loading. This chapter describes the experimental program in detail.

3.1. Test Specimens

There were eight slabs with 2150x2150x150 mm dimensions. Clear cover of the concrete was 25 mm. Slabs have been produced as four identical pairs. One of each pair was tested under static loading, while the other one was tested under impact loading. Other than loading rate, two other parameters were introduced to the study; reinforcement ratio and strengthening method for impact. For all slabs, 8 mm diameter reinforcement bars were used which had a cross-section area of 50 mm^2. Closed hoop shape has been formed by bending straight reinforcing bars in calculated points, making a closed hoop with a length of 2100 mm. These bars have been placed perpendicular to each other to form grids. In both principle directions, spacing has been taken as 150 mm for the two pairs and 200 mm for the other two pairs. Detailing of specimens is presented in Table 3.1. As for strengthening against impact loading, steel fibers and shear studs have been used on individual slabs.

Table 3.1. Detailing of specimens

Name of the Specimen	Longitudinal Reinforcement Layout and Ratio (for both principle directions)	Strengthening Method
YA150a / YA150b	ϕ8/150 - 0.30%	Shear Studs
YA150fa / YA150fb	ϕ8/150 - 0.30%	SFRC (1%in vol.)
YA200a / YA 200b	ϕ8/200 - 0.20%	Shear Studs
YA200fa / YA200fb	ϕ8/200 - 0.20%	SFRC (1%in vol.)
BB150a / BB150b (Batarlar,2013)	ϕ8/150 - 0.30%	-
BB200a / BB200b (Batarlar, 2013)	ϕ8/200 - 0.20%	-

Slabs have been named by the initials of the author, YA. After initials, reinforcement spacing has been written in millimeters. The letter 'f' in the names indicates the usage of steel fibers in the concrete. Also, the letter 'a' means static tested slab and 'b' impact tested slab. For example YA150fa indicates a slab with steel fibers in its concrete mixture, intended for static testing and spacing of reinforcement 150mm. If it was YA200b, then the name would represent a slab with 200 mm reinforcement spacing and with shear studs, intended for impact testing.

3.1.1. Slabs with Shear Studs

A shear stud consists of one rod with two T-section nuts (Figure 3.1) at both ends. Rods had a diameter of 6 mm and a length of 150 mm (Figure 3.2.). Distribution of shear studs can be seen in Figure 3.3. and Figure 3.4. These shear studs were attached to reinforcing bars in three rows. A total of 129 shear studs have been used for each slab. Shear studs had a 65 mm distance from each other, which was roughly half the effective depth.

For slabs YA200a and YA200b, two 2100 mm long bars were attached 200 mm away from each other, one on the left side and one on the right side of the middle bar. For slabs YA150a and YA150b, one 2100 mm long bar was placed in the middle. Again for the back sides of the slabs, this procedure was repeated. These additional bars were used while attaching the studs to the center axes. Three rows of shear studs have been attached on slabs both on horizontal and vertical direction, making a plus sign.

Figure 3.1. T-section nuts

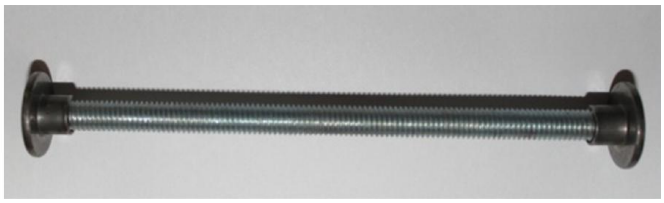

Figure 3.2. Example of a single shear stud

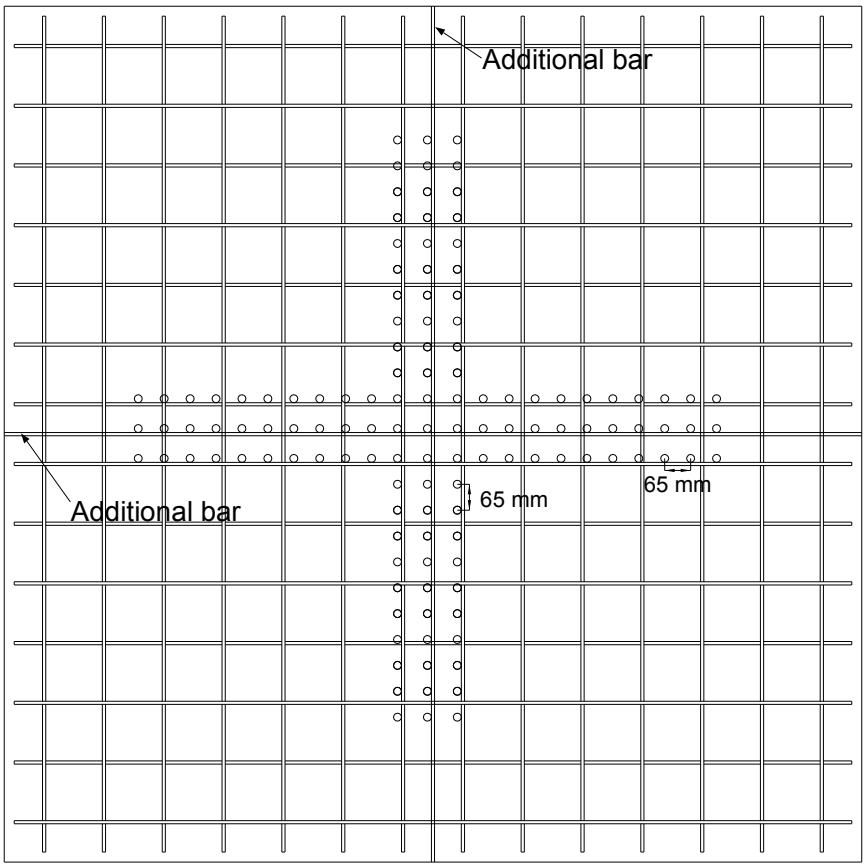

Figure 3.3. Shear stud and strain gauge distribution for specimens YA150a and YA150b

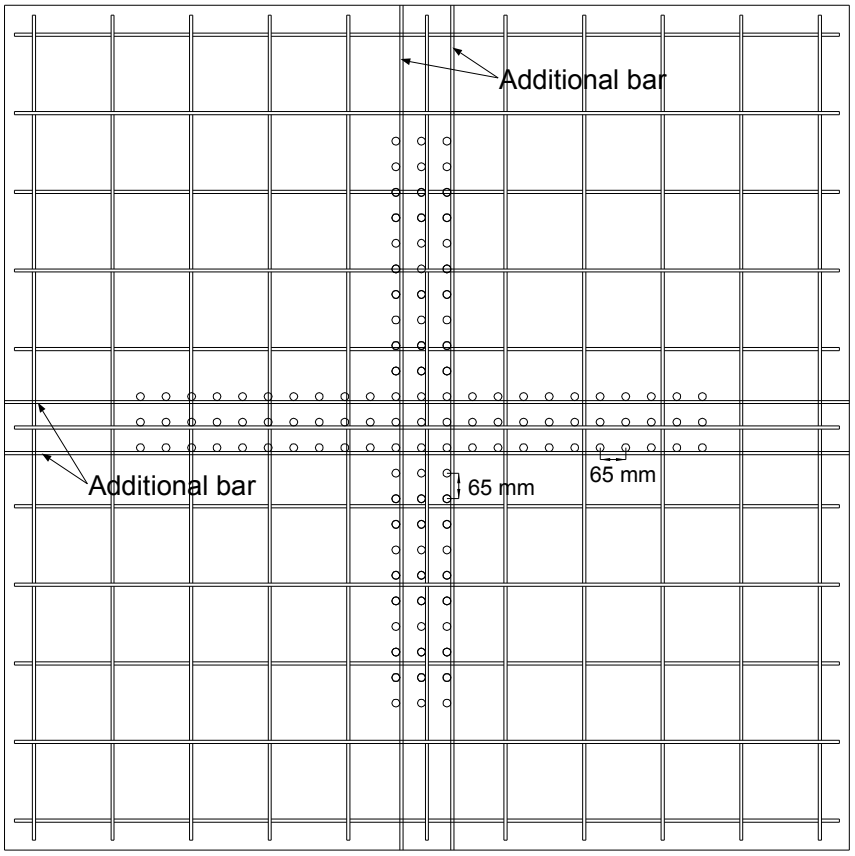

Figure 3.4. Shear stud and strain gauge distribution for specimens YA200a and YA200b

3.1.2. Slabs with Steel Fibers

Steel fibers had a length of 60 mm and diameter of 0.75 mm, with a length/diameter ratio of 80 (Figure 3.5). To reach 1 % volume fraction, 80 kg of steel fibers were mixed in concrete mixer for each cubic meters of fresh concrete. General view of steel fibers is in Figure 3.6. Tensile strength of fibers on the wire was minimum 1050 N/mm^2 and it conforms to EN 10016-2 – C9D, low carbon steel. Other characteristics of the fibers are in Appendix.

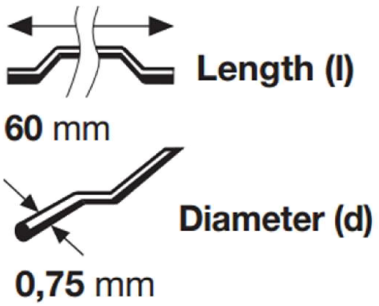

Figure 3.5. Geometric details of steel fibers

Figure 3.6. Steel fibers

3.2. Material Properties

Concrete have been ordered from a local company as one batch. Specimens with shear studs have been cast first. Then, steel fibers were added into the mixer to reach 1% volume fraction. Cylinder concrete specimens were cast during slab specimen casting for both type of concrete. Seven standard cylinder concrete specimens were

cured for 28 days. Four plain and three SFRC were tested under compression and average 27.1 MPa and 29.9 MPa values were found, respectively.

Reinforcement bars were 8 mm in diameter and they had a yield strength of 420 MPa which confirms with B420C standards. Steel rods used to make shear studs were made of cold-drawn steel and their average calculated yield strength was 586.6 MPa. Manufactured shear studs were also tested to confirm that the failure was due to the breaking of the rod, not the slippage of the nut at both ends. Tests confirmed this and studs failed under tension from the rods before the slippage of nuts (Figure 3.7).

Figure 3.7. Testing shear studs

3.3. Test Setup

A test setup was manufactured at the İzmir Institute of Technology as a part of a previous work by Batarlar (2013). In this test setup, both static and impact tests can be done with few alterations. It consists of eight footings, four on corners and four at the mid of the edges, fixed to the strong floor (Figure 3.8). Each two corner footings and the one footing between them were connected to each other by a circular shaft. Load-cells were hinged on these circular shafts in a manner allowing free rotation of the edges. But vertical movement was prevented.

Figure 3.8. Test Setup

3.4. Instrumentation

Numerous instrumentations have been used on the specimens. Following sections give a summary of each measuring instrument used for both static and impact testing.

3.4.1. Load Cells

Three kinds of load cells have been used. Eight load cells had 5000 kg capacity, type S model TB (Figure 3.9.b). Twelve load cells have 10000 kg capacity, type S model SC (Figure 3.9.a). One other load cell was placed on the top of the hydraulic jack and had a capacity of 50 tons (Figure 3.10). The manufacturer of all load cells was ESİT Electronics Production and Trade Co.

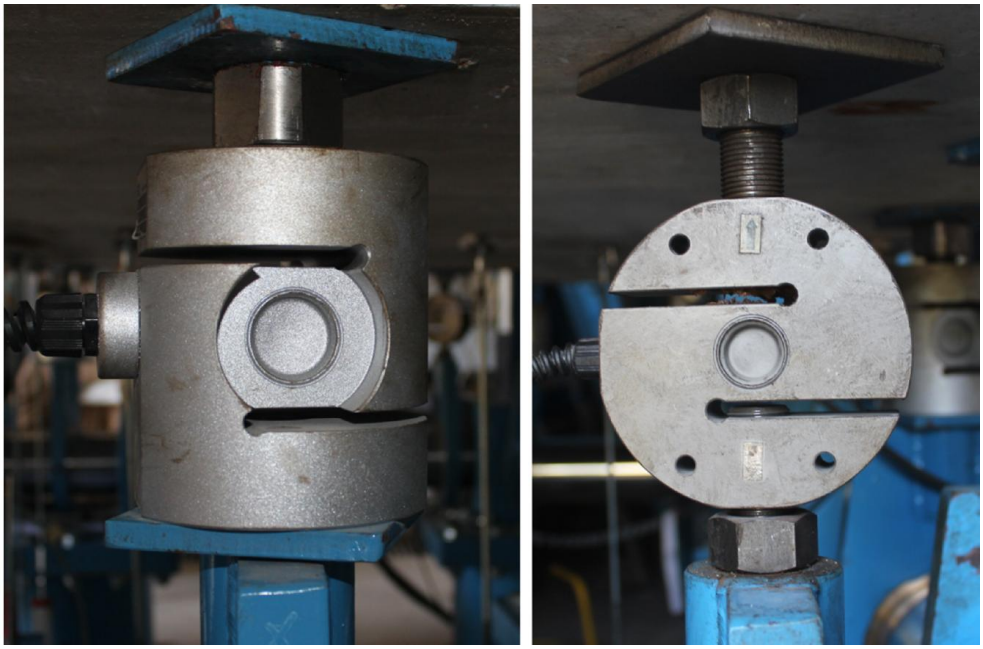

a) b)

Figure 3.9. a) 10000 kg and b) 5000 kg capacity load cells

Figure 3.10. Hydraulic piston with 50 ton capacity load cell on top

There were five load-cells on every edge, 400 mm apart. To attach the load-cells to the slab, thick steel rods with 24 mm diameters have been used. These rods had screw

threads on both ends. One end of the rod went down into the threaded holes in the load cell and the other end went up through the slabs and tightened with a nut. This method also limited vertical movement on the slab edges. To prevent sliding of the nut from the rod, steel plates have been used on both sides of the slab.

3.4.2. Strain Gauges

To measure the strain of reinforcement bars and shear studs, strain gages were used. Type FLA-5-11 strain gauges from Tokyo Sokki Kenkyujo Co. Ltd. had a gauge length of 5 mm. There were ten strain gages on shear stud rods. Also, six strain gages have been placed on reinforcing bars, three on top and three on bottom of the slab. Strain gages on shear studs have been named S1, S2, S3 etc. beginning from the edge. Others on reinforcements have been named as T1, T2, T3 and B1, B2, B3, top and bottom respectively. (Figure 3.11. and Figure 3.12)

Strain gauges were not inserted on slabs with steel fibers because of probable damage. The locations of strain gauges on bars were thoroughly grinded to make a flat and smooth surface. After cleaning grinding residues, glue from the same company was used to attach the strain gauge. Later on, gauges were covered with a thick layer of varnish, paraffin wax and insulation tape. (Figure 3.14. and Figure 3.15.)

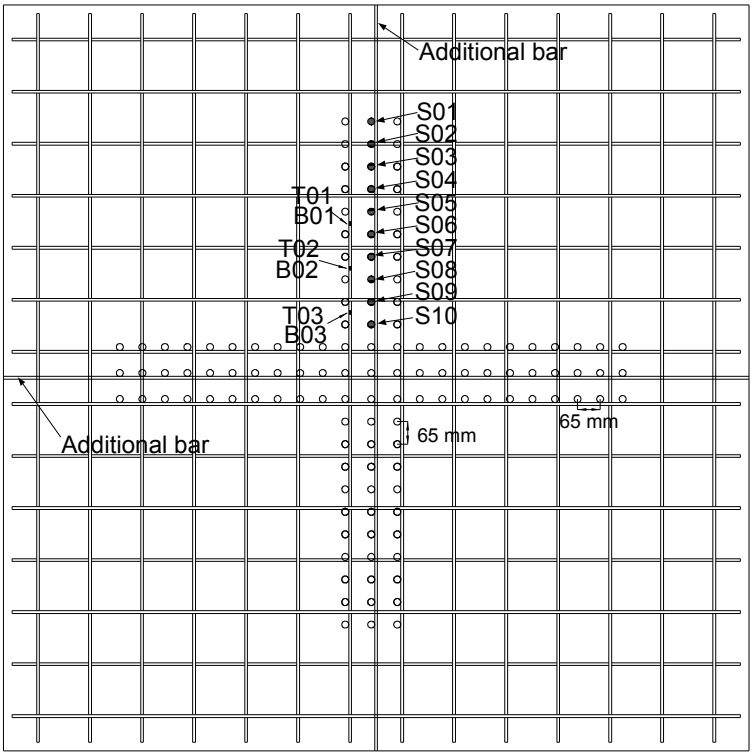

Figure 3.11. Strain gauge distribution for specimens YA150a and YA150b

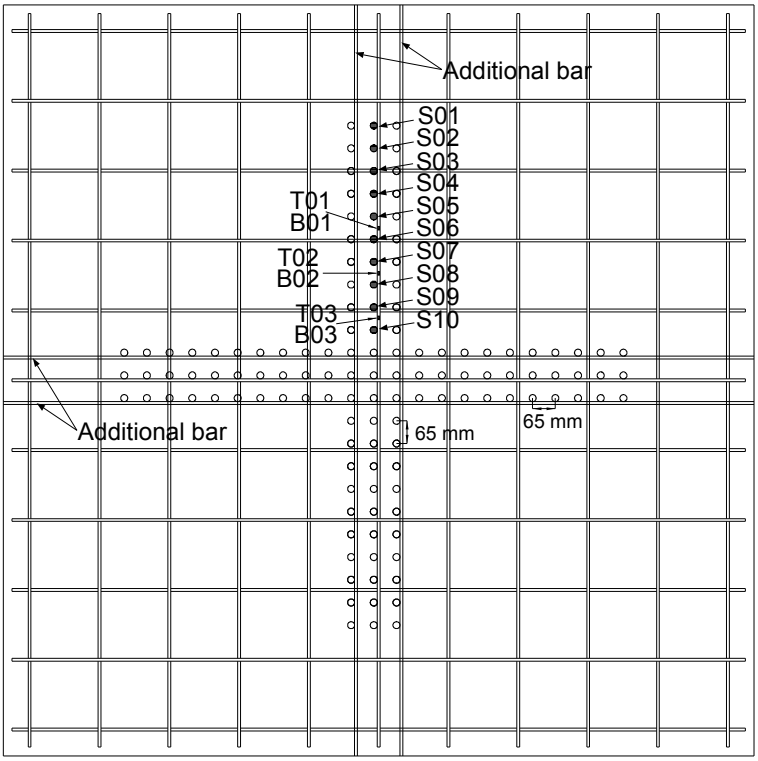

Figure 3.12. Strain gauge distribution for specimens YA200a and YA200b

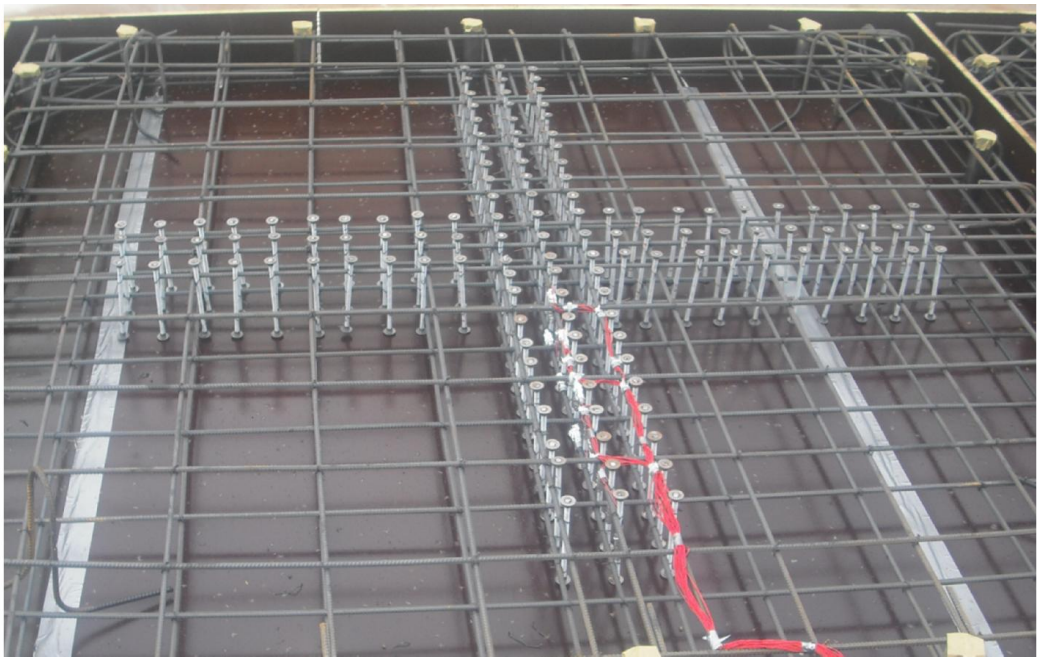

Figure 3.13. Specimen YA200a/b before casting

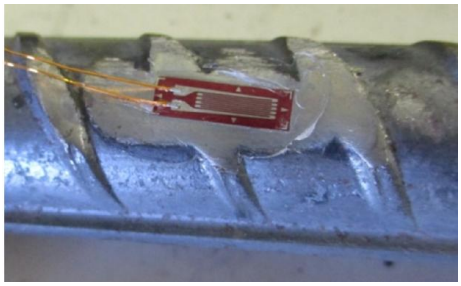

Figure 3.14. Strain gauges on reinforcement (before coating with varnish)

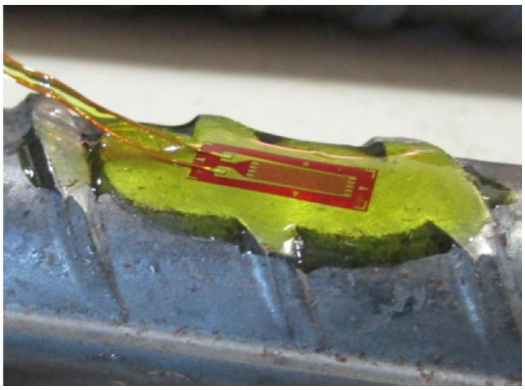

Figure 3.15. Strain gauges on reinforcement after a thick coat of varnish

3.4.3. Resistive Linear Position Transducers (RLPT's)

To record the displacement of the slab during testing, resistive linear position transducers (RLPT) have been used (Figure 3.16). A total of 24 RLPT's were used for each testing (Figure 3.17). A steel base was assembled for each transducer which could ensure vertical movement when needed. The distance between the bottom of the slab and the tip of the transducer was connected by long extension rods. At the end of the extension rod, a pivot head was put to ensure a large angle of movement. This head was fastened to the bottom of the slab via a U-profile, as seen on Figure 3.18. For static tests, U-profiles were screwed to the surface using fixing plugs. As for impact tests, chemical anchor was used for a better hold. Nevertheless, on the moment of impact, some data was lost due to sliding of pivot head.

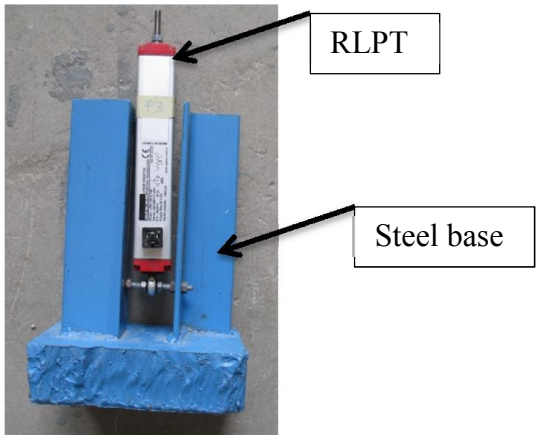

Figure 3.16. General view of RLPT

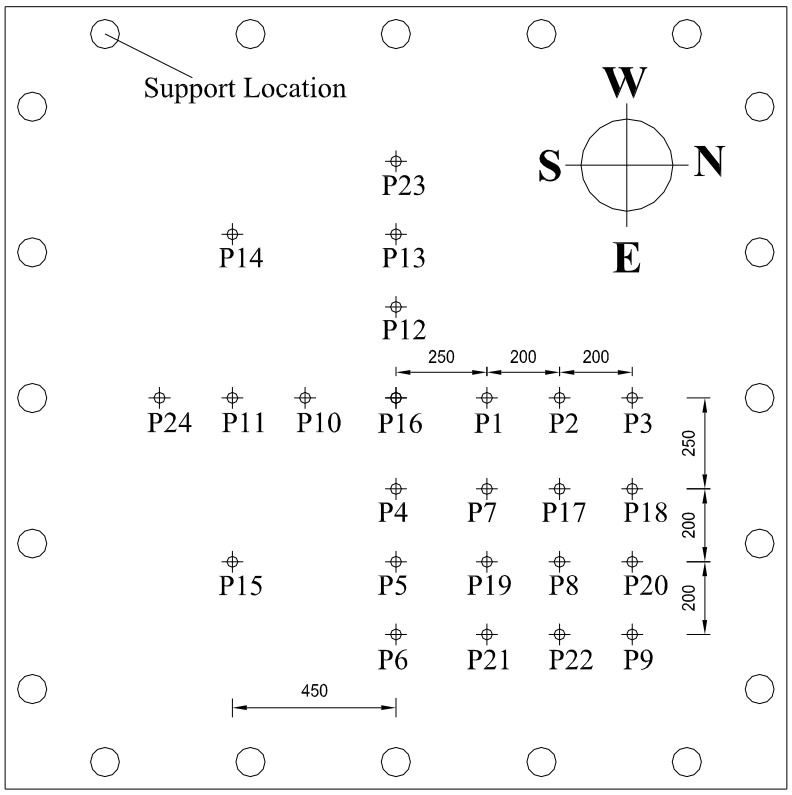

(Numbers indicate crack widths in millimeters)

Figure 3.17. Positions of RLPT's under the specimen

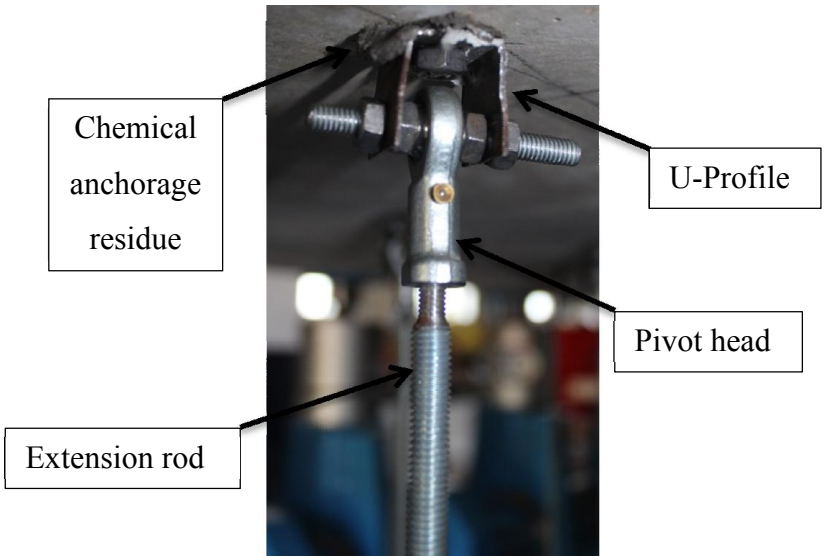

Figure 3.18. Connection of the pivot head to the specimen before impact testing

3.4.4. Accelerometers

Two ± 50000g range, 8742A50 type accelerometers from Kistler Group were mounted on the drop weight. Fourteen accelerometers were mounted on the slab (Figure 3.19.). Four of them had a range of ± 5000g and 8742A5 type from the same manufacturer (Figure 3.20a). The other ten accelerometers were model 350B04 from PCB Piezotronics with a range of ± 5000g (Figure 3.20b).

To reduce the unwanted high frequency vibrations (or the noise), accelerometers were screwed on delrin pieces. These cylinders were attached to the slab with chemical anchor to keep stability. (Figure 3.20.)

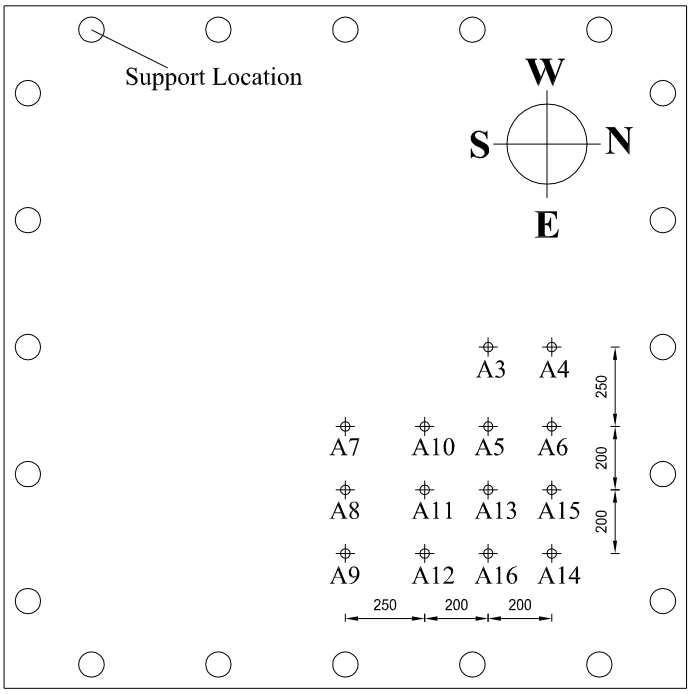

(Numbers indicate crack widths in millimeters)

Figure 3.19. Distribution of accelerometers that are placed on the specimen

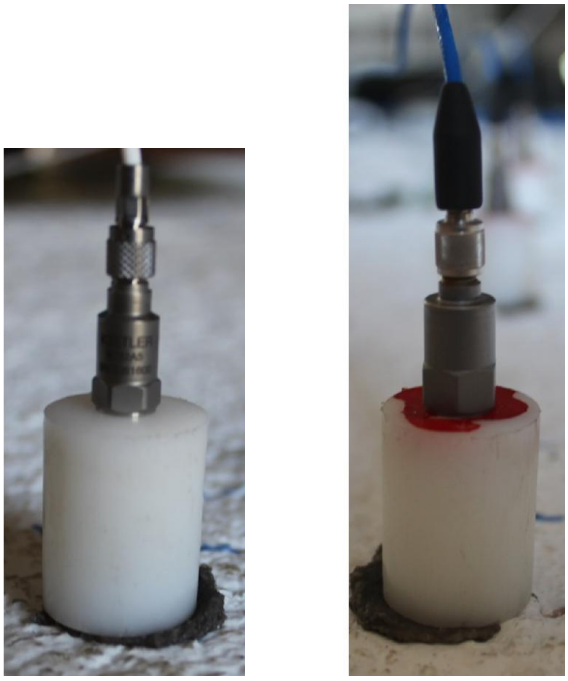

a) b)

Figure 3.20. Two kinds of accelerometers that are used on the surface of the specimen; a) Kistler Group accelerometers, b) PCB Piezotronics accelerometers

3.4.5. Drop Weight

Drop weight was manufactured in İYTE structural lab. A steel bucket with a 200 mm diameter circular bottom surface was filled with steel plates and concrete. Thick steel plates were welded on two sides of this bucket, increasing the weight to 320 kg. (Figure 3.21a)

To cause reasonable damage to the specimen YA200fb, the drop weight has been altered and made in a way that its weight is adjustable. (Figure 3.21b)

a) b)

Figure 3.21. a) Former Drop Weight (320 kg), b) Current Drop Weight (555 kg)

3.4.6. Data Acquisition System

A high speed data acquisition system was employed (Figure 3.22.). National Instruments NI PXI-6143 S series multifunction data acquisition modules with 250 kS/s per channel sampling rate, NI SCXI-1520 8 channel universal strain gauge input modules, NI SCXI-1531 signal conditioning modules and NI SCB-68 shielded I/O connector blocks were used to record data from load cells, strain gauges, accelerometers and RLPT's. As software, Lab VIEW Academic Standard Suite program was used.

Figure 3.22. General view of DAQ

3.4.7. High Speed Camera

A high speed camera was installed to monitor the free fall of the drop weight and to calculate the impact velocity. MotionBLITZ high speed camera system was used (Figure 3.23) manufactured by Mikrotron GmbH. The camera was used at frame rates from 800 fps to 1262 fps.

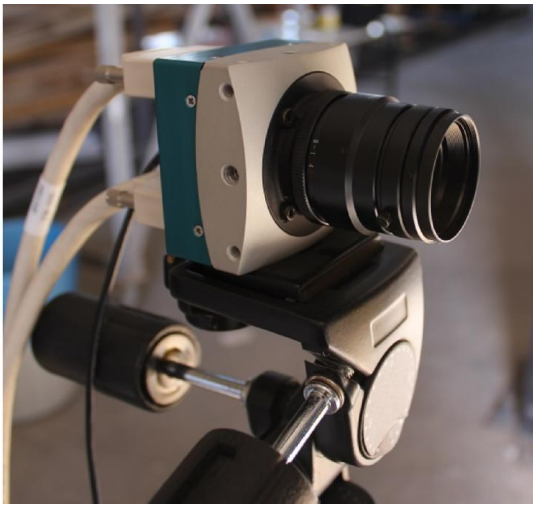

Figure 3.23. Mikroton EoSens high speed camera

3.5. Loading Procedure

3.5.1. Static Testing

Static testing was done by a hydraulic jack installed at the center of the slab, loading upwards. Testing process was paused two to four times, in order to monitor and record crack development. During pauses, widths of the cracks in major points were measured in milimeters and the values were photographed. Crack distributions were hand drawn using the photographs of the specimens.

3.5.1.1. YA150a (05.02.2014)

Loading capacity of specimen YA150a reached 250 kN with a midpoint displacement of 109 mm before tests were stopped due to the limits of test setup. The specimen exhibited a flexural behavior. Crack distribution of this specimen can be seen in Figure 3.26. Also, cracks were observed on the loading face of the specimen (Figure 3.24b and Figure 3.25).

a) b)

Figure 3.24. a) Front face of specimen YA150a after testing, b) Overall look of the loading face of specimen YA150a after testing

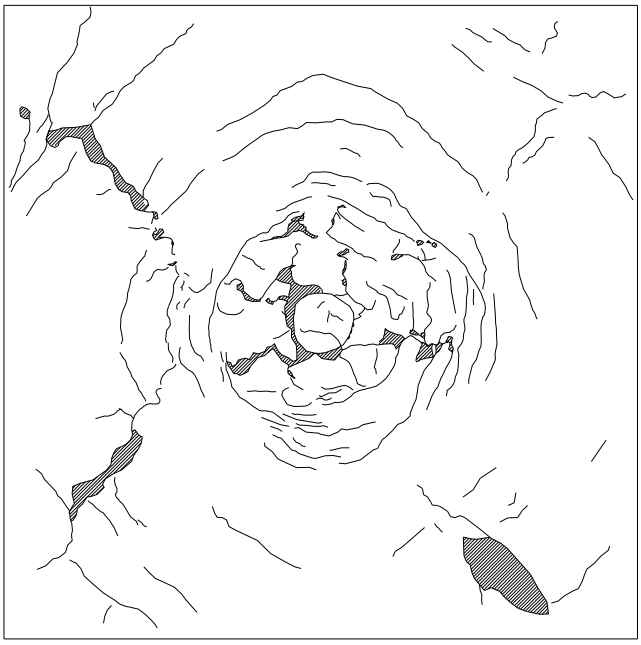

Figure 3.25. Crack profile of the loading face of specimen YA150a after testing

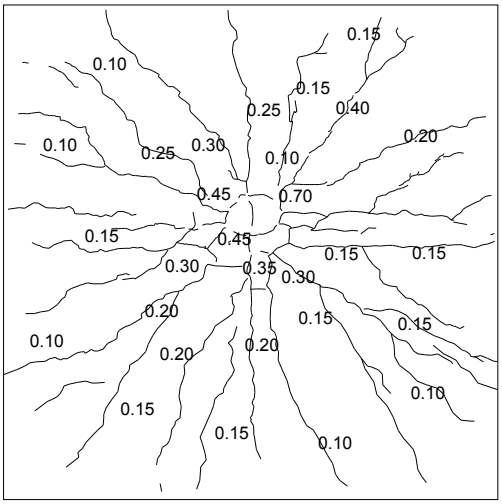

a) P= 141 kN , Δ = 6 mm

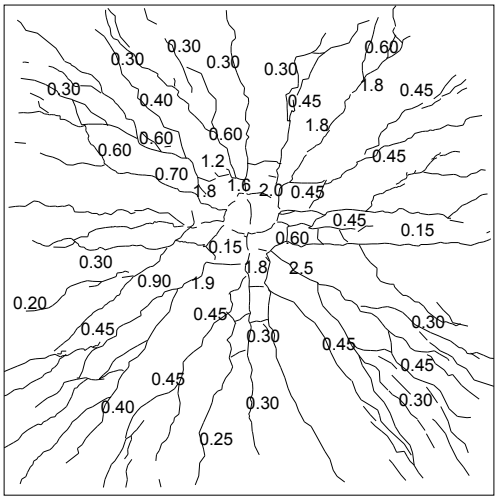

b) P= 205 kN , Δ = 21 mm

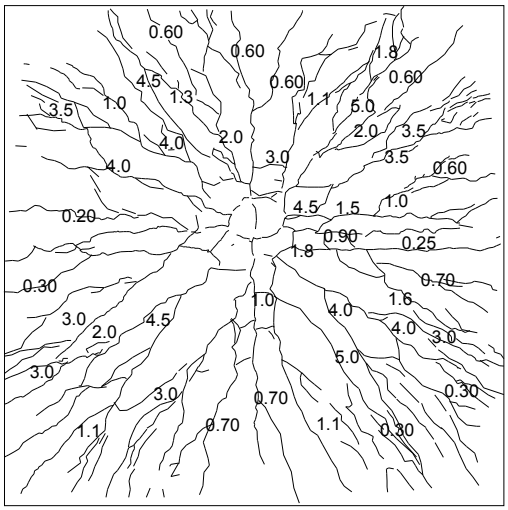

c) P= 250 kN , Δ = 109 mm (after yielding)

(Numbers indicate crack widths in millimeters)

Figure 3.26. Crack profile of the front face of specimen YA150a

3.5.1.2. YA150fa (27.07.2013)

YA150fa reached a midpoint displacement of 54 mm before failing with a load of 309 kN. Specimen's peak load was 325 kN with a midpoint displacement of 42 mm. General view of the specimen is in Figure 3.27. Crack distribution is in Figure 3.28.

a) b)

Figure 3.27. a) Front face of specimen YA150fa after testing, b) Overall look of the loading face of specimen YA150fa after testing

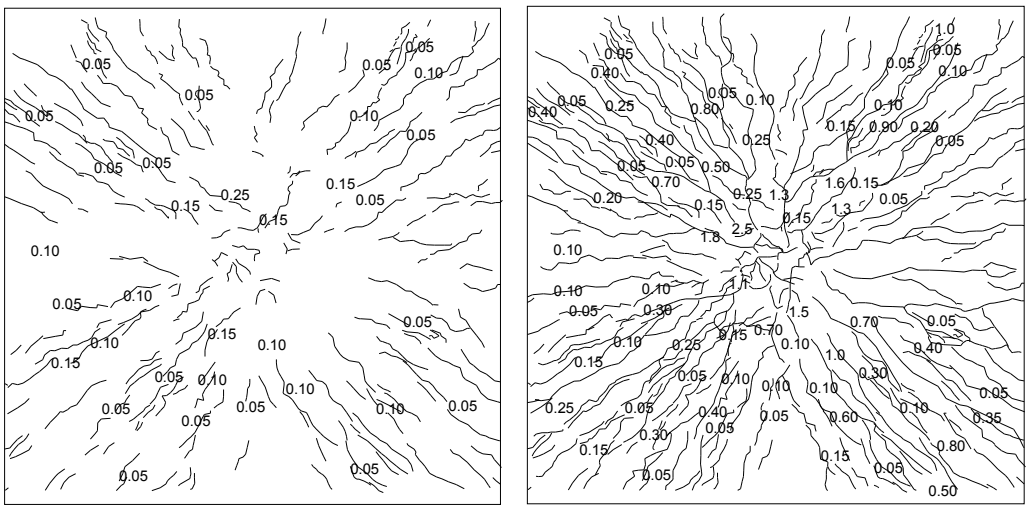

a) P=196 kN , Δ = 8 mm b) P=307 kN , Δ = 33 mm

(Before yielding)

(Numbers indicate crack widths in millimeters)

Figure 3.28. Crack profile of the front face of specimen YA150fa

3.5.1.3. YA200a (16.01.2014)

Specimen YA200a reached a midpoint displacement of 118 mm and a load capacity of 241 kN. Test was not continued until the failure of the specimen due to the

limits of test setup. Crack profiles on the front and the loading face are presented in Figure 3.29a and b. Crack distribution can be seen in Figure 3.30 and Figure 3.31.

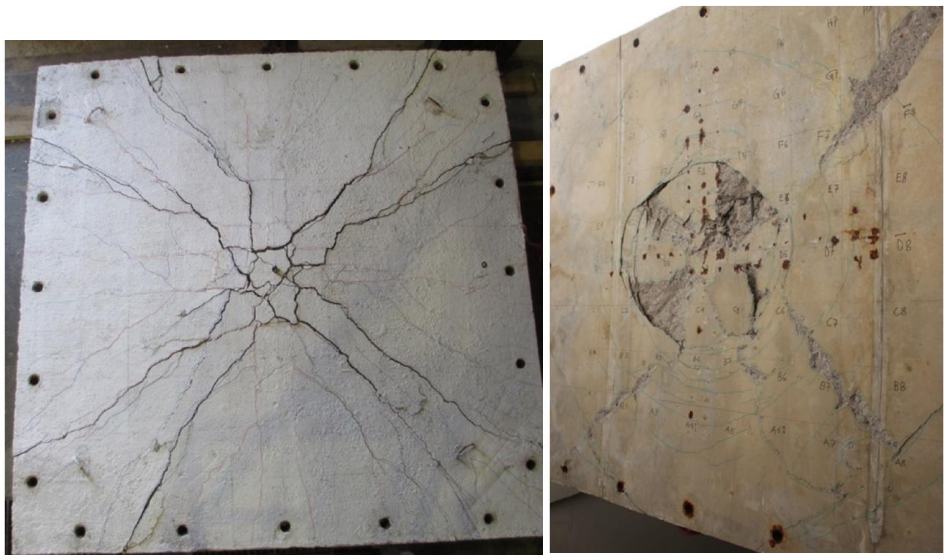

a) b)

Figure 3.29. a) Top side of specimen YA200a after testing, b) Overall look of the bottom side of specimen YA200a after testing

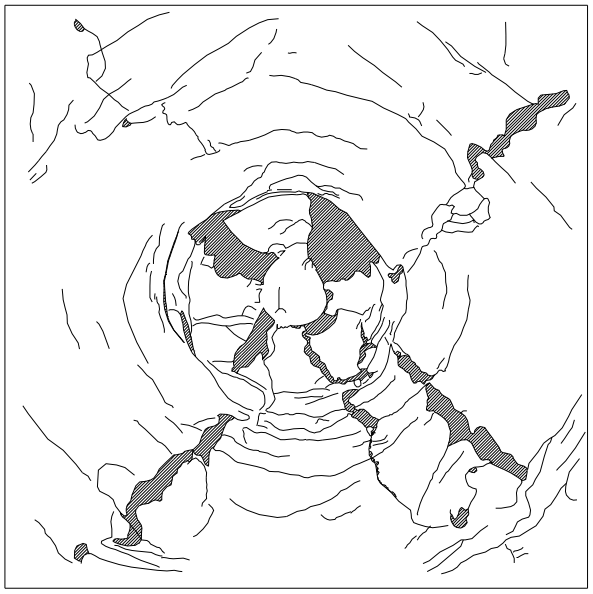

Figure 3.30. Crack profile of the loading face of specimen YA200a

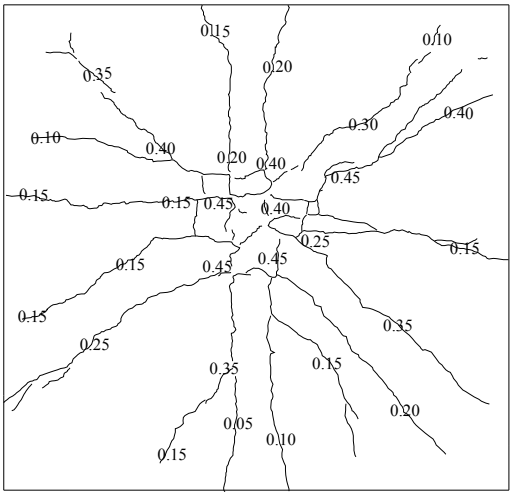

a) P= 150 kN , Δ = 6 mm

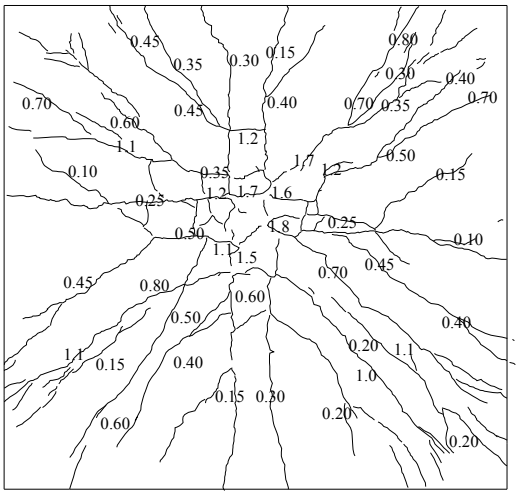

b) P= 197 kN , Δ = 19 mm

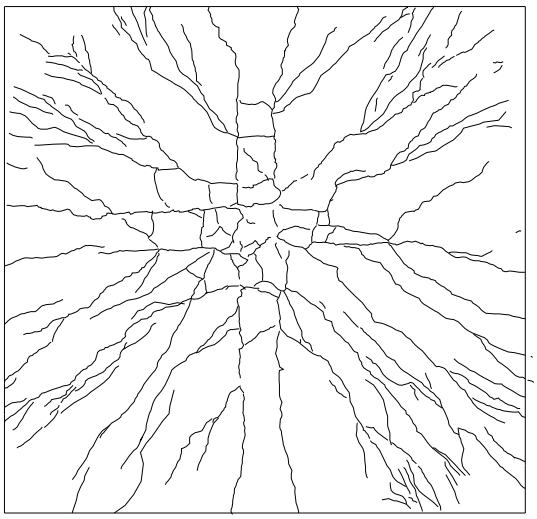

c) P= 241 kN , Δ = 119 mm (After yielding)

(Numbers indicate crack widths in millimeters)

Figure 3.31. Crack profile of the front face of specimen YA200a

3.5.1.4. YA200fa (01.08.2013)

Specimen YA200fa reached 320 kN load carrying capacity and a midpoint displacement of 55 mm before failing. Crack distribution of the specimen is in Figure 3.32 and Figure 3.33.

a) b)

Figure 3.32. a) Front face of specimen YA200fa after testing, b) Loading face of the specimen YA200fa after testing

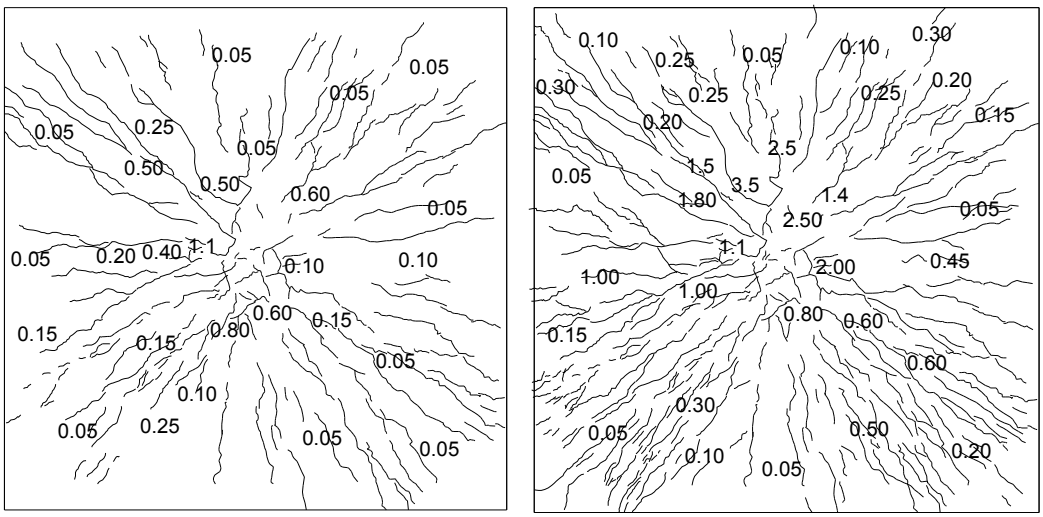

a) P= 254 kN , Δ = 13 mm b) P= 298 kN , Δ = 25 mm

(Before yielding)

Figure 3.33. Crack profile of the front face of specimen YA200fa

(cont. on next page)

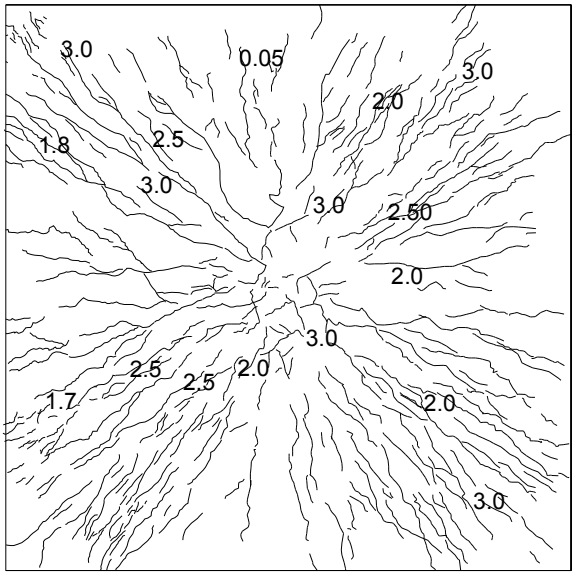

c) P= 125 kN , Δ = 68 mm (After failure)

(Numbers indicate crack widths in millimeters)

Figure 3.33. (cont.)

3.5.1.5. BB150a (Control specimen, Batarlar, 2013)

Testing of control specimen BB150a was stopped five times in order to monitor the crack distribution. Specimen failed by punching which can be seen from Figure 3.34e.

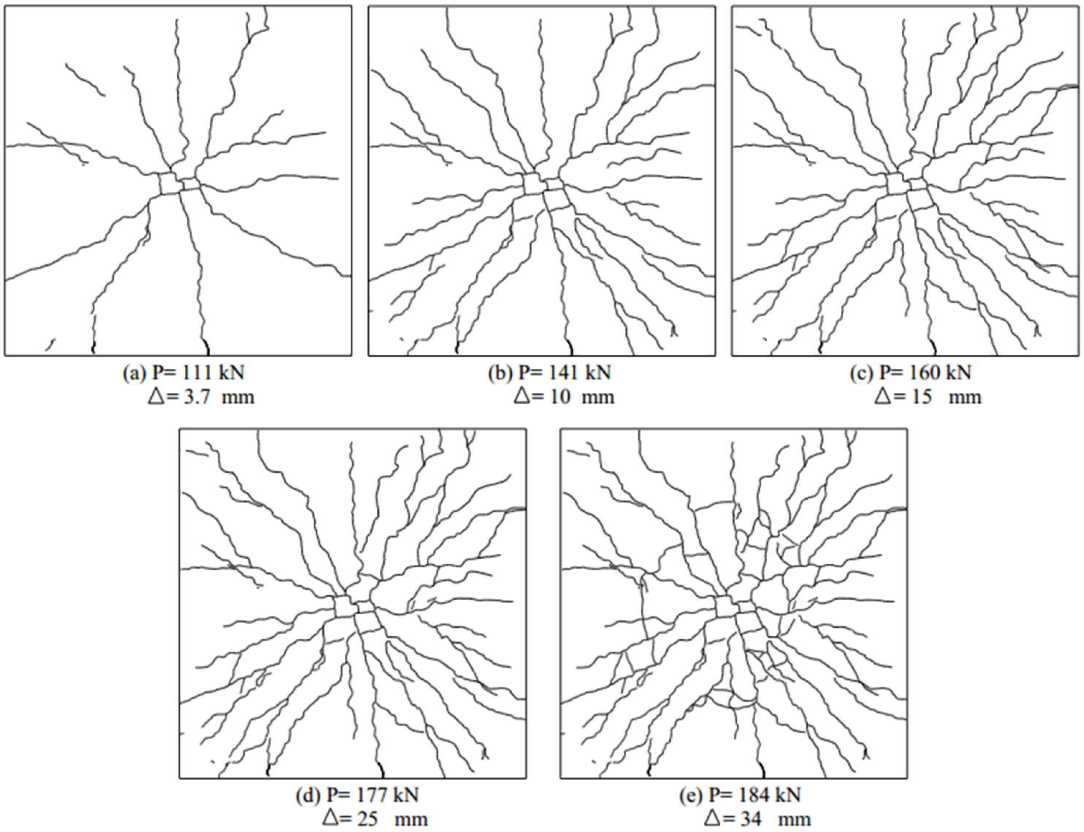

Figure 3.34. Cracks distribution of control specimen BB150a
(Source: Batarlar, 2013)

3.5.1.6. BB200a (Control specimen, Batarlar, 2013)

Crack distribution of control specimen BB200a was recorded five times. Sudden punching failure was observed. (Figure 3.35)

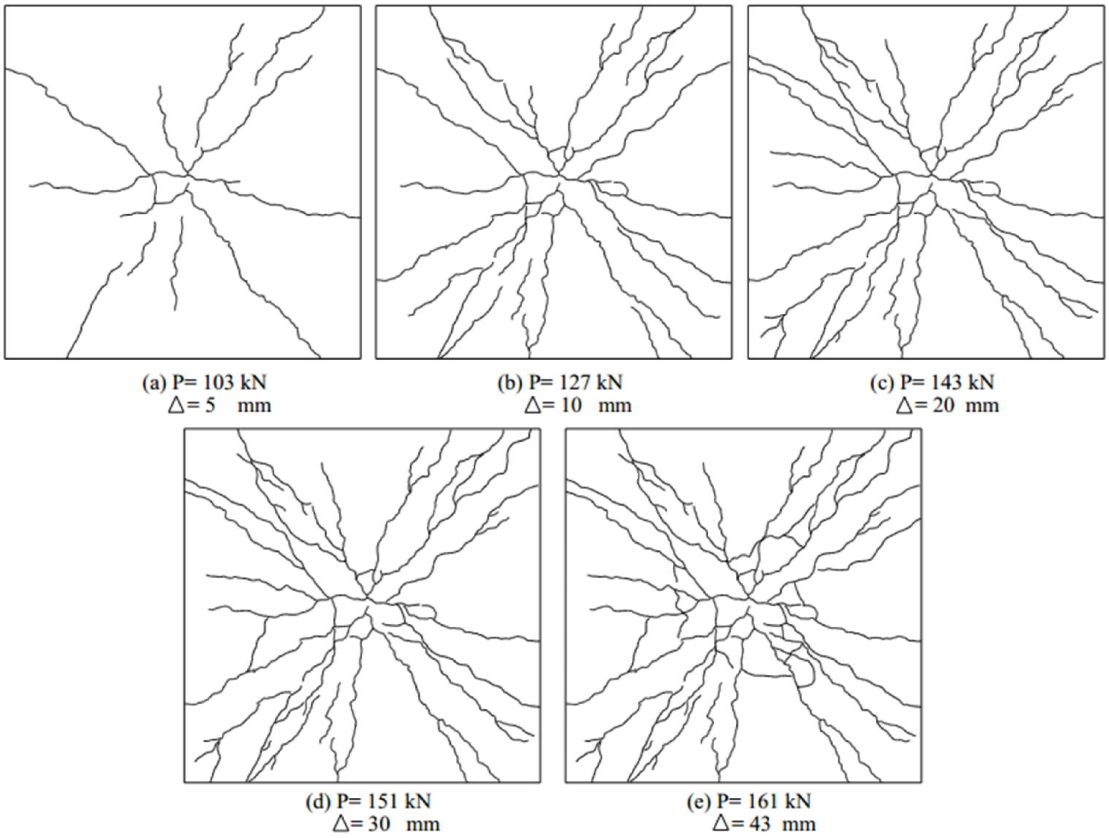

Figure 3.35. Cracks distribution of control specimen BB200a
(Source: Batarlar, 2013)

3.5.2. Impact Testing

For impact testing, the hydraulic mechanism was removed from underneath the specimen. A drop tower established from four rails was mounted on the top of the test setup (Figure 3.8.). Specimens were impacted several times. Individual tests are referred as the drop number following the specimen name. Drop height was kept constant at 2.5 m for all impact tests except tests YA200fb-2, YA200fb-3 and YA200fb-4, which the drop height was 2.44 m. Sixteen accelerometers have been placed on slab and on the drop-weight. After every drop, the cracks underneath and the crack on top of the slab were marked and photographed. Major cracks were measured in milimeters and documented. Crack distributions were hand drawn using the photographs of the specimens.

3.5.2.1. YA150b (Test Dates: 28.03.2014 – 31.03.2014 - 03.04.2014)

320 kg drop weight was dropped from 2.5 m three times. The last one caused scabbing on the bottom of the specimen (Figure 3.36.). Additionally, cracks formed on the impact surface in a circular manner, as can be seen in Figure 3.37. Crack distributions are in Figure 3.38 and Figure 3.39.

a) b)

Figure 3.36. a) Closer and b) general look of the back face of the specimen YA150b after testing

Figure 3.37. Impacted face of the specimen YA150b after tests

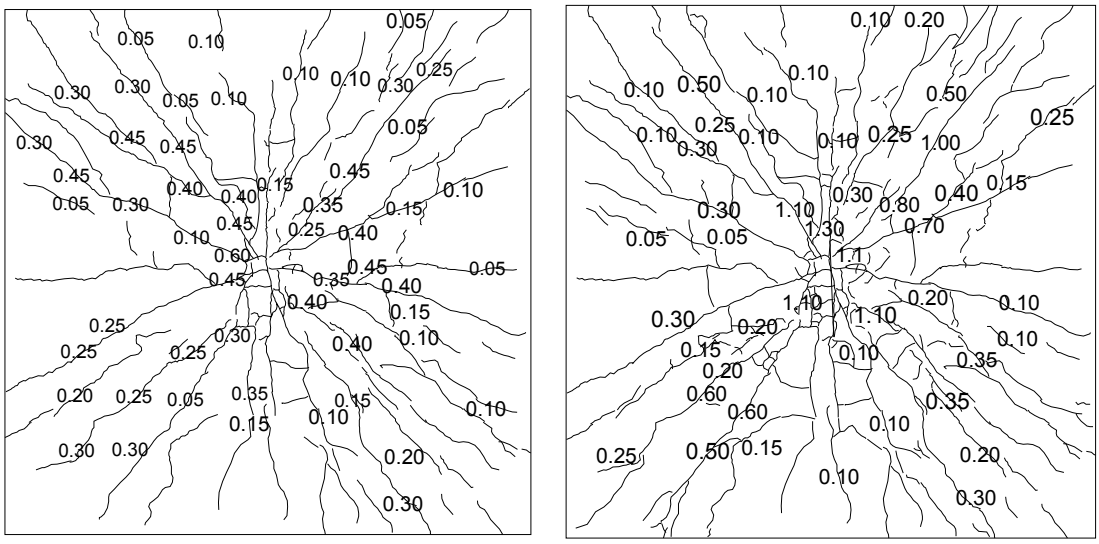

a) YA150b-1 b) YA150b-2

c) YA150b-3

(Numbers indicate crack widths in millimeters)

Figure 3.38. Impact crack profiles on the back face of the specimen YA150b

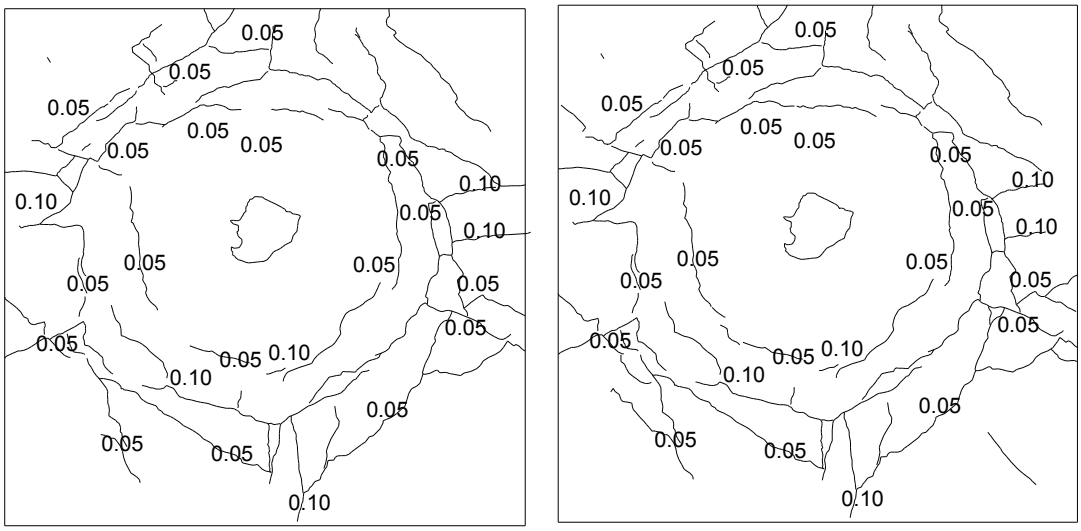

a) YA 150b-2 b) YA150b-3

(Numbers indicate crack widths in millimeters)

Figure 3.39. Crack profiles on the impacted face of the specimen YA150b

3.5.2.2. YA150fb (Test Dates: 10.03.2014 – 12.03.2014(twice) – 13.03.2014(twice))

Specimen YA150fb endured five impact loadings from 2.5 m with the 320 kg drop weight. Almost no scabbing occurred (Figure 3.40). No cracks formed on the impacted surface of the specimen (Figure 3.41.). Crack distribution of specimen is in Figure 3.42.

a) b)

Figure 3.40. a) Formation of punching cone and b) General view of the back face of the specimen YA150fb after testing

Figure 3.41. Impacted face of the specimen YA150fb after testing

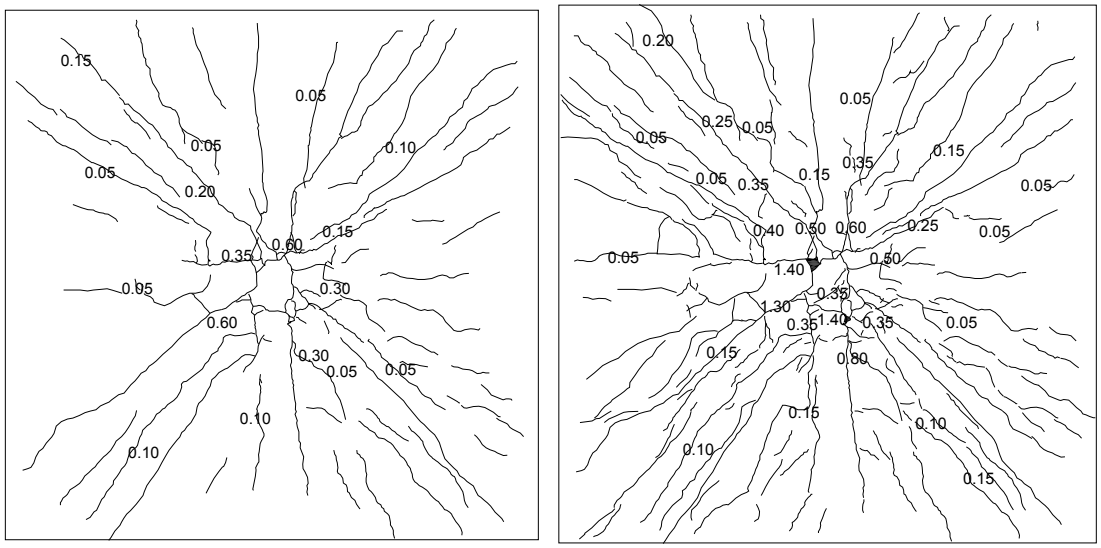

a) YA150fb-1 b) YA150fb-2

Figure 3.42. Impact crack profiles on the back face of the specimen YA150fb

(cont. on next page)

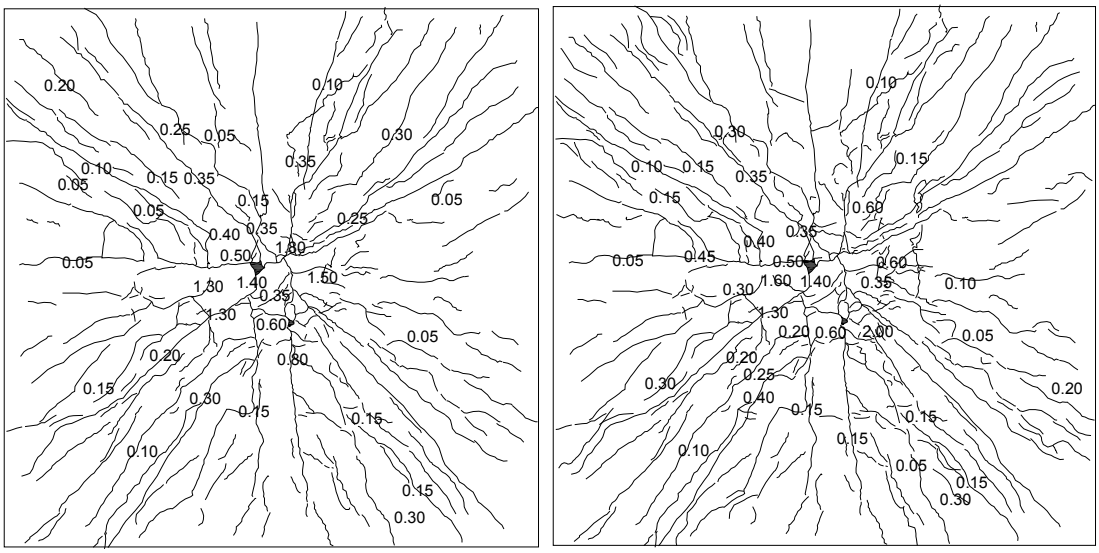

c) YA150fb-3 d) YA150fb-5

(Numbers indicate crack widths in millimeters)

Figure 3.42. (cont.)

3.5.2.3. YA200b (Test Dates: 21.04.2014 – 24.04.2014)

Specimen YA200b was subjected to impact loading twice with a drop weight of 320 kg, from 2.5 m. Scabbing occurred as can be seen in Figure 3.43. Circular cracks formed on the impacted surface of the specimen.

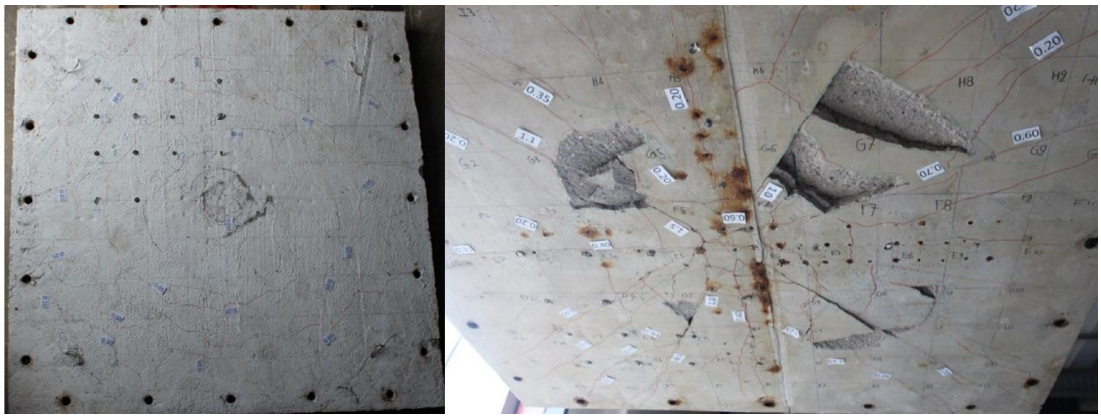

a) b)

Figure 3.43. a) Impacted face of the specimen YA200b after the tests, b) Back of the specimen YA200b after tests

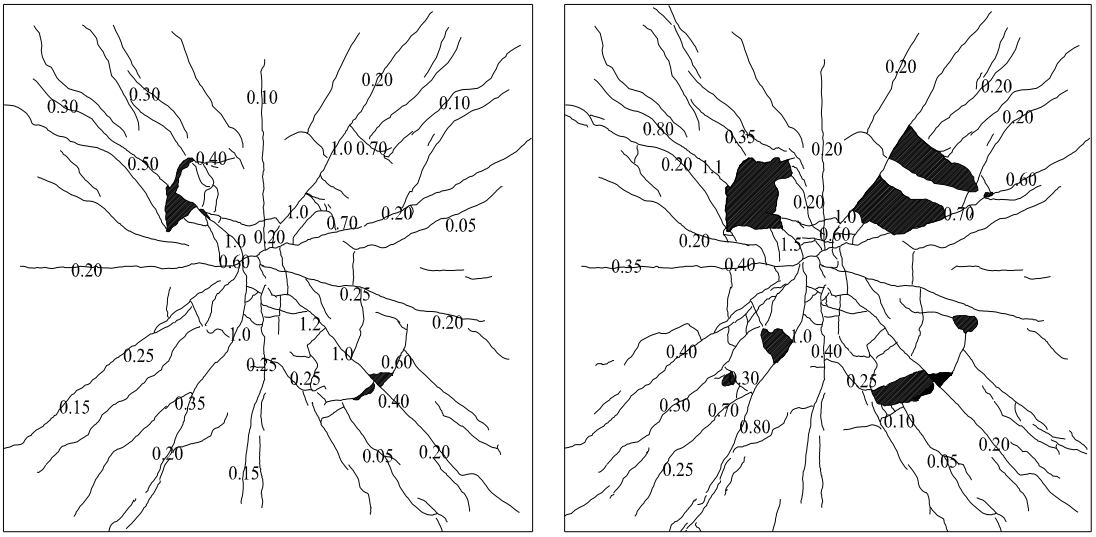

a) YA200b-1 b) YA200b-2

(Numbers indicate crack widths in millimeters)

Figure 3.44. Impact crack profiles on the back face of the specimen YA200b

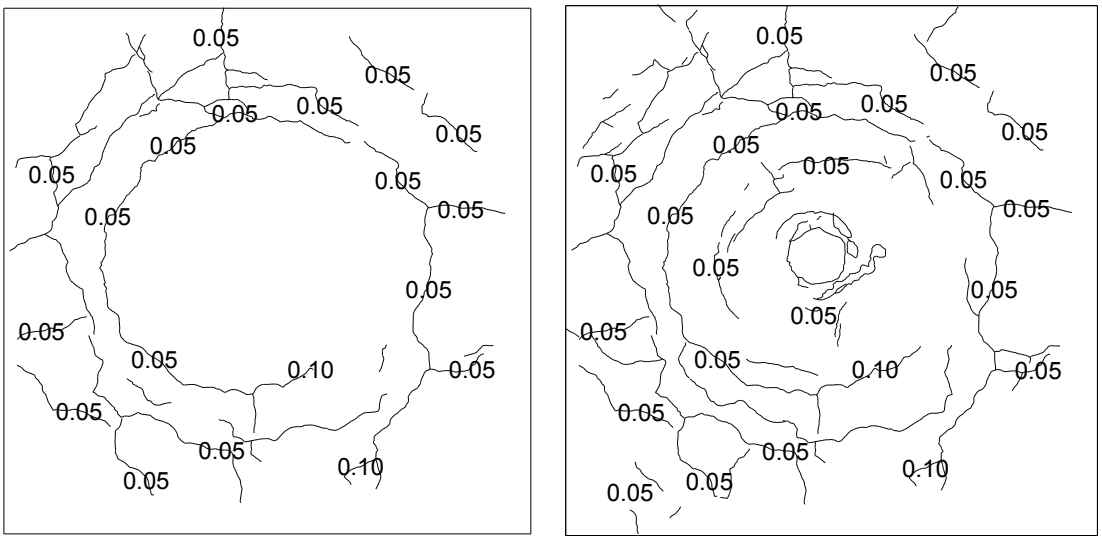

a) YA200b-1 b) YA200b-2

(Numbers indicate crack widths in millimeters)

Figure 3.45. Crack profiles on the impacted face of the specimen YA200b

3.5.2.4. YA200fb (Test Dates: 05.05.2014 – 07.05.2014 – 09.05.2014(twice))

320 kg drop weight was dropped on specimen YA200fb only for the first impact. Since this impact did not introduce a significant level of damage to the specimen, a heavier drop weight was used in subsequent impacts to cause a sizeable damage, allowing observations under near failure conditions. Hence, subsequent three impact loadings were made with the heavier 555 kg drop weight from 2.44 m. Cracks on the impacted surface are in Figure 3.46 and Figure 3.47. Circular cracks occurred on the impacted face of the specimen (Figure 3.48).

a) b)

Figure 3.46. a) Impacted face of the specimen YA200fb after tests, b) Back face of specimen YA200fb after tests

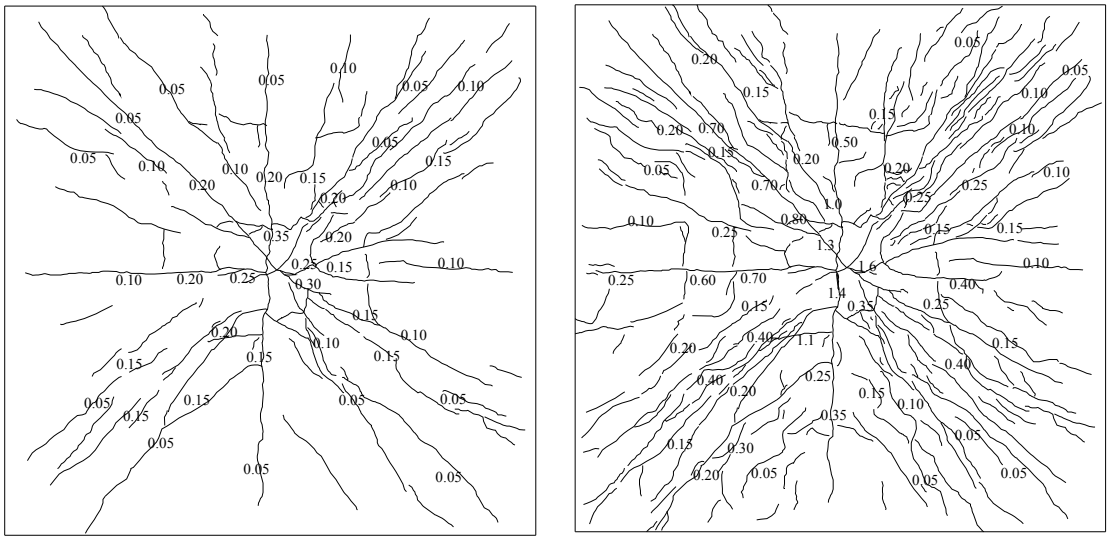

a) YA200fb-1 b) YA200fb-2

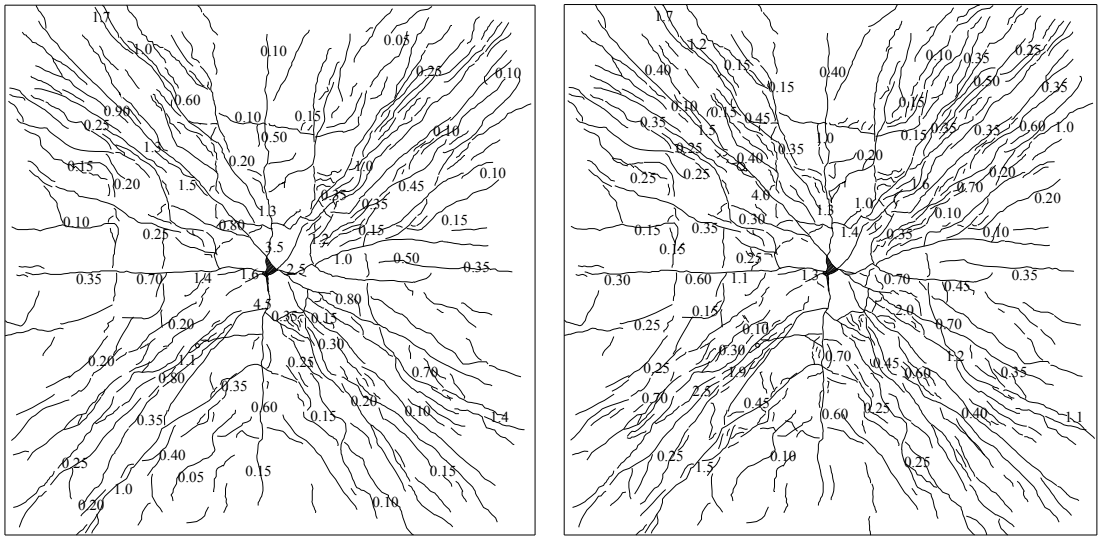

c) YA200fb-3 d) YA200fb-4

(Numbers indicate crack widths in millimeters)

Figure 3.47. Impact crack profiles on the back face of the specimen YA200fb

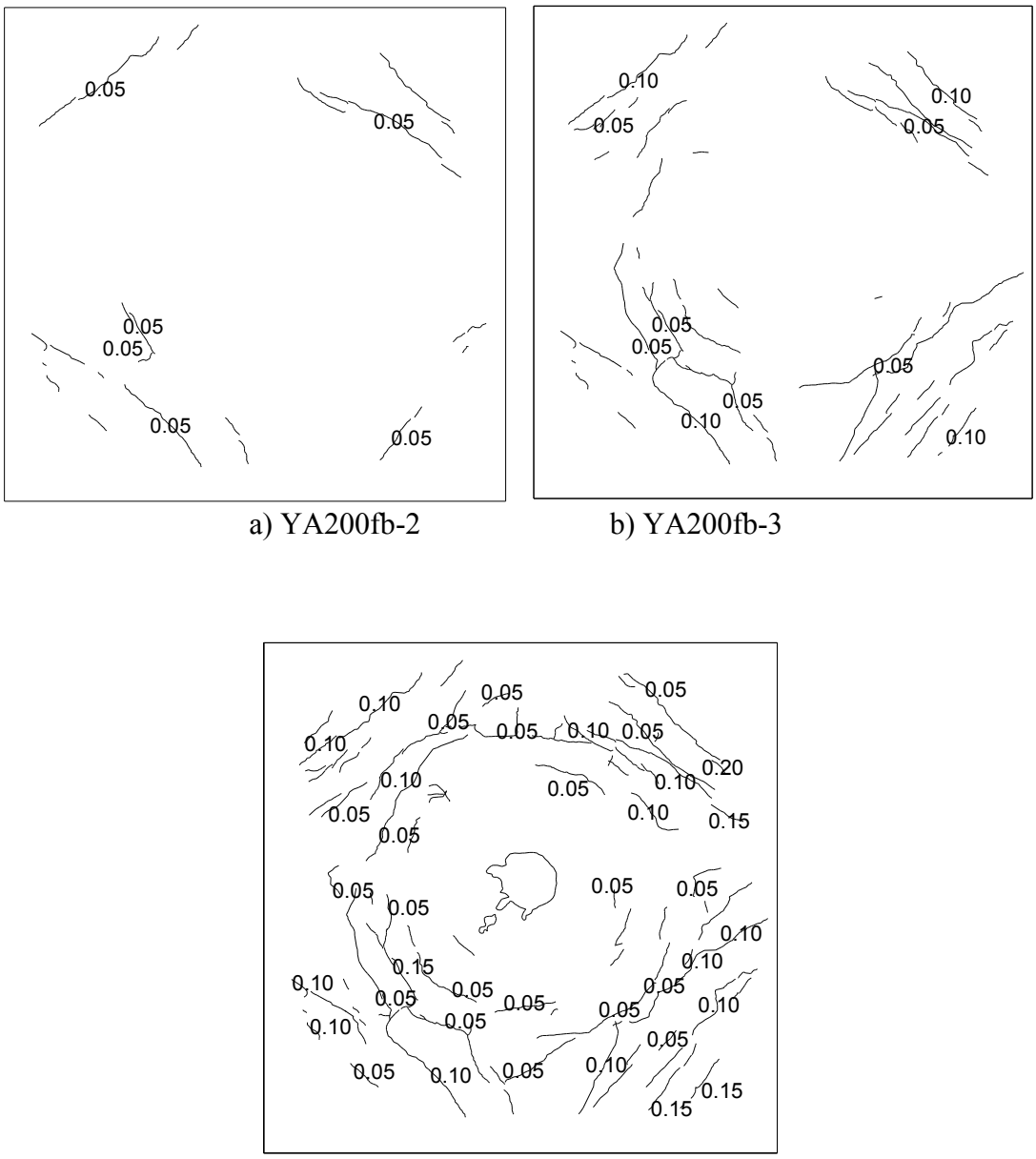

a) YA200fb-2 b) YA200fb-3

c) YA200fb-4

(Numbers indicate crack widths in millimeters)

Figure 3.48. Crack profiles on the impacted face of the specimen YA200fb

3.5.2.5. BB150b-1 (Control Specimen, Batarlar, 2013)

Control specimen was subjected to impact loading once with a drop weight of 320 kg from 2.5 m. General view and crack distribution of specimen BB150b is in Figure 3.50 and Figure 3.50.

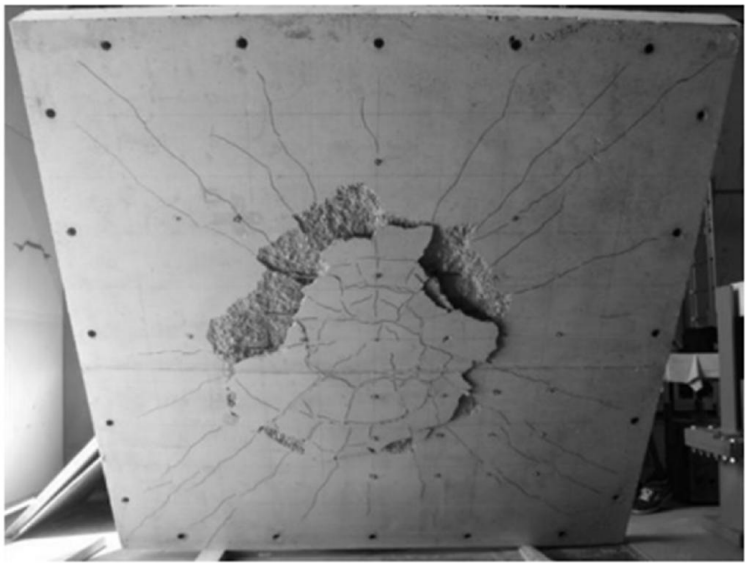

Figure 3.49. Back surface of the control specimen BB150b after tests
(Source: Batarlar, 2013)

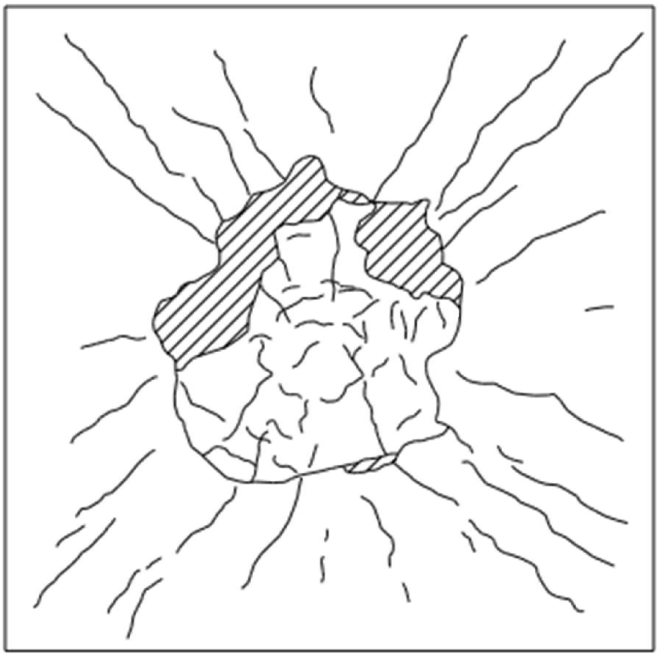

Figure 3.50. Impact crack profiles on the back face of the specimen BB150b
(Source: Batarlar, 2013)

3.5.2.6. BB200b-1 (Control Specimen, Batarlar, 2013)

Control specimen BB200b was subjected to impact loading twice with a drop weight of 210 kg from 2.5 m. Occurred scabbing and the crack distribution can be seen in Figure 3.51 and Figure 3.52.

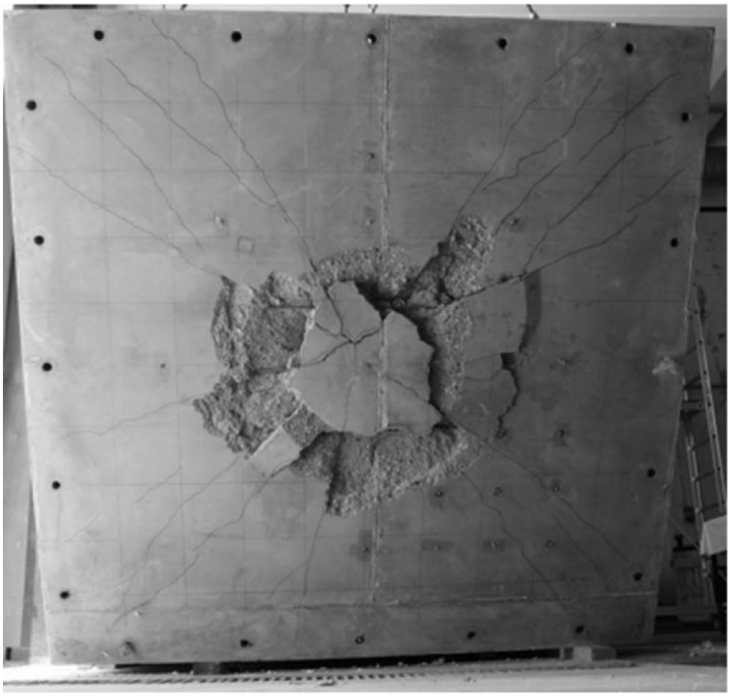

Figure 3.51. Back surface of the control specimen BB200b after tests
(Source: Batarlar, 2013)

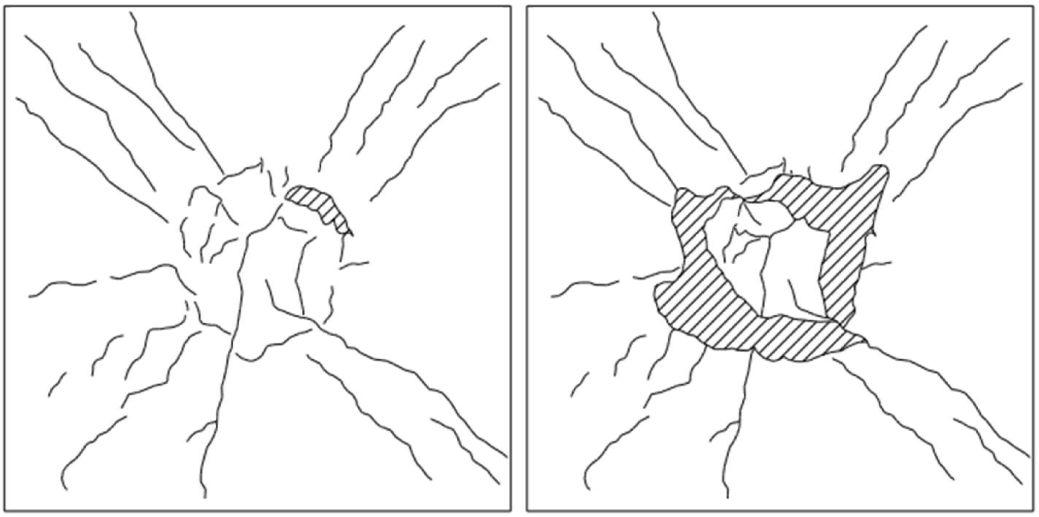

Figure 3.52. Impact crack profiles on the back face of the specimen BB200b (Source: Batarlar, 2013)

Table 3.2. Calculated kinetic energies applied on each specimen during impact tests

	Kinetic Energy ($kg.m^2/s^2$)					
Specimen	1st impact	2nd impact	3rd impact	4th impact	5th impact	Total Kinetic Energy ($kg.m^2/s^2$)
YA150b	7840	7840	7840	-	-	23520
YA200b	7840	7840	-	-	-	15680
YA150f-b	7840	7840	7840	7840	7840	39200
YA200f-b	7840	13288.5	13288.5	13288.5	-	47705.5
BB150b	7840	-	-	-	-	7840
BB200b	5145	5145	-	-	-	10290

CHAPTER 4

DISCUSSION OF RESULTS

Data obtained from measurements and comparisons of specimen behaviours are being discussed in this chapter.

4.1. Static Tests

Static loading was applied on the bottom midpoint of the specimens. During the static tests, the process was halted at certain displacements and was resumed afterwards in order to mark, measure and record the distribution of the cracks. In this section, the crack distribution and related comments are presented along with comparisons of specimens with the same longitudinal reinforcement ratios in terms of crack distribution and displacement profiles. Peak loads and corresponding midpoint displacements are presented in Table 4.1.

Table 4.1. Maximum loads and corresponding displacements for static tests

Specimen	Peak Load (kN)	Corresponding Displacement (mm)
YA150a	250	109
YA200a	241	118
YA150f-a	325	42
YA200f-a	329	38
BB150a	184	35
BB200a	161	43

4.1.1. YA150a – YA150fa – BB150a

All three specimens have the same longitudinal reinforcement. BB150a is the control specimen and was tested by Batarlar (2013). Specimen YA150a has shear studs addition to longitudinal reinforcement and specimen YA150fa has SFRC instead of plain concrete. Crack profiles after the testing of all three specimens are presented in Figure 4.2.

By looking at the load displacement graph (Figure 4.1), it is visible that contributions of steel fibers and shear studs changed the failure from brittle punching to ductile flexural. Control specimen reached a peak load of 184 kN with a midpoint displacement of 35 mm before failing.

Specimen YA150fa reached its peak load at 325 kN, providing a 77% increase in load carrying capacity compared to the control specimen. Midpoint displacement for the peak load is 42 mm, which is a 20 % increase again compared to the control specimen, BB150b. Testing specimen YA150a was stopped at a load of 250 kN and with a displacement of 109 mm due to test setup limitations. This specimen exhibited a 36% increase in load carrying capacity and 211% increase in deformation capacity.

Even though the specimen YA150a did not fail, it showed a ductile behavior. Specimen YA150fa reached the highest load among the specimens and exhibited some level of ductility before failing. Control specimen failed by punching.

Crack distribution of the specimen YA150a was even in the early stages of testing. Cracks were spread on the top surface of the specimen. Cracks widths were observed to be larger on the central region compared to the other regions. With the increasing load, more cracks formed while the older ones got wider. Cracks widths of those parallel to the edges were smaller compared to the cracks on the diagonal axes and the ones near the center.

Due to the wide cracks on the diagonal axes, compression formed on the rear diagonals of the specimen. Compression of the concrete caused scabbing, as can be seen from Figure 4.2b. Additionally, circular cracks formed on the loading face, which exhibits ductile flexural behavior of the member.

Specimen YA150fa had evenly distributed cracks along the diagonals. Cracks near the central region developed on the following stages. Denser crack distribution was observed compared to the other two specimens. Crack widths were much smaller

compared to specimen YA150a for the same midpoint displacements. With the increasing load, cracks got wider along diagonals. No crack was observed on the loading face of the specimen.

Crack distribution of control specimen BB150a was similar to the specimen YA150a in the beginning. However, with the increasing load, old cracks got wider while few numbers of new cracks formed leading to punching failure. Punching shear cone can be seen from the Figure 4.2d.

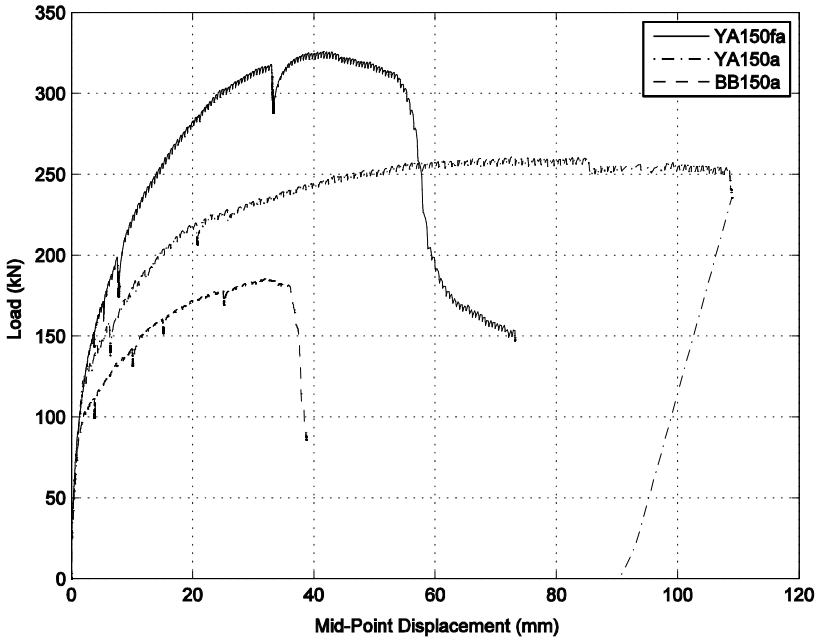

Figure 4.1. Load – Midpoint displacement graph for specimens YA150fa, YA150a and BB150a

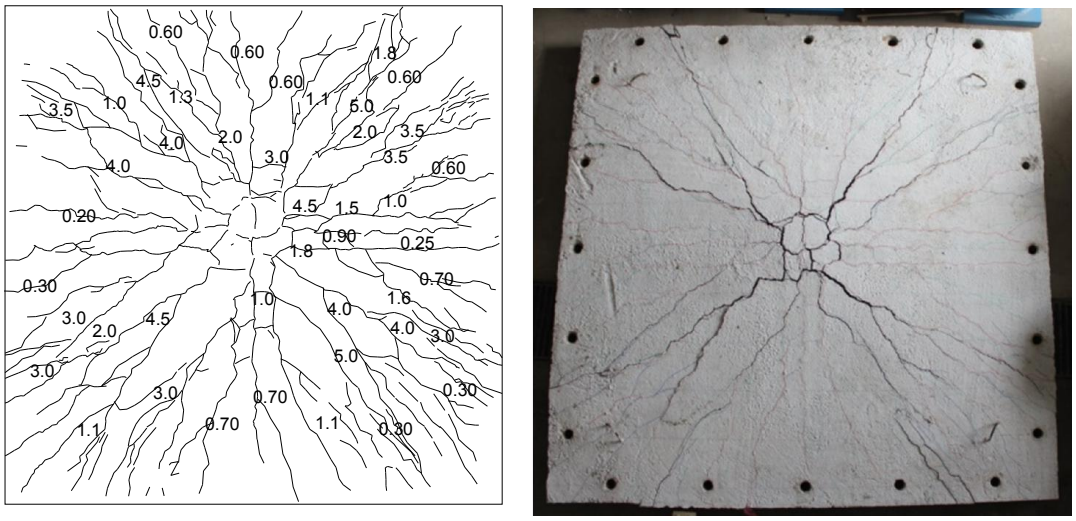

a) Front face of the specimen YA150a, after testing

(Numbers indicate crack widths in millimeters)

b) Loading face of the specimen YA150a, after testing

Figure 4.2. Drawings and photographs of specimens with the same longitudinal reinforcement ratio, after testing

(cont. on next page)

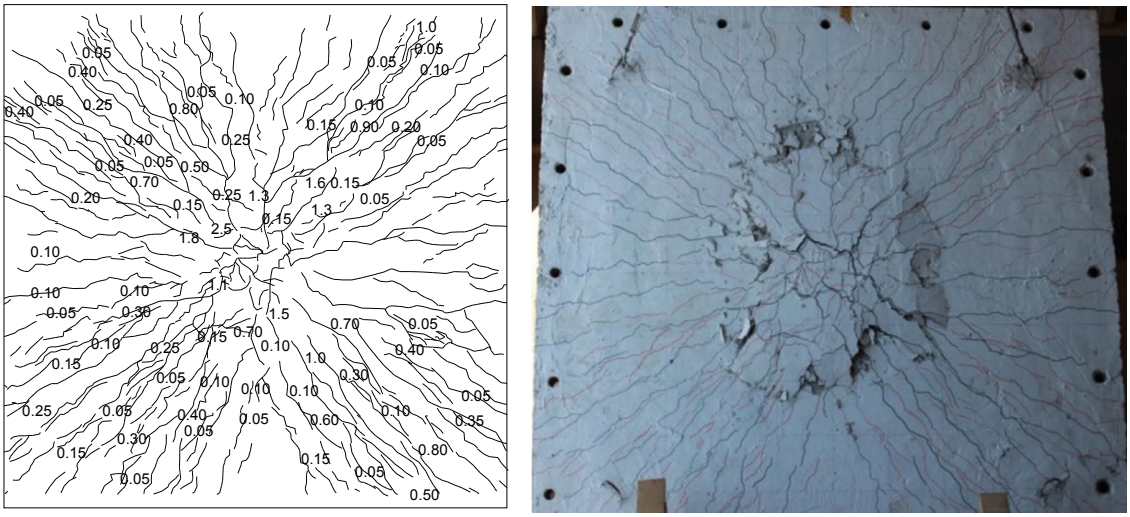

c) Front face of the specimen YA150fa, after testing

(Numbers indicate crack widths in millimeters)

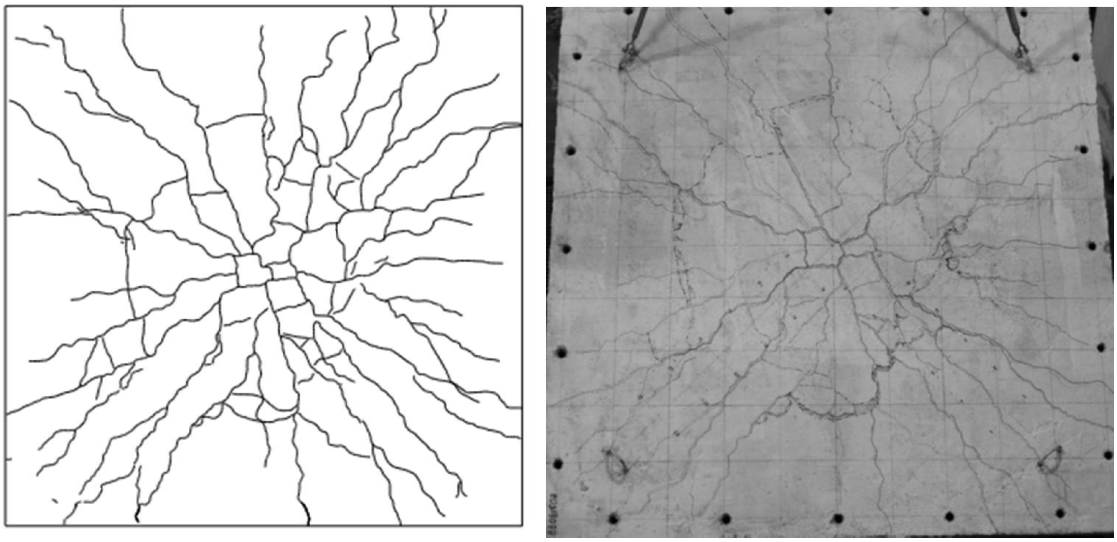

d) Front face of the control specimen BB150a, after testing

(Source: Batarlar,2013)

Figure 4.2. (cont.)

4.1.2. YA200a – YA200fa – BB200a

A comparison will be made between specimens with same longitudinal reinforcement ratio. Specimen BB200a is the control specimen and was tested by Batarlar (2013). YA200a is the specimen that has shear studs as addition. Specimen YA200fa has SFRC instead of plain concrete.

By looking at Figure 4.3, it is visible that specimens with shear studs and with steel fibers exhibited ductile behaviors compared to the control specimen. Control specimen reached a load of 161 kN with a midpoint displacement of 43 mm before failing suddenly. Specimen with steel fibers reached the highest load capacity with 329 kN, a 104% increase compared to control specimen. At that point, its midpoint displacement was 38 mm, Specimen YA200a reached a load of 241 kN with 118 mm displacement. Its load carrying capacity was 50% more than control specimen while its deformation capacity at that point, was 174% more than the control specimen. Test was terminated before the failure of specimen YA200a due to the limits of the test setup.

Due to the lesser amount of reinforcement, less cracks was observed than the specimens with 150 mm reinforcement spacing.

For specimen YA200a, cracks were extending from center to corners and edges on the early stages of testing. Specimen had fewer number of cracks compared to specimen YA150a. Cracks around the center were wider than the others. Similar to specimen YA150a, as the applied load increased, cracks around the diagonals got wider while new narrow cracks formed. Due to the wide diagonal cracks, compression formed on the rear diagonal axes, leading to scabbing. Compared to specimen YA150a observed scabbing area was larger, which could be because of higher midpoint displacement than YA150a at the last stages. Also at the loading face of the specimen more circular cracking was observed compared to specimen YA150a which could again be explained with higher midpoint displacement at the last stages.

Specimen YA200fa experienced more even cracking compared to YA150fa for the same midpoint displacements. Cracks were wider compared to specimen YA150fa and narrower compared to YA200a. With the increasing load, more cracks appeared especially around the diagonals. Older ones got wider particularly the ones on the diagonal axes. At the end of the testing, less cracking was observed than YA150fa.

Control specimen BB200a had fewer cracks compared to BB150a due to less amount of reinforcement. Cracks got wider with the increasing load. Specimen failed in a brittle manner with a sudden crack sound. Punching cone occurred. (Figure 4.4d)

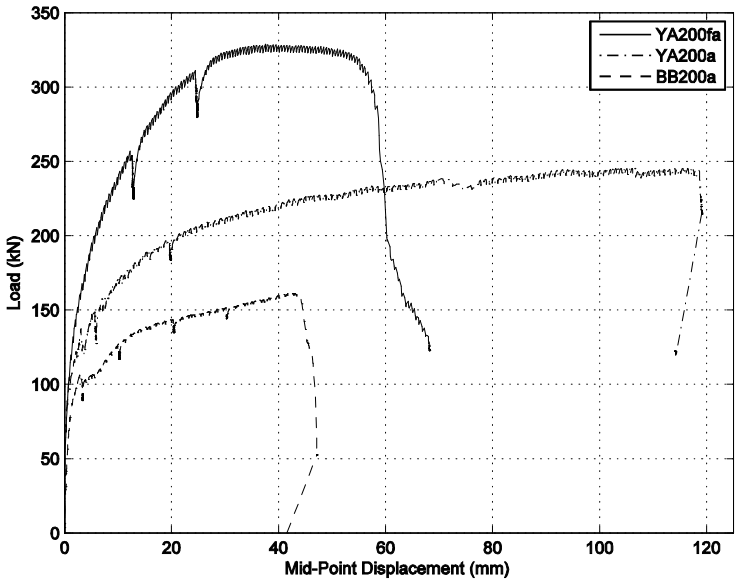

Figure 4.3. Load – Midpoint displacement graph for specimens YA200fa, YA200a and BB200a

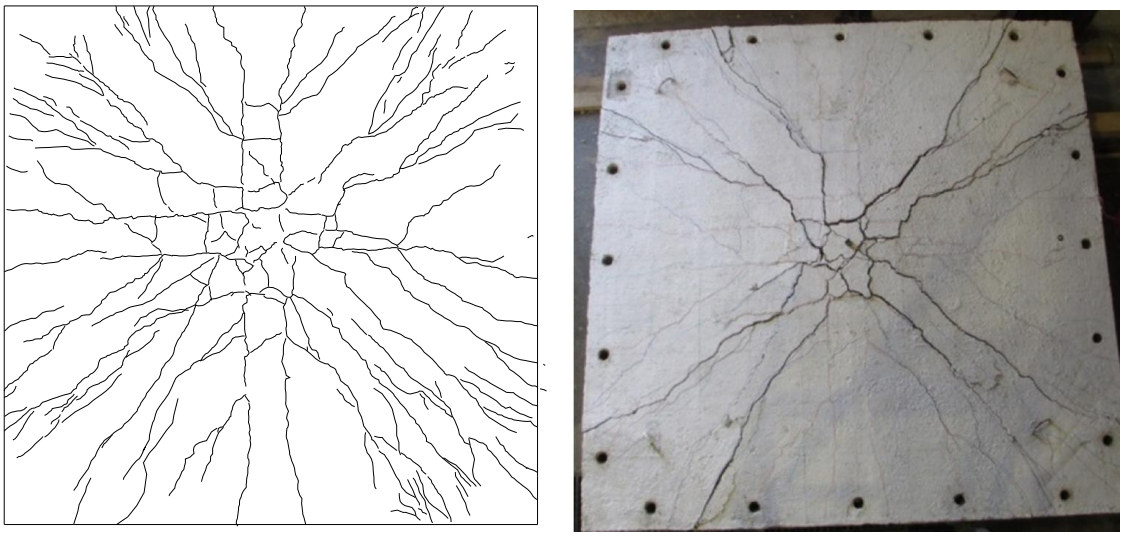

a) Front face of the specimen YA200a, after testing

b) Loading face of the specimen YA200a, after testing

Figure 4.4. Drawings and photographs of specimens with the same longitudinal reinforcement ratio, after testing

(cont. on next page)

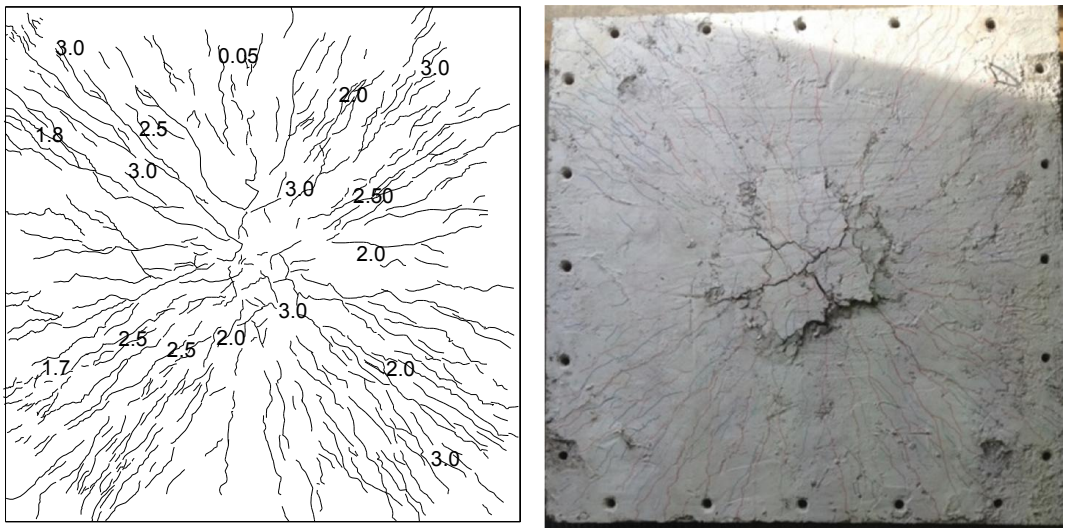

c) Front face of the specimen YA200fa, after testing

(Numbers indicate crack widths in millimeters)

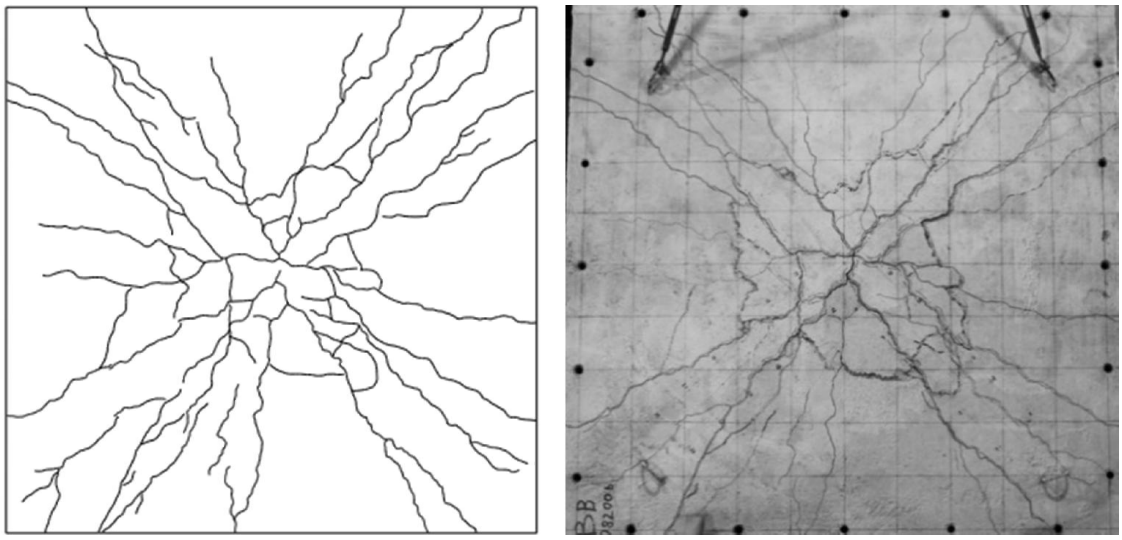

d) Front face of the control specimen BB200a, after testing

(Source: Batarlar, 2013)

Figure 4.4. (cont.)

4.2. Impact Test Comparisons

Impact load was generated by dropping a weight on the top center of the specimen from a certain drop height. Drop weight and height are stated below for each specimen. Specimens with same longitudinal reinforcement ratios are going to be compared according to their crack distributions in this section.

At the instant of loading, as a result of the impact behavior, the impacted zone starts to go downwards. But the remaining parts cannot follow this movement due to their inertia and an upward curvature is formed at the instant of the impact. (Figure 4.5)

4.2.1. YA150b – YA150fb – BB150b

Drop weight for all three specimens was 320 kg with a drop height of 2.5 m.

Specimen YA150b was subjected to impact loading three times (Figure 4.6). Cracks around the diagonals were wide and the width increase more near the impact center. Second impact caused some crack lines to get narrow while some cracks near the center and the diagonals got wider. Third impact caused scabbing in an unusual form compared to the control specimen which can be explained by the nature of impact.

Under impact loading, as the impacted zone starts to go to a direction, remaining areas cannot follow this movement because of their inertia. In that instance, a shape close to the one in Figure 4.5b forms. Under the arcs compression occurs while tension develops on the top. Plus shaped shear studs on specimen YA150b keeps concrete around its region intact while other parts experience scabbing due to compression. Tension of the impacted face causes cracks to occur as can be seen from Figure 4.7.

Specimen YA150fb was subjected to impact loading five times (Figure 4.8). Few narrow cracks was observed for the first impact. Other impacts caused more cracks which are distributed evenly on the surface. Crack widths were mainly equal except around the center. Uniformly distributed steel fibers avoided punching shear failure and increase specimen's resistance against impact loading. Nearly no scabbing was observed due to the grip of the fibers.

Control specimen BB150b was subjected to impact loading once. Scabbing and punching failure occurred as can be seen from Figure 4.9.

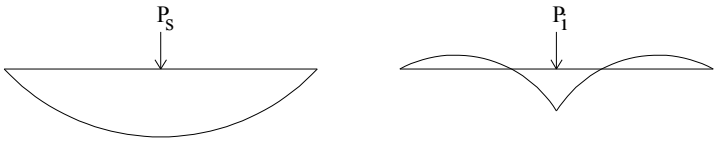

a) b)

Figure 4.5. a) Shape under static loading, b) Shape under impact loading

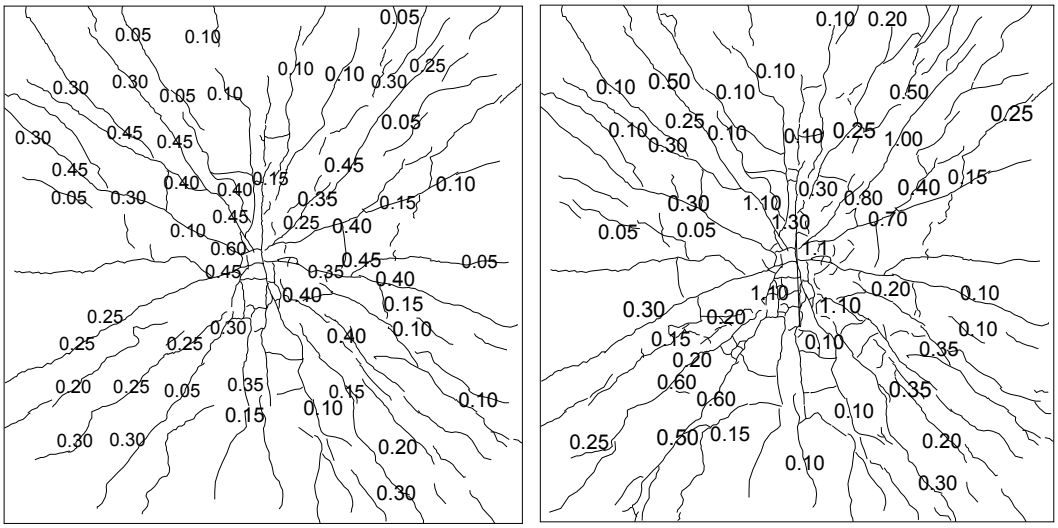

a) YA150b-1 b) YA150b-2

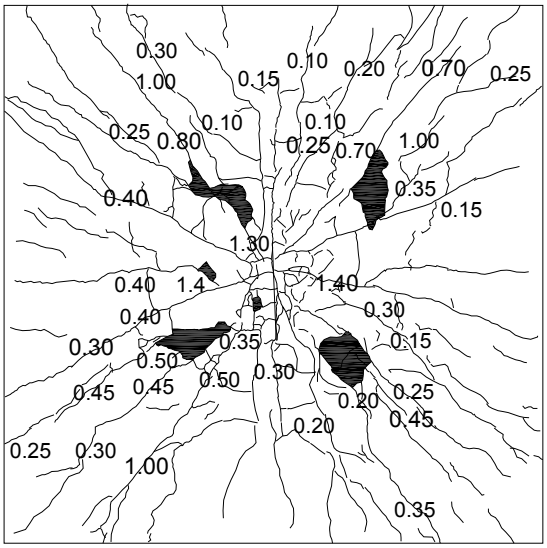

c) YA150b-3

(Numbers indicate crack widths in millimeters)

Figure 4.6. Crack profiles of the back face of YA150b

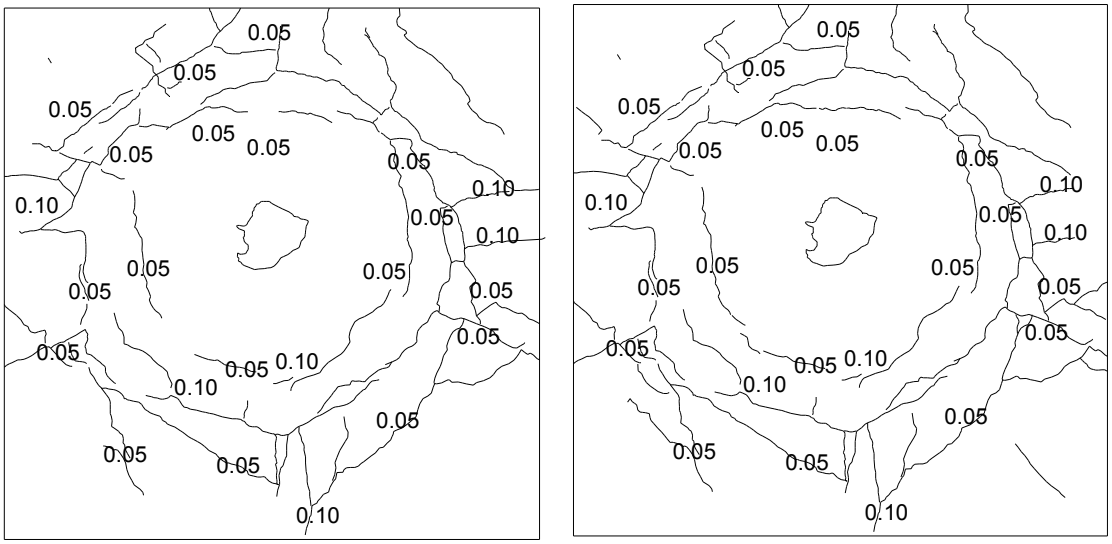

a) YA 150b-2 b) YA150b-3

(Numbers indicate crack widths in millimeters)

Figure 4.7. Crack profiles on the loading face of the specimen YA150b

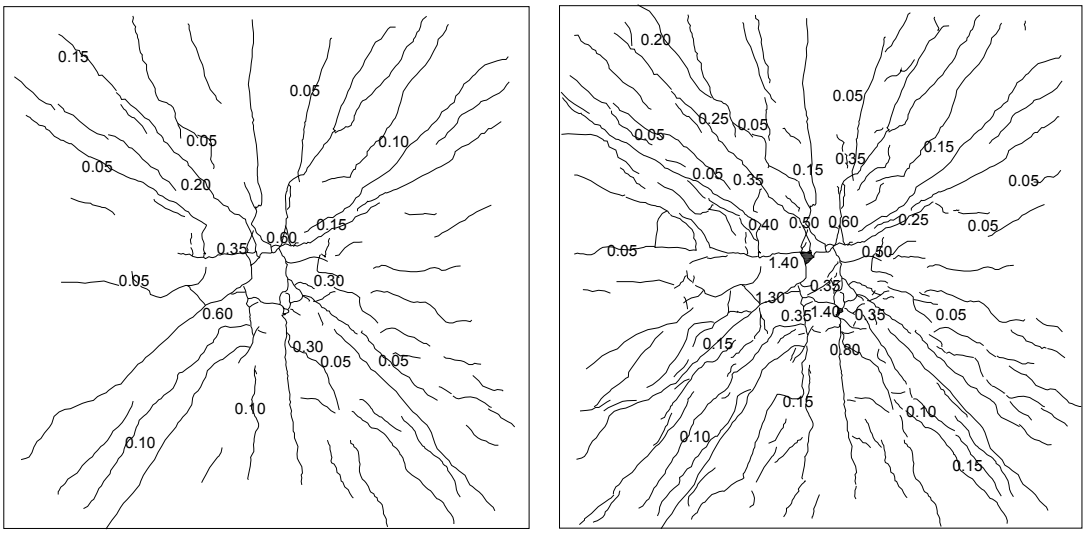

a) YA150fb-1 b) YA150fb-2

(Numbers indicate crack widths in millimeters)

Figure 4.8. Crack profiles of the back face of YA150fb

(cont. on next page)

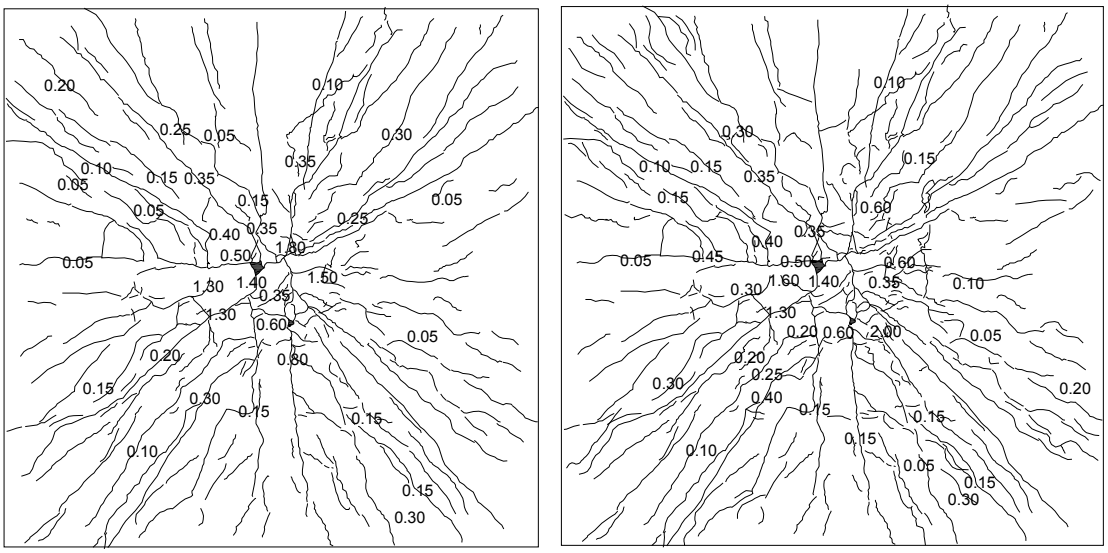

c) YA150fb-3 d) YA150fb-5

(Numbers indicate crack widths in millimeters)

Figure 4.8. (cont.)

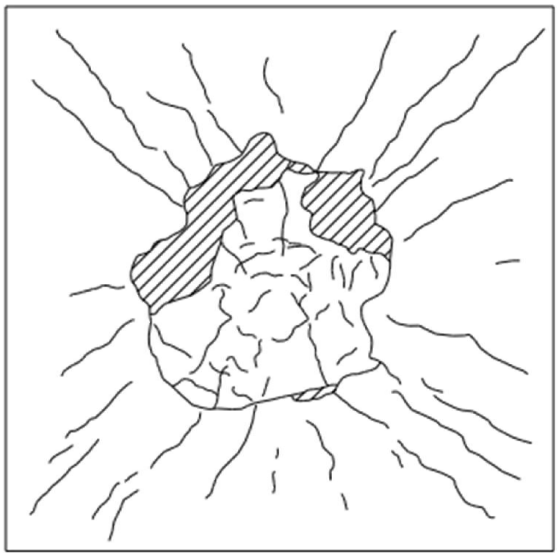

Figure 4.9. Crack profiles of the back face of BB150b
(Source: Batarlar,2013)

4.2.2. YA200b – YA200fb – BB200b

Specimen YA200b was subjected to impact loading two times with a drop weight of 320 kg, from a drop height of 2.5 m. Cracks were grouped on diagonals (Figure 4.10). Second impact caused almost no cracks. Previous cracks got wider and scabbing occurred. Lesser amount on longitudinal reinforcement lead to larger scabbing compared to YA150b. As explained before on the previous section, cracks on the loading face develop due to tension during the impact (Figure 4.11).

Specimen YA200fb was subjected to impact loading once with a drop weight of 320 kg and three times with a weight of 555 kg. Drop height was 2.5 m for 320 kg and 2.44 m for 555 kg. More cracks occurred on the first impact compared to YA150fb but the crack widths were almost the same as YA150fb. Upcoming impacts generated lots of cracks distributed on the surface. More cracks were observed compared to specimen YA150fb. Cracks around the center were wider compared to the ones on diagonals (Figure 4.12). And cracks on the diagonal axes were wider than the rest of the cracks. Similar to YA15fb, no scabbing occurred. Different from specimen YA150fb, circular cracks formed on the impacted face of the specimen (Figure 4.13).

Control specimen was subjected to impact loading twice with a drop weight of 210 kg from 2.5 m. Cracks developed on diagonals on the first impact and scabbing occurred (Figure 4.14). Second impact generated even more scabbing. Formed cracks got wider and no new cracks formed.

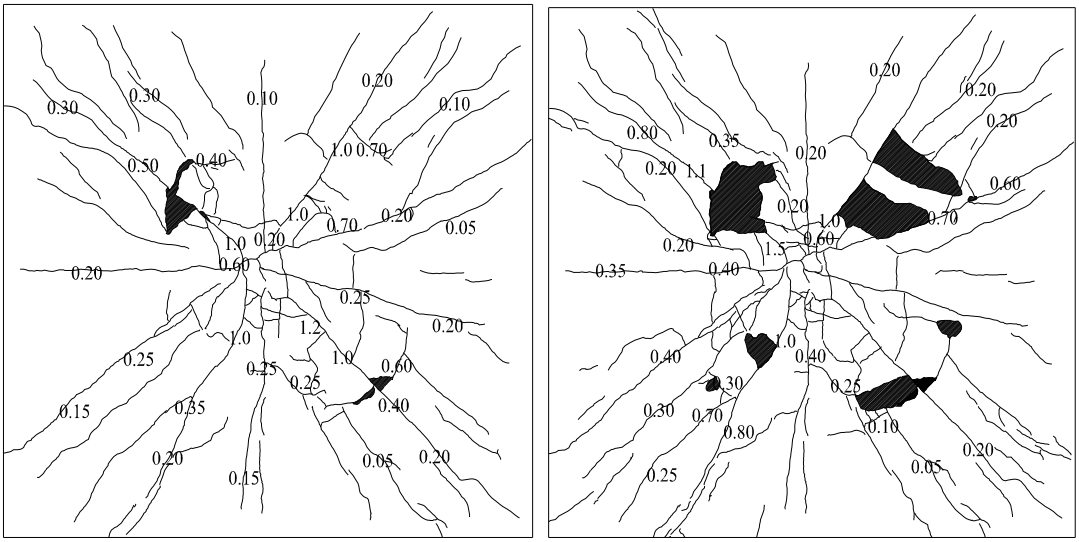

a) YA200b-1 b) YA200b-2

(Numbers indicate crack widths in millimeters)

Figure 4.10. Crack profiles of the back face of YA200b

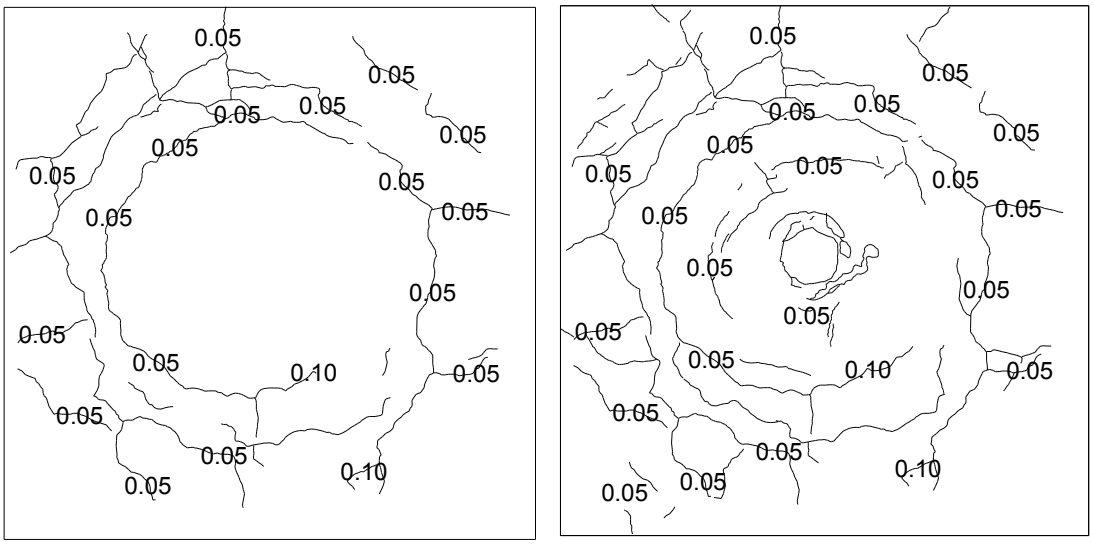

a) YA200b-1 b) YA200b-2

(Numbers indicate crack widths in millimeters)

Figure 4.11. Crack profiles on the loading face of YA200b

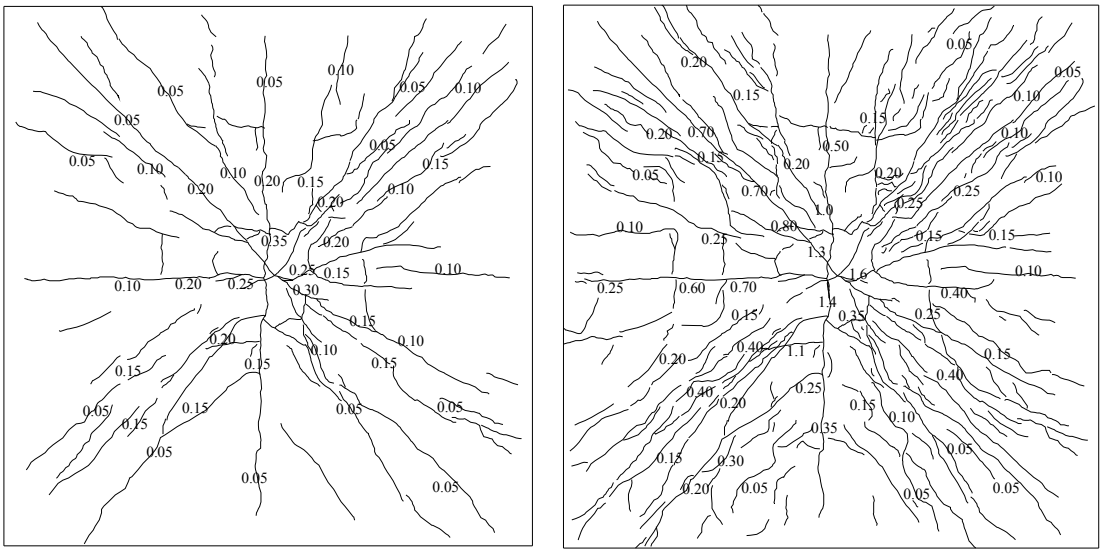

a) YA200fb-1 b) YA200fb-2

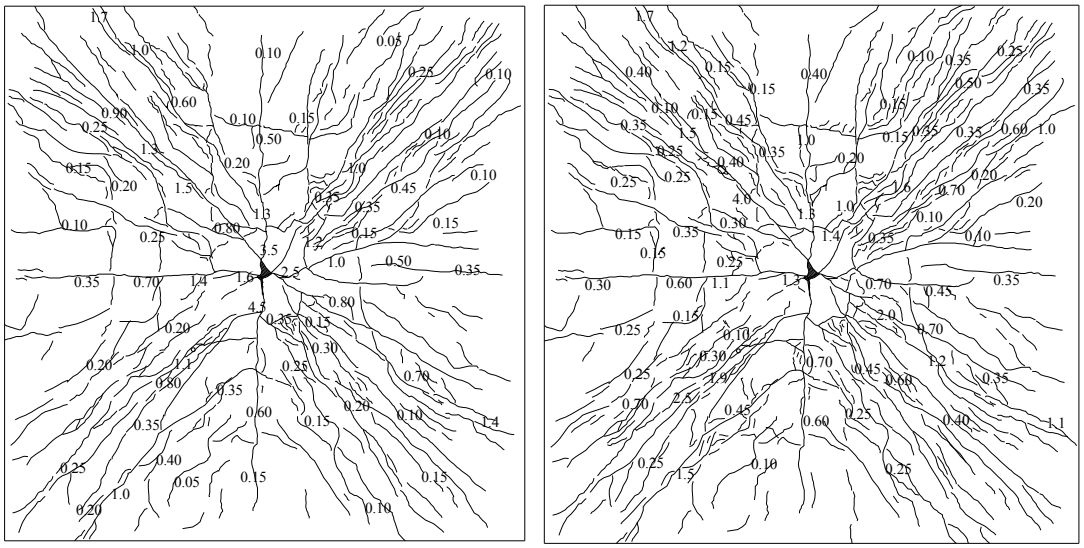

c) YA200fb-3 d) YA200fb-4

(Numbers indicate crack widths in millimeters)

Figure 4.12. Crack profiles of the back face of YA200fb

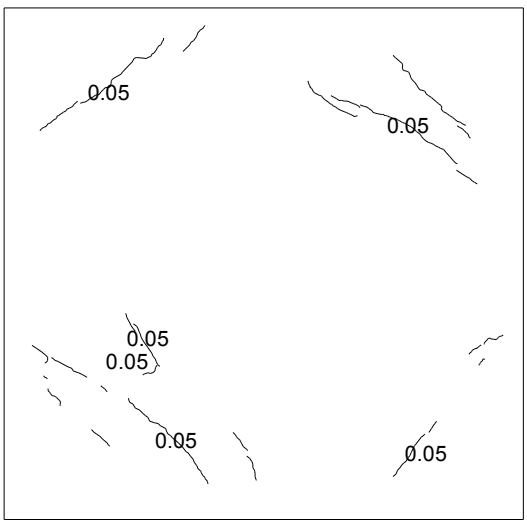

a) YA200fb-2

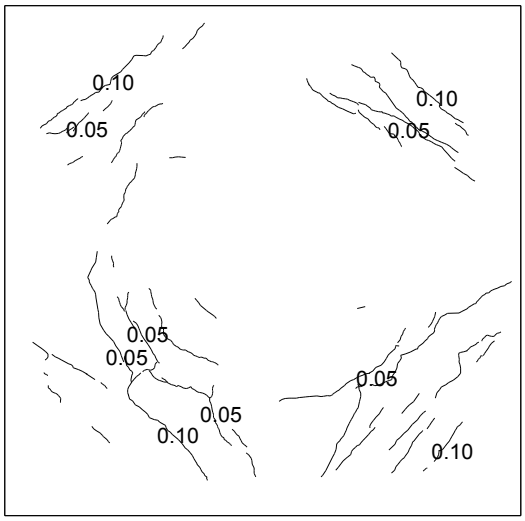

b) YA200fb-3

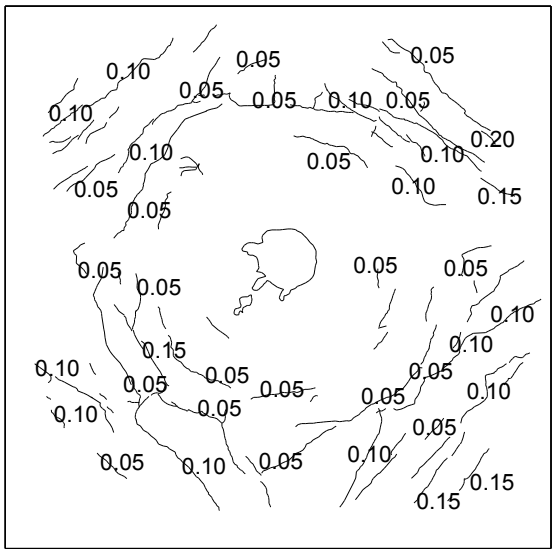

c) YA200fb-4

(Numbers indicate crack widths in millimeters)

Figure 4.13. Crack profiles on the loading face of YA200fb

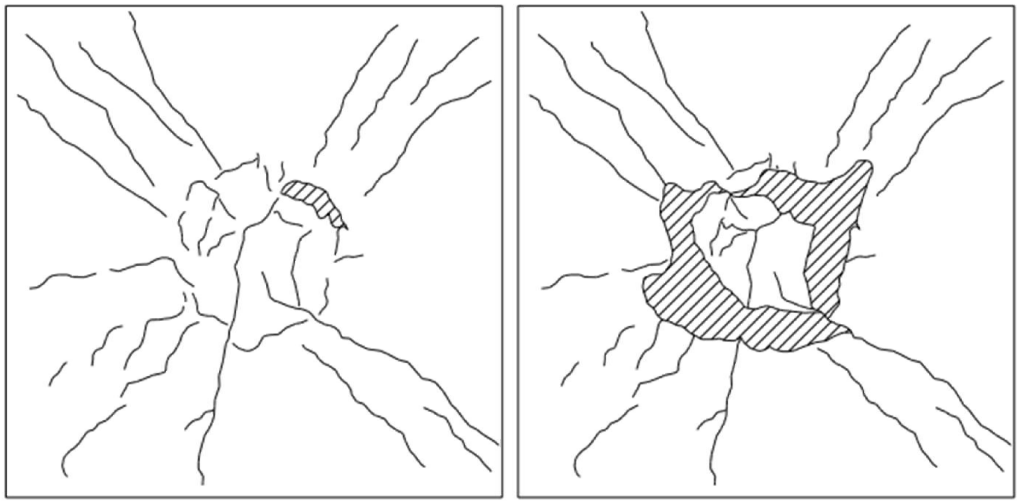

Figure 4.14. Crack profiles of the back face of BB200b (Source: Batarlar,2013)

4.3. Displaced Shapes

In order to obtain the displacement profiles, 24 RLPT's were placed under the specimen during testing. During the course of the tests, a few of the RLPT's were fallen due to impact. Therefore, the middle line axis for each slab was chosen as the N-S or E-W direction depending on the fallen RLPTs' (see Figure 4.15. and Figure 4.16.).

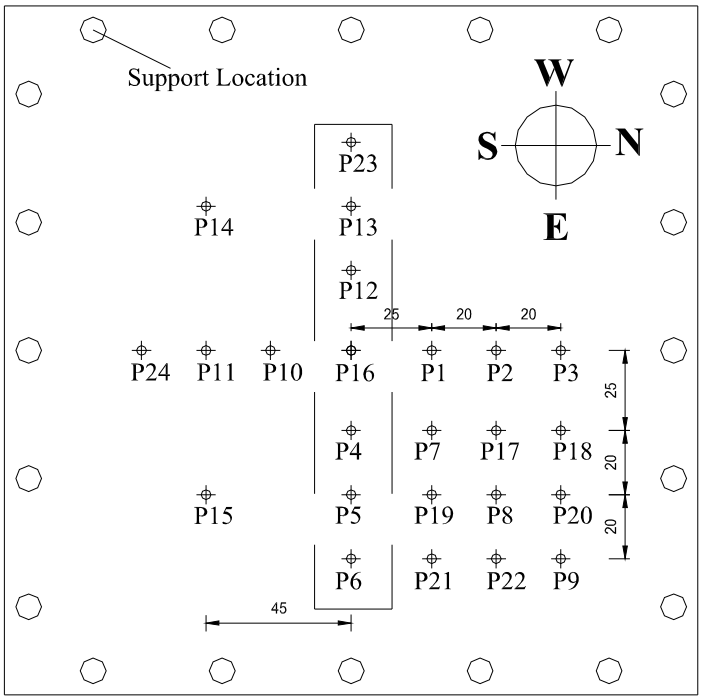

Figure 4.15. RLPT's selected for YA150fb-1 and YA200fb-1 (Numbers indicate crack widths in centimeters)

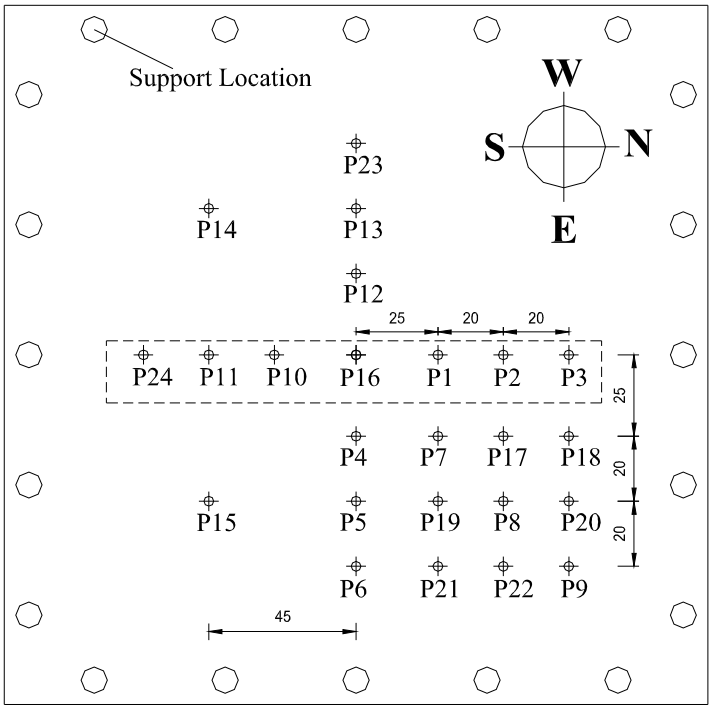

Figure 4.16. RLPT's selected for YA150b-1 and YA200b-1 (Numbers indicate crack widths in centimeters)

Shear studs had a length of 150 mm, same length as the specimen thickness. Due to stud distribution, some of RLPTs' were re-located. Modified locations of RLPTs' are in Figure 4.17. Also, fallen RLPTs' are presented in Figure 4.17, between rectangular dashed lines.

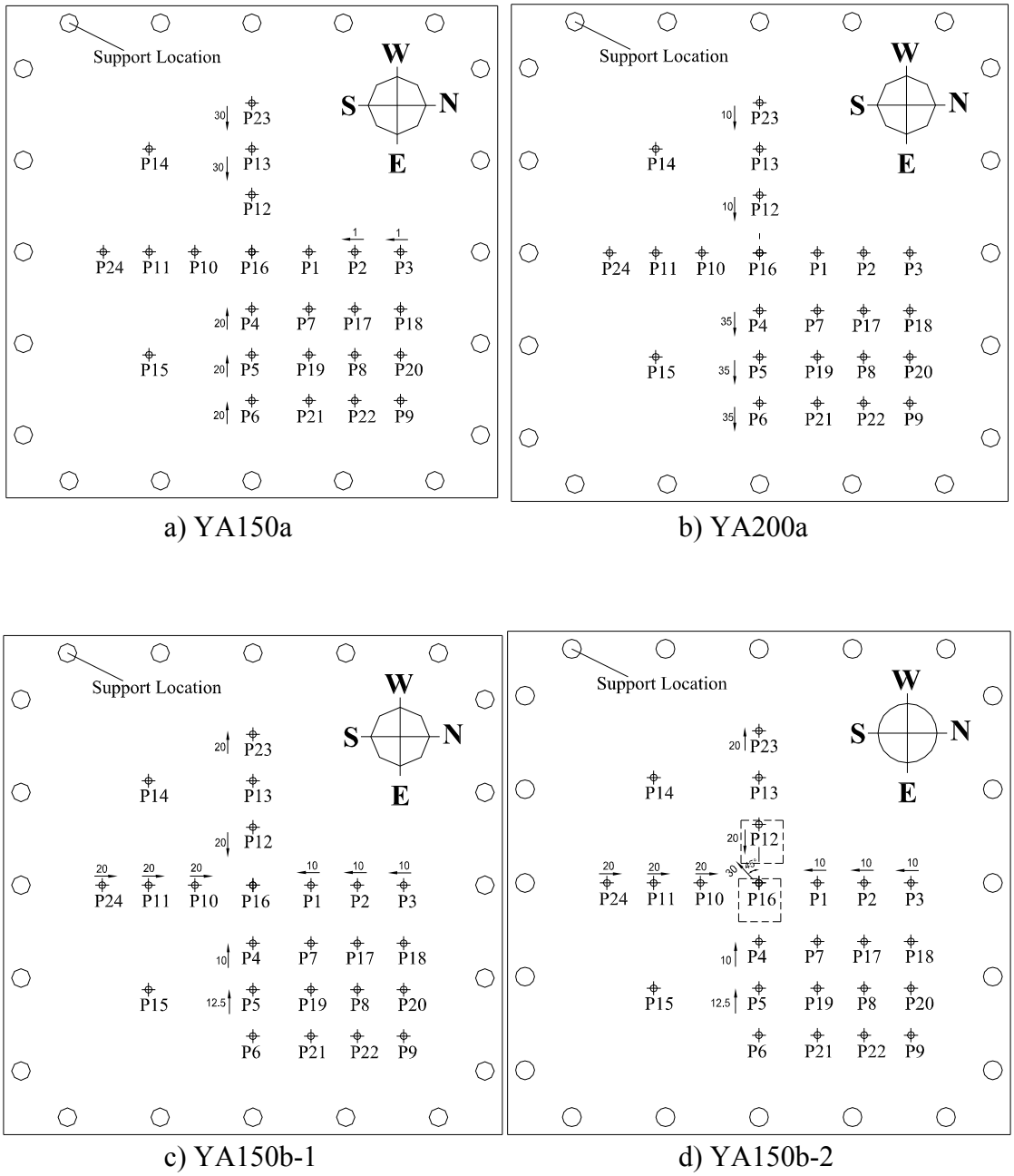

a) YA150a b) YA200a

c) YA150b-1 d) YA150b-2

Figure 4.17. Modifications done to relocate RLPT's (Numbers indicate modifications in millimeters)

(cont. on next page)

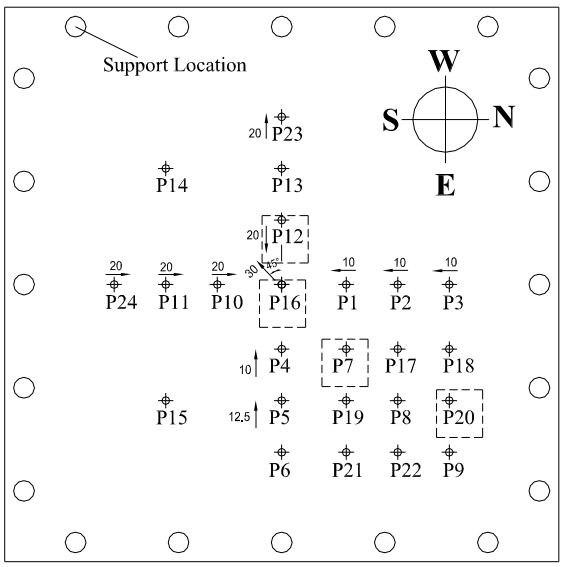

e) YA150b-3

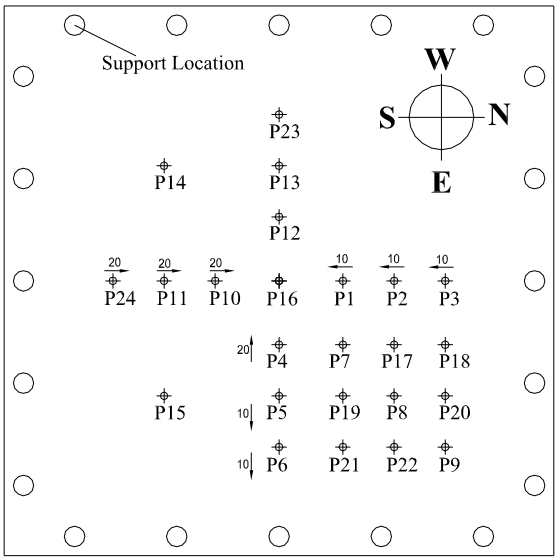

f) YA200b-1

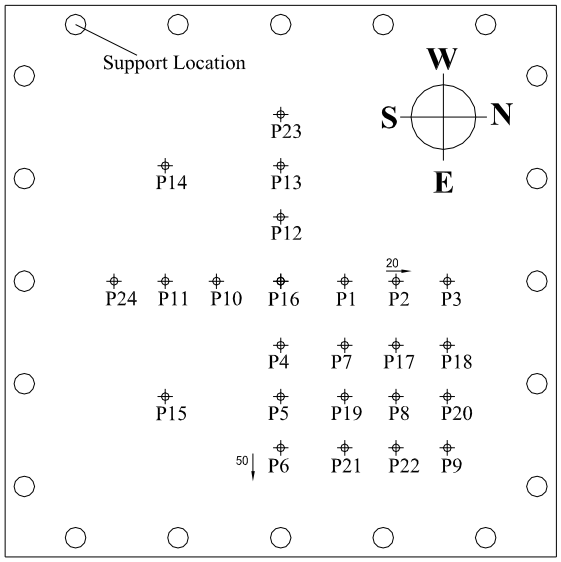

g) YA200fb-1

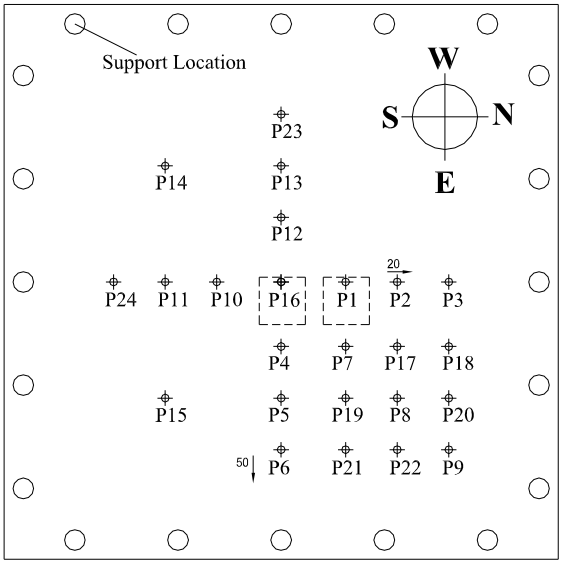

h) YA200fb-2

Figure 4.17. (cont.)

(cont. on next page)

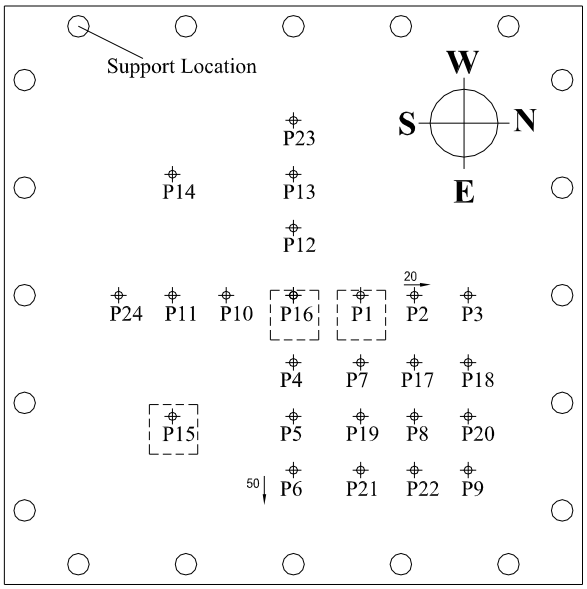

i) YA200fb-4

Figure 4.17. (cont.)

Deformation profile of each specimen for the first impact loading is in Figure 4.18. Figures were plotted according to modifications of RLPTs in Figure 4.17.

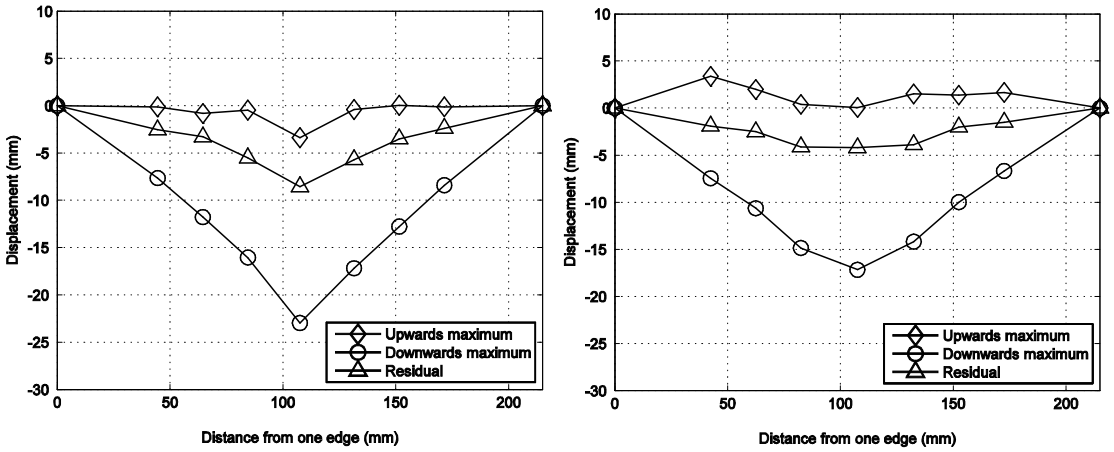

a) YA150b-1 b) YA150fb-1

Figure 4.18. Deformation profiles of each specimen for the first impacts

(cont. on next page)

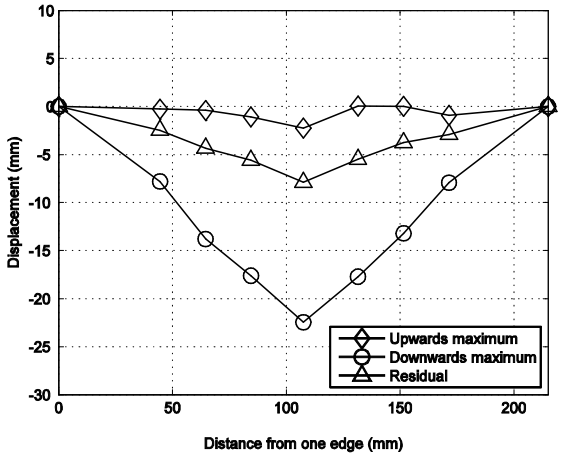

c) YA200b-1

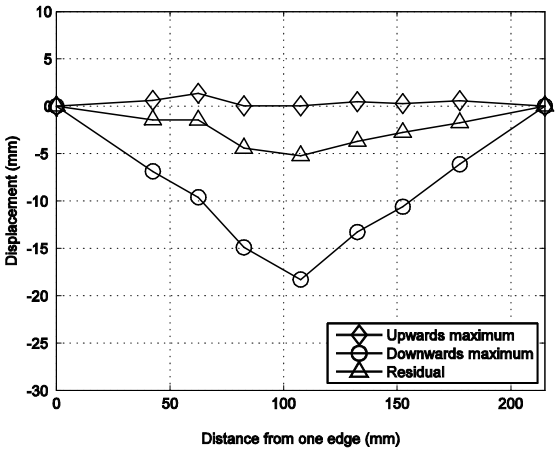

d) YA200fb-1

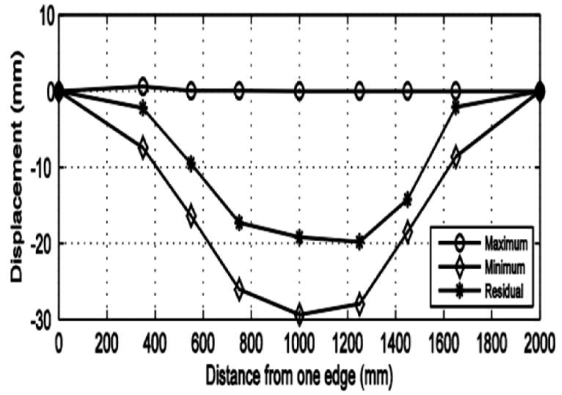

e) BB150b (320 kg)
(Source: Batarlar, 2013)

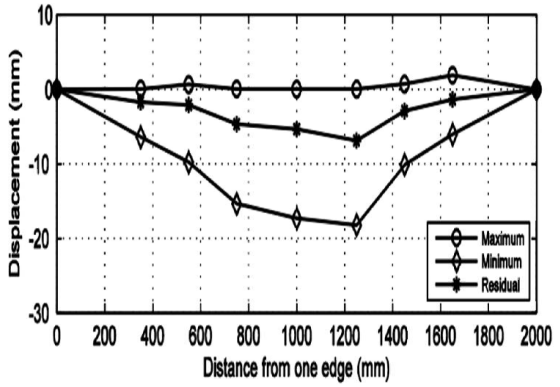

f) BB200b-1 (210 kg)
(Source: Batarlar, 2013)

Figure 4.18. (cont.)

According to the deformation profiles of each specimen, it can be said that steel fibers and shear studs enhance the behavior of the specimen under impact loading. Punching shear cone of the control specimen BB150b is clearly visible on Figure 4.18e. Even though a lighter drop weight (210 kg) was used for the control specimen BB200b, general shape in Figure 4.18f is a punching cone.

Comparing Figure 4.18a with Figure 4.18b and Figure 4.18c with Figure 4.18d, the stiffness of the specimens with steel fibers are noticeable from the maximum upward movements. Due to this higher stiffness of the specimens with uniformly distributed steel fibers, maximum downward deformation is less than specimens with shear studs.

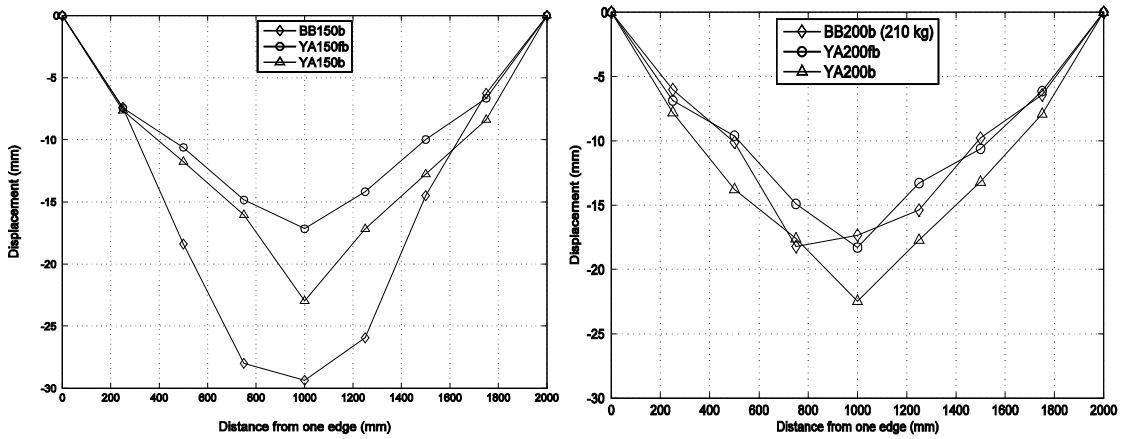

Figure 4.19. Maximum displacements of the specimens with same longitudinal reinforcements

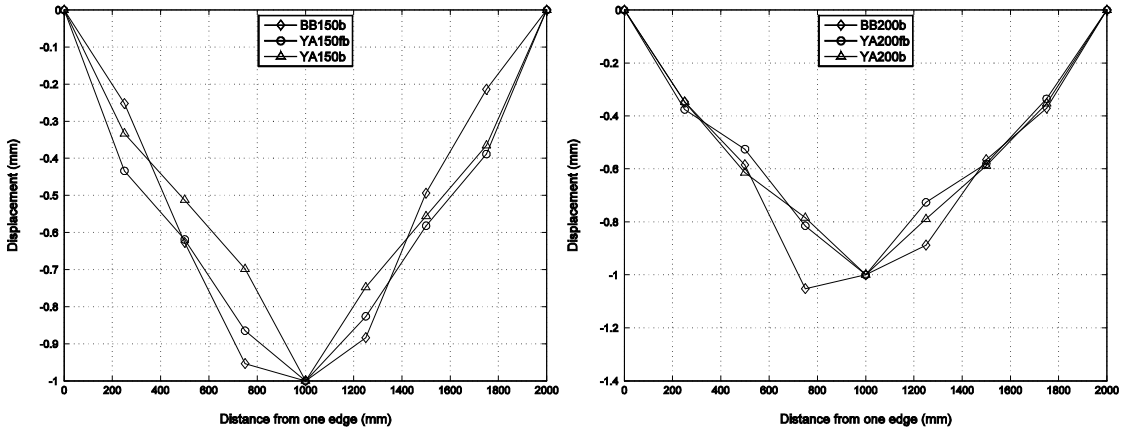

Figure 4.20. Maximum displacements of the specimens with same longitudinal reinforcements, normalized with respect to their midpoint deflection

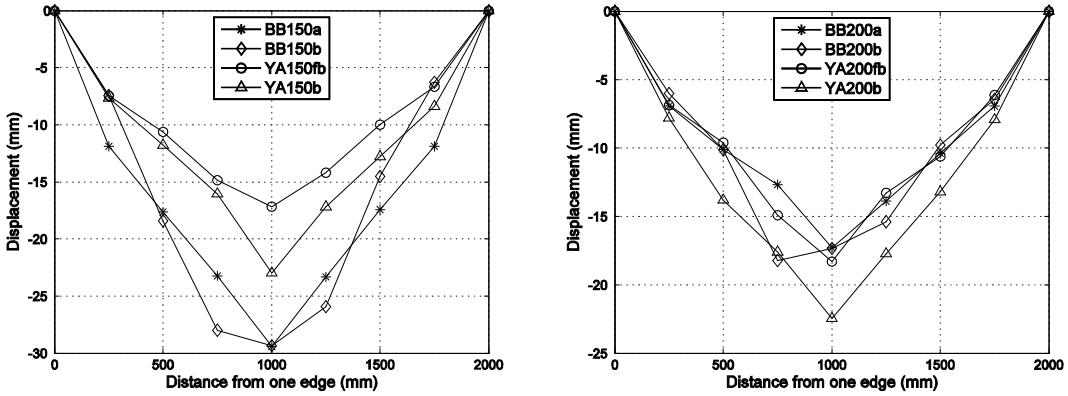

Figure 4.21. Maximum displacements of the specimens with same longitudinal reinforcements and corresponding static tested control specimens

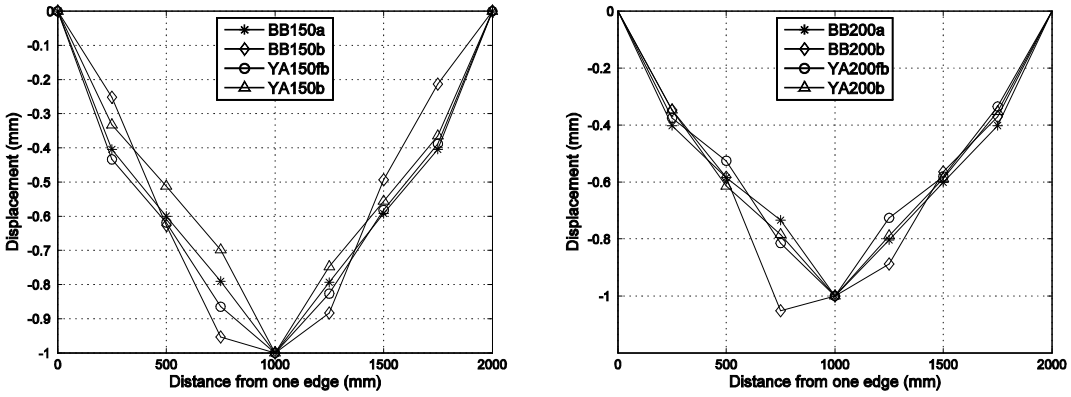

Figure 4.22. Maximum displacements of the specimens with same longitudinal reinforcements and corresponding static tested control specimens, normalized with respect to their midpoint deflection

Maximum deformations are plotted in Figure 4.19, Figure 4.20, Figure 4.21 and Figure 4.22. Deformations under impact loading are in Figure 4.19 and the punching shear cone of control specimen BB150b is noticeable. Deformation profile of YA150b is similar to the one in Figure 4.5b. YA150fa shows more of a static shape close to the one in Figure 4.5a. Specimens with less reinforcement exhibit higher deformations under impact except control specimen BB200b. When the deformations are normalized (Figure 4.20), punching behavior of the control specimens is visible. To differentiate the displacement shape difference between impact loading and static loading, Figure 4.21 and Figure 4.22 were plotted. Displacement profiles of specimens BB150a and BB200a

were plotted for the maximum midpoint deformations of BB150b and BB200b. Control specimens of BB150a and BB200a exhibit a deformation close to Figure 4.5a.

Figure 4.23, Figure 4.24, Figure 4.25 and Figure 4.26 are displacement profiles of static and impact tested specimens plotted together for same midpoint deformations. The general shape under impact loading (Figure 4.5b) can be seen on YA150b clearly in Figure 4.23. While specimen YA200b exhibits a profile more or less similar to YA200a in Figure 4.24, displacement profiles of specimens with fiber is generally the same as static tested specimens (Figure 4.5c). However shape in Figure 4.5b can still be seen on Figure 4.25 and Figure 4.26 on early moments of impact loading.

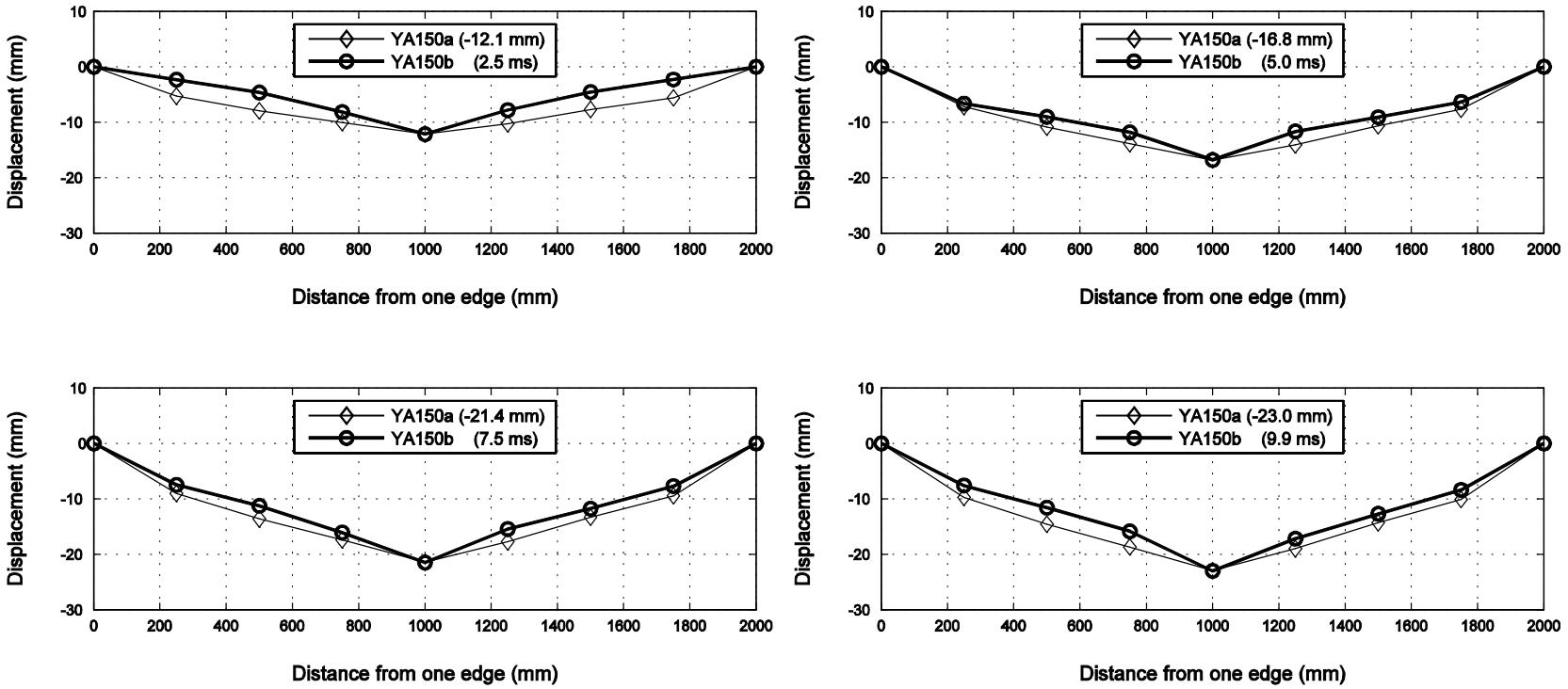

Figure 4.23. Displacement profiles of YA150a and YA150b-1 for the same midpoint displacements

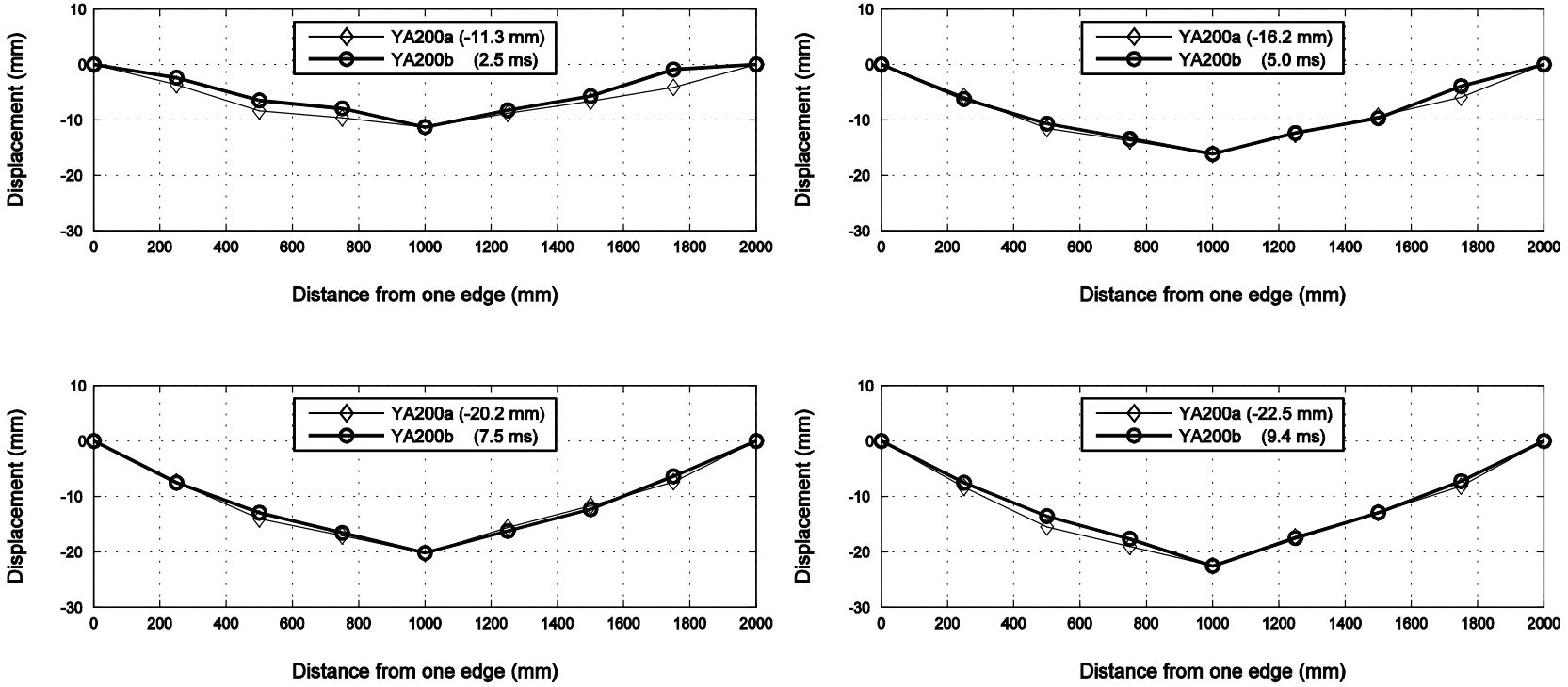

Figure 4.24. Displacement profiles of YA200a and YA200b-1 for the same midpoint displacements

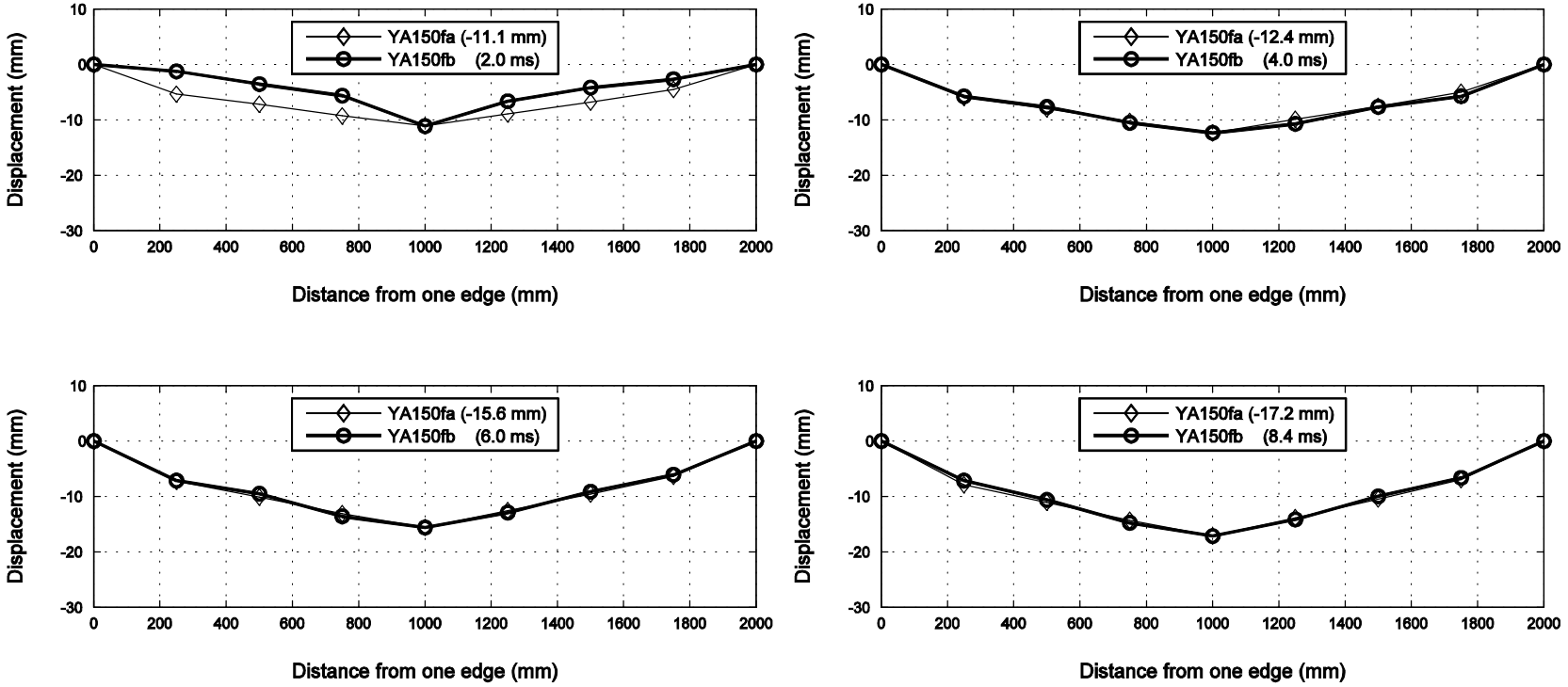

Figure 4.25. Displacement profiles of YA150fa and YA150fb-1 for the same midpoint displacements

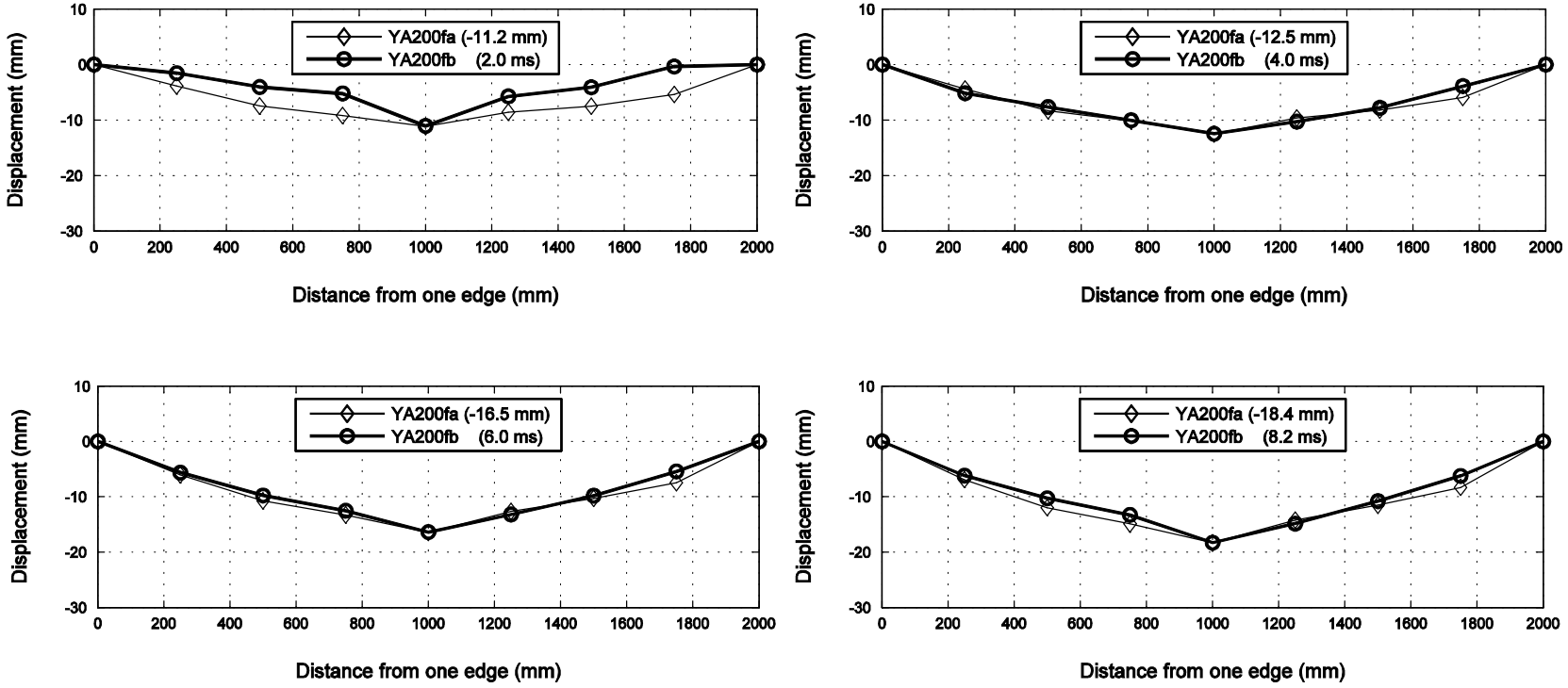

Figure 4.26. Displacement profiles of YA200fa and YA200fb-1 for the same midpoint displacements

4.4. Support Reactions

Total reaction force-time histories for the first impact loadings of all specimens are in Figure 4.27. Support reactions of specimen YA200fb-1 is highest among the specimens for both peaks. First impacts of other specimens are seen in Figure 4.28, Figure 4.29 and Figure 4.30. Unfortunately, support reactions for second impact loading of specimen YA200b-2 were not recorded. Peak support reactions for all impact tests are in Table 4.2.

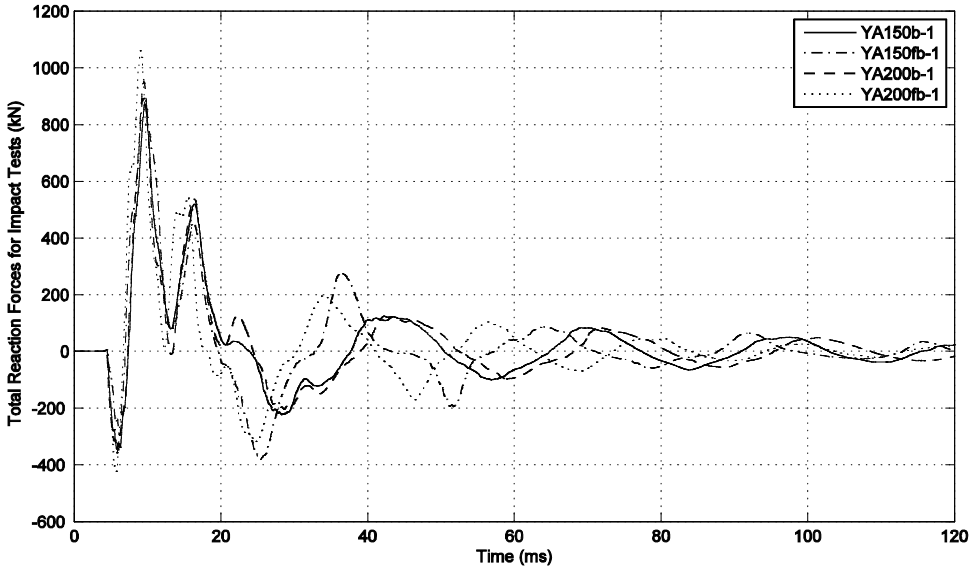

Figure 4.27. Total reaction force – time histories for all first impact tests

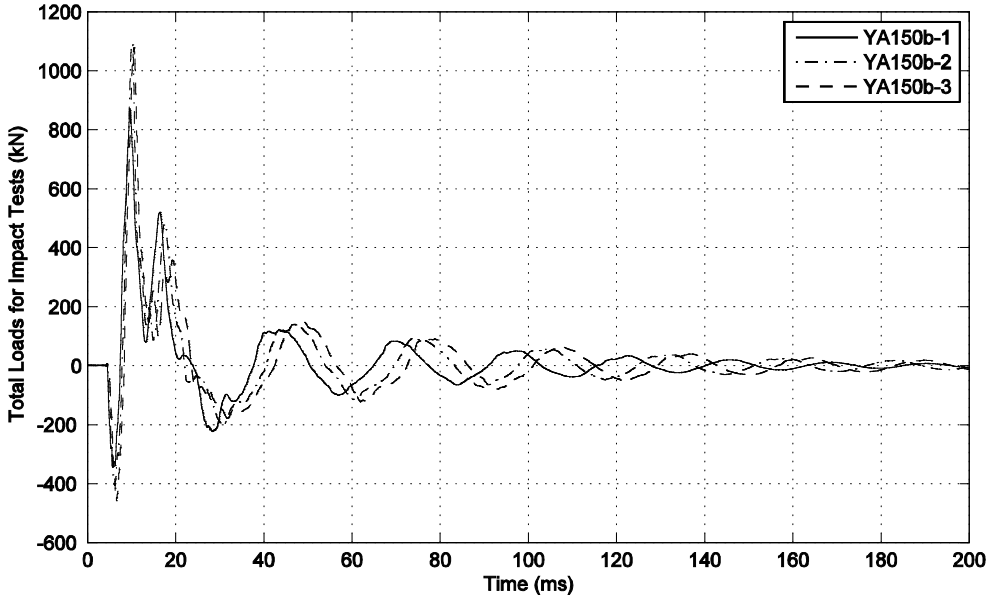

Figure 4.28. Total reaction force – time histories for specimen YA150b

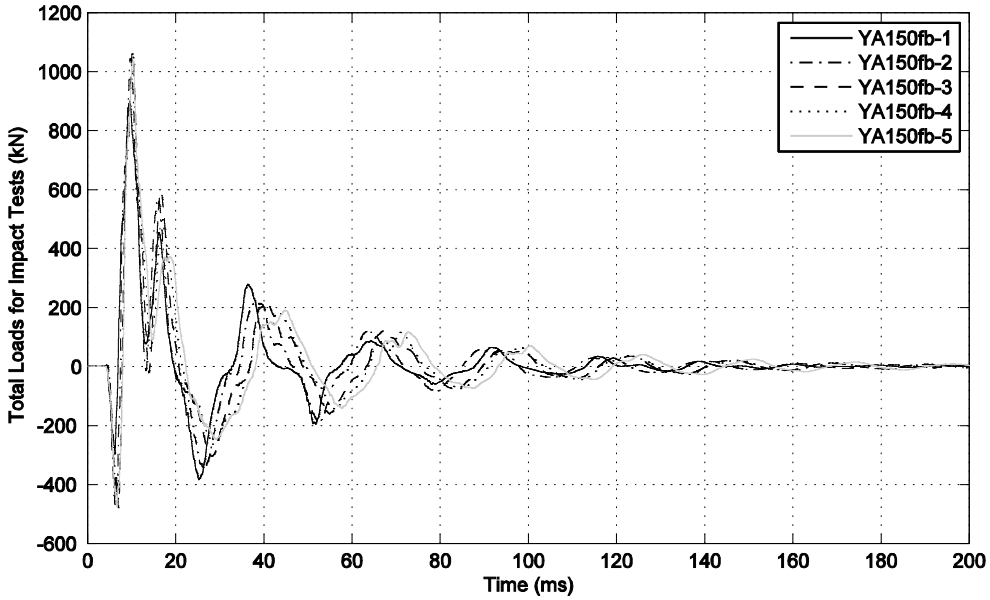

Figure 4.29. Total reaction force – time histories for specimen YA150fb

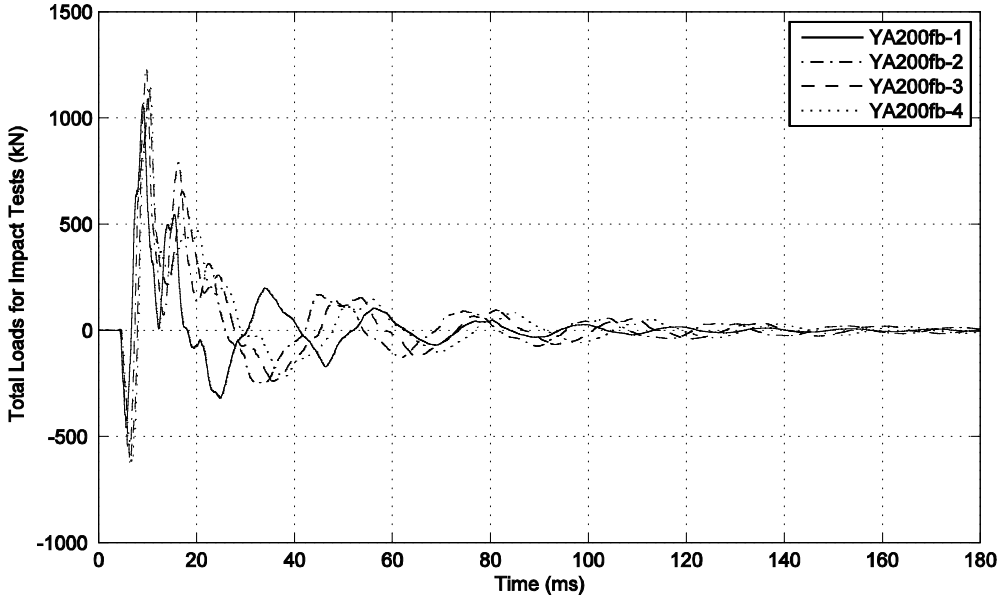

Figure 4.30. Total reaction force – time histories for specimen YA200fb

Table 4.2. Peak support reactions (all values are in kN)

	1st Impact	**2nd Impact**	**3rd Impact**	**4th Impact**	**5th Impact**
YA150b	872	1092	1078	-	-
YA150fb	878	1044	1062	1052	1036
YA200b	950	x	-	-	-
YA200fb	1061	1234	1136	1153	-
(Drop weight of YA200fb-2, YA200fb-3 and YA200fb-4 are 555 kg)					

4.5. Strain Gauges

16 strain gauges were placed on shear studs and reinforcements (Figure 3.11 and Figure 3.12) for four specimens in order to record strains during static and impact loading. Strain gauges on specimen YA150b-1 were broken. Maximum strain values of YA200b-1 and the instance of maximum strains are in Figure 4.31.

According to obtained data, highest strain values were achieved by the shear stud strain gauge closest to the center. For the gauge values on reinforcements, it was seen that bottom strains were higher than the top strains.

In Figure 4.32 and Figure 4.33, maximum strain values for specimens under static loading are presented. It was observed that strains on studs under impact loading were higher than strains on studs under static loading. For specimen YA150a, strain gauges on reinforcing bars and stain gauge on stud S08 were unreliable. Similarly, for specimen YA200a, strain gauges on studs S09 and S10 were unreliable. It should be noted that strain gauge readings for static tests were completely questionable.

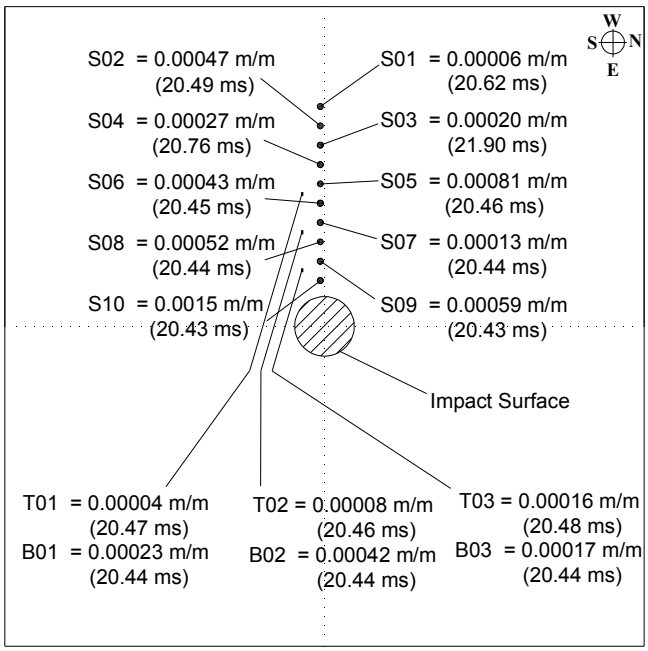

Figure 4.31. Maximum strain gauge values of YA200b-1

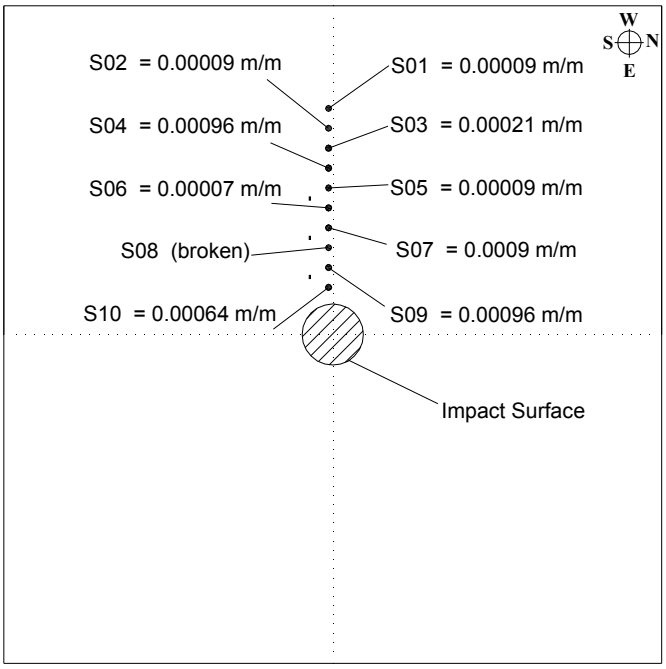

Figure 4.32. Maximum strain gauge values of YA150a

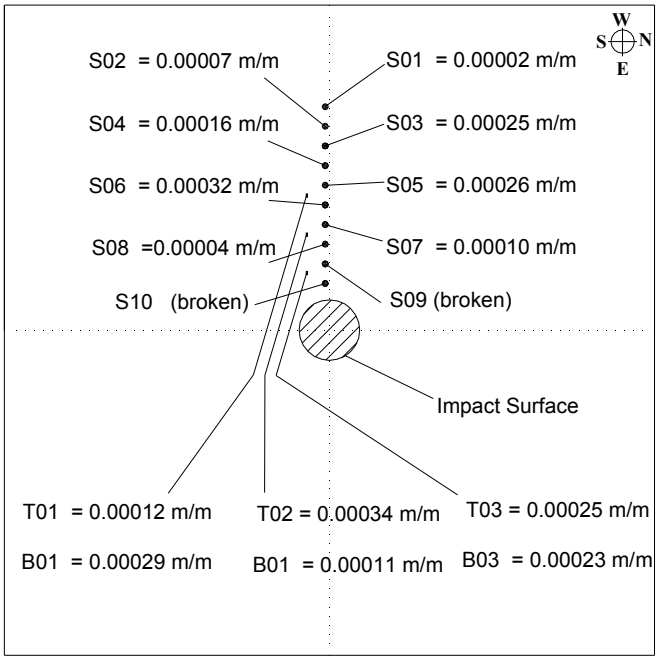

Figure 4.33. Maximum strain gauge values of YA200a

CHAPTER 5

CONCLUSIONS

This study investigated the impact behavior of RC slabs strengthened for punching using steel fibers and shear studs. Eight slab specimens were manufactured as four identical pairs and while one was tested under static loading, the other was tested under impact loading. Four pairs had a longitudinal reinforcement spacing of 150 mm and the other four had a spacing of 200 mm. Observations and obtained data were compared with four control specimens tested in a previous study of Batarlar (2013).

According to the results under static loading,

- Specimens with steel fibers reached the highest load carrying capacity.
- Specimens with shear studs carried a smaller load for large deformations.
- Steel fibers and shear studs changed the brittle failure mode. Steel fibers prevented sudden brittle failure and introduced a slight ductility, whereas shear studs provided significant ductility to the specimens.
- Even surface cracking was observed for specimens with steel fibers due to fibers' ability to distribute the tensile stresses through the specimen.
- Cracking was observed at the loading face of the specimens with shear studs due to bending of the specimen.

According to the results under impact loading,

- Control specimens failed by punching.
- Specimens with uniformly distributed steel fibers displayed a close to static behavior under impact loading, influenced only slightly by inertial forces due to impact.
- Specimens with shear studs were largely influenced by inertial forces and scabbing occured at some areas.
- Specimens with steel fibers endured more impacts compared to control specimens and specimens with shear studs due to their higher energy dissipating capabilities.

REFERENCES

ACI Committee 318, (2005). Building Code Requirements for Structural Concrete (ACI 318-05) and Commentary (318R-05). American Concrete Institute, Farmington Hills, Mich.

Adetifa, B., Polak, M.A., (2005). Retrofit of Slab Column Interior Connections Using Shear Bolts. ACI Structural Journal Title no. 102-S27

Batarlar, B., (2013). Behavior of Reinforced Concrete Slabs Subjected to Impact Loads. Graduate School of Engineering and Sciences of İzmir Institute of Technology.

Bu, W., Polak, M.A., (2009). Seismic Retrofit of Reinforced Concrete Slab-Column Connections Using Shear Bolts. ACI Structural Journal Title no. 106-S49

Cheng, M.-Y., Parra-Montesinos, G.J., (2010). Evaluation of Steel Fiber Reinforcement for Punching Shear Resistance in Slab-Column Connections- Part I: Monotonically Increased Load. ACI Structural Journal Title no. 107-S11

Dinh, H.H., Parra-Montesinos, G.J., Wight, J.K., (2010). Shear Behavior of Steel Fiber-Reinforced Concrete Beams without Stirrup Reinforcement. ACI Structural Journal Title no. 107-S59

El-Salakawy, F., Polak, M.A., Soudki, K.A., (2002). Rehabilitation of Reinforced Concrete Slab-Column Connections. Canadian Journal of Civil Engineering: Vol. 29, 2002.

El-Salakawy, F., Polak, M.A., Soudki, K.A., (2003). New Shear Strengthening Technique for Concrete Slab-Column Connections. ACI Structural Journal Title no. 100-S32

Ghali, A., Youakim, S.A., (2005). Headed Studs in Concrete: State of the Art. ACI Structural Journal Title no. 102-S67

Kiski, N., Kurihashi, Y., Ghadimi Khasraghy, S.,, Mikami, H., (2011). Numerical Simulation of Impact Response Behavior of Rectangular Reinforced Concrete Slabs under Falling – Weight Impact Loading. Applied Mechanics and Materials, Vol. 83, 266-271

Li, Q.M., Reid, S.R., Wen, H.M., Telford, A.R.,(2005). Local impact effects of hard missiles on concrete targets. International Journal of Impact Engineering 32 (2005) 224-284

Trautwein, L.M., Bittencourt, T.N., Gomes, R.B., Bella, J.C.D., (2011). Punching Strength of Flat Slabs with Unbraced Shear Reinforcement. ACI Structural Journal Title no. 108-S20

Ong, K.C.G., Basheerkhan, M., Paramasivam, P., (1999). Resistance of Fibre Concrete Slabs to Low Velocity Projectile Impact. Cement and Concrete Composites 21 (1999) 391 -401

Xu, H., Mindess, S., (2006). Behavior of Concrete Panels Reinforced With Welded Wire Mesh and Fibres Under Impact Loading. ASCE 2006, Shotcrete.

Zineddin, M., Krauthammer, T., (2007). Dynamic response and behavior of reinforced concrete slabs under impact loading. International Journal of Impact Engineering 34 1517-1534

APPENDIX A

TECHNICAL DATA SHEETS

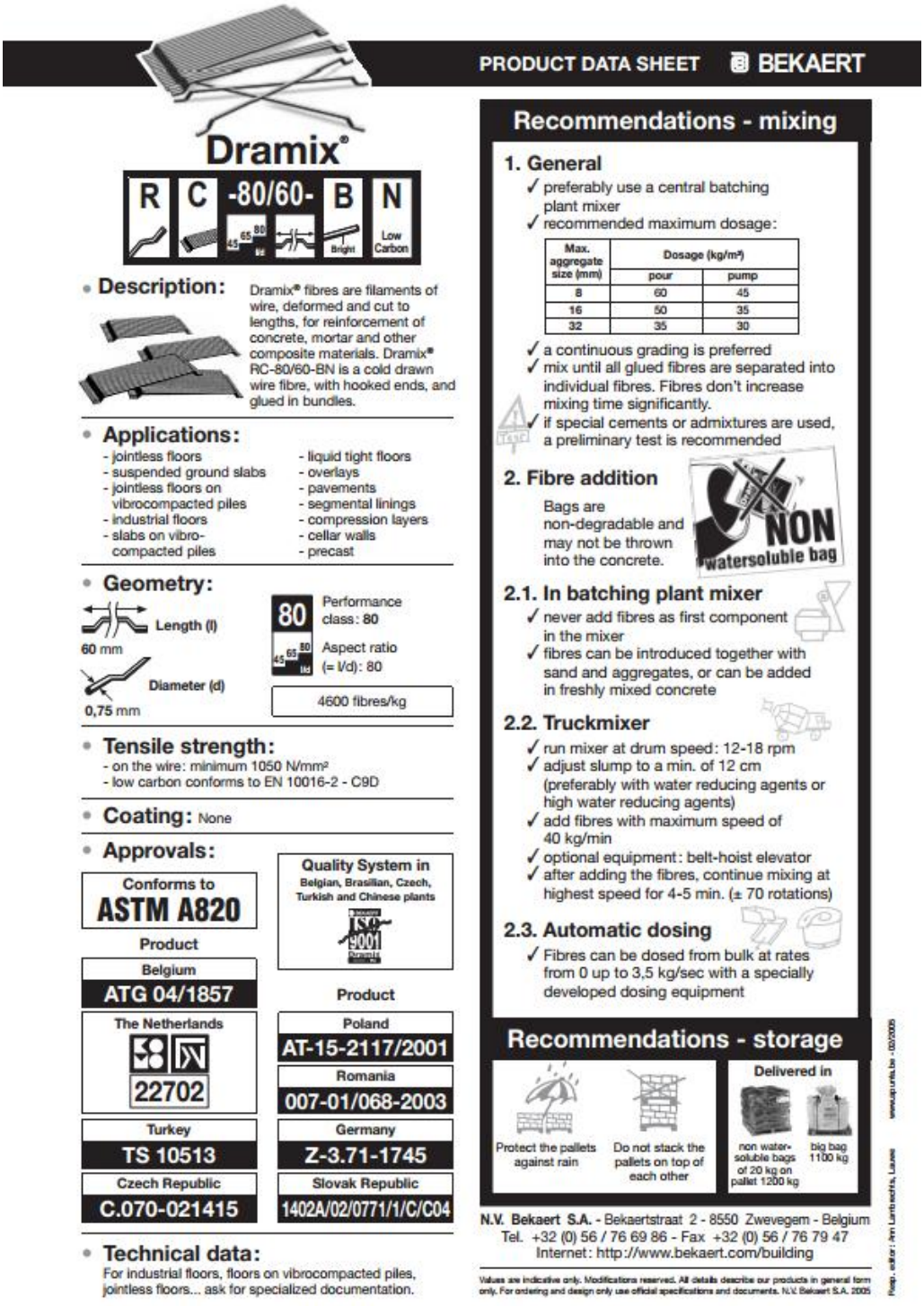

Figure A.1. Steel fibers' product data sheet

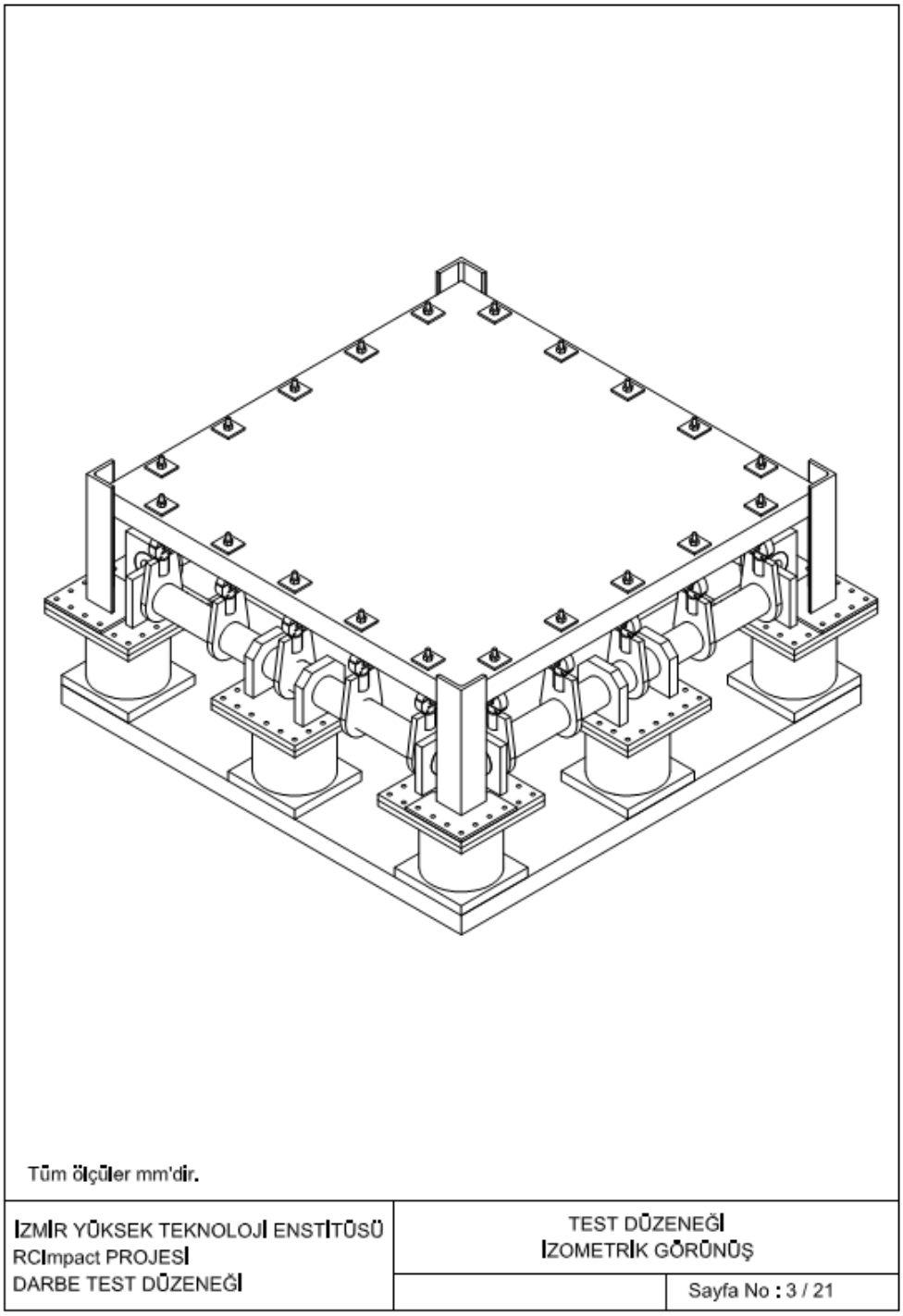

Figure A.2. Isometric view of the test setup